AD NUMBER

AD852062

NEW LIMITATION CHANGE

TO

Approved for public release, distribution unlimited

FROM

Distribution: Further dissemination only as directed by Air Force Aero Propulsion Lab., Wright-Patterson AFB, OH 45433, MAY 1969, or higher DoD authority.

AUTHORITY

AFAL ltr, 26 Apr 1979

AFAPL-TR-69-35
Volume III

FINAL REPORT

ADVANCED TURBINE ENGINE GAS GENERATOR CONCEPTUAL STUDIES AND FEASIBILITY EXPERIMENTAL TEST PROGRAM (UNCLASSIFIED TITLE)

Volume III: Materials Section (Table LXXV)

Frederick G. Groh
Pratt & Whitney Aircraft Division
United Aircraft Corporation

TECHNICAL REPORT AFAPL-TR-69-35, VOLUME III
May 1969

NOTICES

All distribution of this report is controlled. Qualified Defense Documentation Center users will request through AF Aero Propulsion Laboratory (RTD), Attn: APTP, [redacted], Wright-Patterson AFB, Ohio 45433.

When Government drawings, specifications, or other data are used for any purpose other than in connection with a definitely related Government procurement operation, the United States Government thereby incurs no responsibility nor any obligation whatsoever; and the fact that the Government may have formulated, furnished or in any way supplied said drawings, specifications or other data, is not regarded by implication or otherwise as in any manner licensing the holder or any other person or corporation, or conveying any rights or permission to manufacture, use or sell any patented invention that may in any way be related thereto.

Copies of this report should not be returned unless return is required by security considerations, contractual obligations, or notice on a specific document.

OK

(9) FINAL REPORT. 1 Jun 66 - 31 Aug 67,

(6) ADVANCED TURBINE ENGINE GAS GENERATOR CONCEPTUAL STUDIES AND FEASIBILITY EXPERIMENTAL TEST PROGRAM
(UNCLASSIFIED TITLE)

Volume III: Materials Section (Table LXXV).

(10) Frederick G. Groh

(11) May 69 from cover (12) 1446.

(15) AF 33(657)-15504

(16) AF-681B

(14) PWA-3219-Vol-3

SPECIAL HANDLING REQUIRED
NOT RELEASABLE TO FOREIGN NATIONALS
The information contained in this document will not be disclosed to foreign nationals or their representatives.

(18) AFAPL (19) TR-69-35-Vol-3

1473

FOREWORD

This report was produced in accordance with contract AF33(657)-15504, Project No. 681B, P. ~~E. C. No. 69216~~F, under the direction of Captain J. A. Baca (APTP) of the Air Force Aero Propulsion Laboratory. It discusses the work conducted by the Pratt & Whitney Aircraft Division of United Aircraft Corporation, East Hartford, Connecticut in accordance with Exhibit A of the contract during the period from June 1, 1966, through August 31, 1967. The report has been assigned the contractor number PWA-3219 and was submitted for review in October 1967.

This report contains no classified information extracted from other classified documents. The report has been classified in accordance with DD Form 254 of the contract.

Publication of this report does not constitute Air Force approval of the report's findings or conclusions. It is published only for the exchange and stimulation of ideas.

ERNEST C. SIMPSON
Chief, Turbine Engine Division
Air Force Aero Propulsion Laboratory

UNCLASSIFIED ABSTRACT

(U) Materials research and development was performed under Contract AF33 (657)-15504 on diffusion bonding of titanium, machining of small-diameter holes, determination of the abrasive properties of materials in a simulated jet-engine environment, and determination of the properties of selected materials in a high-temperature corrosive and erosive environment. Satisfactory diffusion bonds were formed in hollow titanium specimens at a temperature of 1800°F under isostatic pressure of 10,000 psi using machined steel mandrels to support the walls of the cavities within the specimens. Although satisfactory results were obtained using steel mandrels, the difficulty of accurately machining mandrels to fill cavities with complicated shapes makes this technique impractical for production processes. Five-mil diameter holes, which were subsequently coated to reduce the diameter to three mils, were successfully drilled into 80-mil thick alloys by the ECID (electrochemical impingement drilling) and the EDM (electrochemical discharge machining) processes. Low-cycle fatigue testing of specimens with arrays of three-mil diameter holes indicated the superiority of directionally solidified U-700 alloy over other forms of the same alloy and over Mar-M-509 alloy. None of the materials evaluated for abrasion properties demonstrated satisfactory abradability concurrently with a capability for withstanding the jet-engine environment, nor did any of the materials evaluated for use in a high-temperature corrosive and erosive environment meet the program requirements. Best results were obtained with chrome-aluminide-coated TD nickel, but cracks were observed in the specimen after only 46 hours of testing, and oxidation followed the cracks.

TABLE OF CONTENTS

LIST OF ILLUSTRATIONS

LIST OF ILLUSTRATIONS (Cont'd)

LIST OF ILLUSTRATIONS (Cont'd)

LIST OF ILLUSTRATIONS (Cont'd)

LIST OF ILLUSTRATIONS (Cont'd)

LIST OF ILLUSTRATIONS (Cont'd)

LIST OF ILLUSTRATIONS (Cont'd)

LIST OF ILLUSTRATIONS (Cont'd)

LIST OF ILLUSTRATIONS (Cont'd)

SECTION I

INTRODUCTION

(U) Materials research and development work was performed in four areas with funding provided by Contract AF33(657)-15504. The first of these involved an investigation of techniques for diffusion bonding hollow titanium specimens with internal supporting webs. The second task involved evaluation of techniques for machining small-diameter holes and determination of the effects of the holes on the properties of the material. The third task consisted of determination of the abrasion properties of a number of nonmetallic and metallic materials in a simulated jet-engine environment, and the fourth task was an evaluation of the properties of coated and uncoated materials in a high-temperature corrosive and erosive environment. The results of the work expended in each of these areas with contract funding is discussed in the following sections.

SECTION II

DIFFUSION BONDING

A. INTRODUCTION

(U) Diffusion bonding is of interest for joining surfaces which are not accessible after a part has been assembled. A typical example would be a hollow structure with internal supporting webs which might be fabricated in two halves and then bonded together. In such a structure, the interface of the web sections are completely inaccessible and cannot be bonded by more conventional bonding techniques such as welding. A diffusion bond can be achieved, however, by heating both halves of the part to a temperature below the melting point of the material used and pressing the halves together for a sufficient time period to allow diffusion of the material across the interface. For bonding to be achieved, the surfaces to be bonded must be brought into intimate contact, which requires that the mating surfaces be accurately machined and that sufficient pressure be used to ensure that contact is obtained over the entire interface. The pressure used generally will be high enough to cause the material to yield, and, therefore, in a hollow webbed structure, some type of support is required to prevent the hollow sections between the webs from collapsing.

B. DISCUSSION OF BONDING EFFORT

(U) Diffusion bonding techniques were studied by bonding a number of titanium specimens of the form shown in Figure 1. As shown, the hollow sections of these specimens were supported by an internal mandrel.

(U) The selection of materials for use as mandrels was based on several considerations. The mandrel material must be compatible with titanium and it must be capable of providing the required support. It also must be capable of being formed relatively precisely to the cavity dimensions, and it must be readily removable from the cavity following bonding.

(U) The mandrel materials initially considered were molybdenum, Armco iron, and Armco iron coated with aluminum oxide or graphtie. All of these materials produced a reaction zone in the titanium alloy which was unacceptably brittle. Subsequently, medium-carbon steel was tested, and it was found that the carbon in this material reacts with the titanium to form a titanium-carbide layer which acts as a reaction barrier, as shown in Figure 2. Steels with carbon contents between 0.24 and 0.47 percent were found to produce the desired barriers to prevent diffusion of the mandrel material into the titanium.

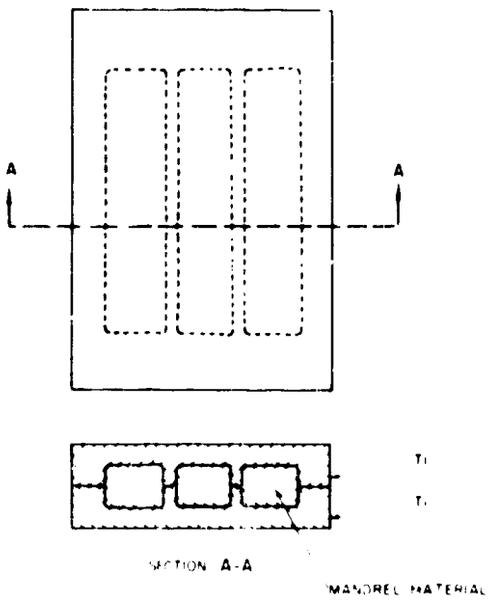

Figure 1 Sketch of Diffusion-Bonded Specimen

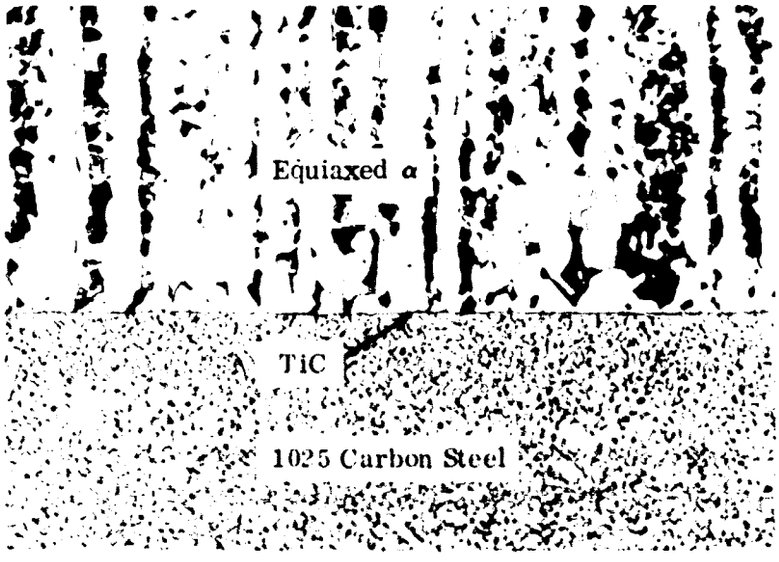

Mag: 100X

Figure 2 Photomicrograph of Interface Between Ti-6Al-4V Alloy and 1025 Steel in Hollow Diffusion-Bond Specimen

NOFORN

(U) Initially, machined steel strips used for mandrels were found to be satisfactory for parts with hollow cavities which have a relatively simple shape. The mandrel must fit the cavity precisely, however, and, therefore, machined mandrels do not appear to be feasible for supporting cavities which complex shapes, since the time required to produce complicated, accurately machined mandrels would be excessive for producing parts on a production basis. Consequently, several alternate methods of producing mandrels were attempted. These included electroplating, plasma spraying, and filling the cavity with small-diameter steel balls. None of these techniques were satisfactory. Electroplating resulted in severe corrosion at the interface of the mandrel material and the titanium, and the plasma-sprayed material failed to fill the corners of the cavities. The small-diameter steel balls did not provide adequate support, and the walls over the cavities collapsed during bonding. Methods of supporting the cavity walls without mandrels have been developed under other programs, and these methods appear to be more practical than those using mandrels when parts with complex internal cavities must be bonded. These methods are proprietary and are not discussed in this volume.

(U) Whenever mandrels are used, a method must be available for removing the mandrels after the blade halves are diffusion bonded together. The only practical method available for removing steel mandrels from the complex blade cavities is leaching with an acid solution. During this program, a 50-percent solution of nitric acid was found to be a satisfactory leaching agent. The process was slow, and, when the specimens were simply immersed in the leaching solution, periods of several weeks were sometimes required to completely remove the mandrel material. A pumped stream of leaching solution would be considerably faster, but would also be more complicated. The simple immersion process was considered to be adequate for the purposes of this program, and no effort was spent on developing a faster technique.

(U) All bonding was performed with a pressure of 10,000 psi and a temperature of 1800°F, which is the maximum temperature below that at which the beta transformation occurs. These conditions were maintained for three hours to permit some creep of the titanium to occur. Experience has shown that titanium can be bonded successfully at atmospheric pressure and a temperature of 1500°F in a very short time if the surfaces to be bonded are initially in intimate contact. The higher pressures and temperatures were used, however, because of the difficulty in machining two perfectly mated surfaces. The bonding parameters used were selected to permit bonding of surfaces with gaps up to 0.005 inch.

(U) A total of eleven specimens were bonded with mandrels at Battelle Memorial Institute. A typical bonded joint is shown in Figure 3. Four of the specimens were peel tested, and all of these failed in the parent metal away from the joint (see Figures 4 and 5). Metallographic examination revealed that good bonding was achieved in all areas. However, some deformation occurred at the edges of

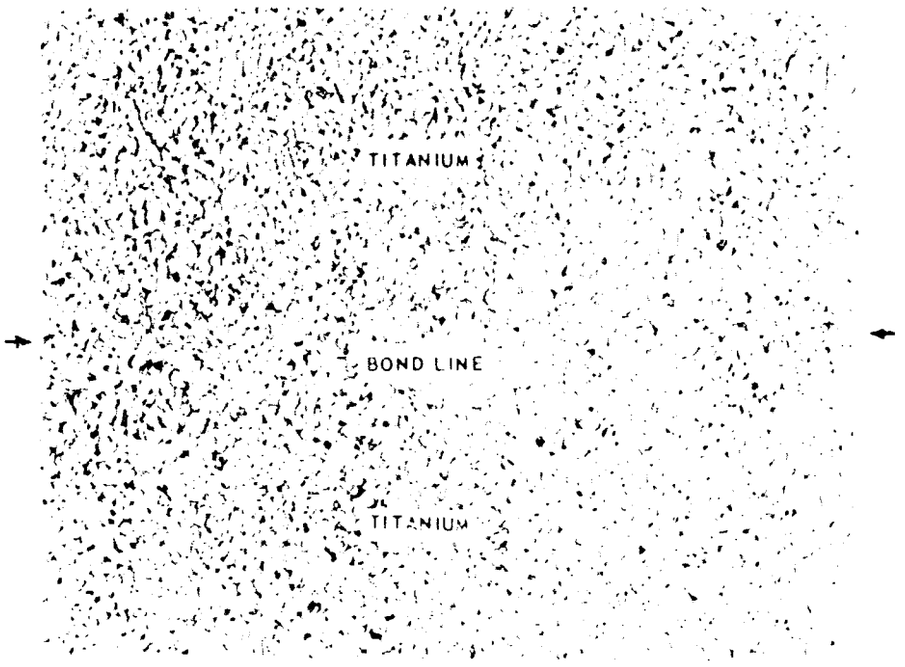

Figure 3 Typical Titanium Joint Diffusion Bonded at 10,000 psi and 1800 F for Three Hours XP-67627

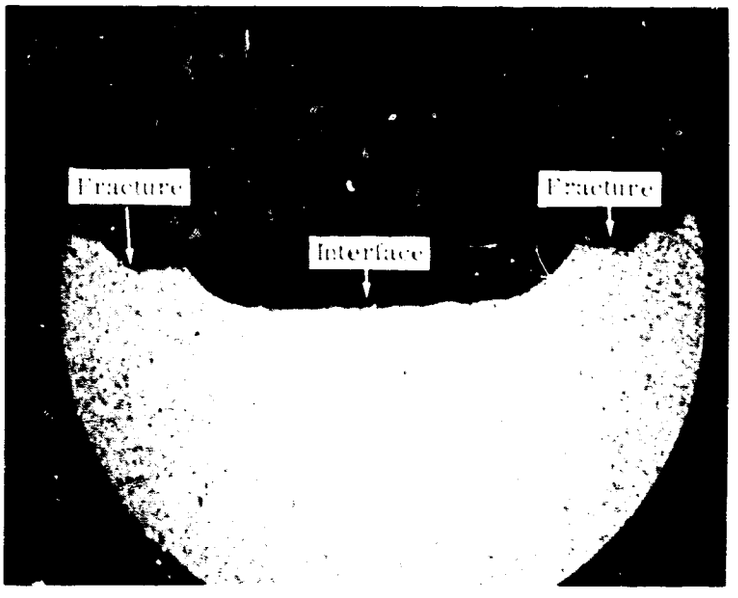

Mag: 3.5X

Figure 4 Photomicrograph of Peel-Tested AMS 4911 Diffusion-Bonded Specimen Showing That No Separation Occurred at Diffusion-Bonded Joint EM-1816-3

NOFORN

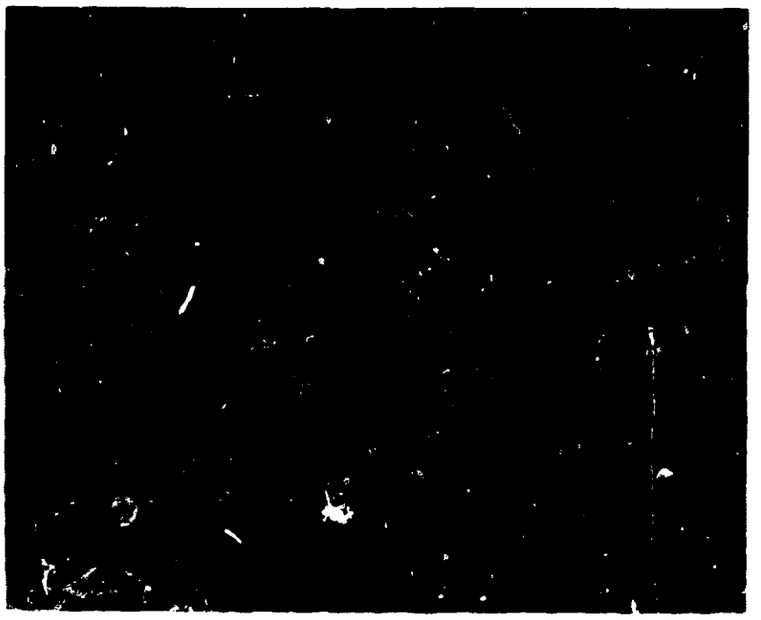

Mag: 500X

Figure 5 Photomicrograph of Diffusion-Bonded Section of Peel-Tested AMS 4911 Specimen EM-1816-1

the specimen cavities where the mandrel did not precisely conform to the contour of the cavity.

C. CONCLUSIONS AND RECOMMENDATIONS

(U) Diffusion bonding was shown to be a feasible method of joining titaniun specimens. For parts with cavities with simple shapes, solid, machined mandrels are satisfactory. However, better results, both technically and economically, can be obtained by using a proprietary process which does not require mandrels to support the cavity walls.

SECTION III

TECHNIQUES FOR DRILLING SMALL-DIAMETER HOLES

A. INTRODUCTION

(U) A program involving fabrication trials and mechanical testing was conducted to determine the best technique for producing closely spaced arrays of small-diameter holes. Hole-diameters of approximately three mils were desired.

(U) The initial phase of the program was devoted to selecting the more promising methods for producing holes, and the second phase of the program involved preparation and testing of axial push-pull and strip-bend low-cycle fatigue specimens. The specimens were prepared with 100 holes in each specimen arranged in a rectangular array with a center-to-center spacing of 50 mils.

B. INITIAL EVALUATION OF HOLE-DRILLING TECHNIQUES

1. Preliminary Selection

(U) Several methods of drilling small-diameter holes were selected for evaluation. The laser process was considered to be promising because of its speed and because one vendor reportedly had drilled a one-mil diameter hole through 40-mil thick tungsten carbide. The process needed development, however, because the metal which melted during the drilling process resolidified on the hole surface, leaving a recast layer which had a tendency to crack. The ECID process (electrochemical impingement drilling) had been under study at Pratt & Whitney Aircraft prior to this program and was considered to be quite promising for this application. The EDM process (electrodischarge machining) was initially rejected because it was believed that suitable three-mil diameter holes could not be obtained. Later, however, the required hole size diameter was increased to five mils, and the EDM process was evaluated. The increase in diameter was permissible because it was found that a three-mil diameter hole could be made by proper coating of a five-mil diameter hole. The ECM process was not studied because it is not possible to construct a satisfactory nozzle for producing a three-mil diameter hole, since in this process the nozzle must pass through the hole.

2. Laser Development

(U) Holes are produced by a laser beam as a result of the melting and vaporization of the material struck by the beam. Since the beam can be concentrated into a very small area, holes on the order of one mil in diameter can be produced. However, some of the metal melted by the beam remains to form a remelt

or recast layer. Since the properties of the recast layer differ from those of the remainder of the material, cracks frequently develop in the recast layer as a result of thermal cycling. Consequently, development was required to reduce the thickness of the recast layer to an acceptable level.

(U) Three laser vendors were requested to develop drilling techniques to eliminate or minimize the recast layer on a best-effort basis. Each was given samples of 80-mil thick cast Udimet-700 and requested to submit what they considered to be their best results at the end of a specified time period. The vendor achieving the greatest progress would then be given an opportunity to continue development on all candidate materials.

(U) Table I shows the range of variables studied and the optimum values determined by one vendor. The geometry is shown in Figure 6. However, even with the optimum geometry, satisfactory holes could not be produced. Since no significant improvement was achieved, the development of laser hole-drilling techniques was discontinued.

(U) TABLE I

RESULTS OF LASER DRILLING OPTIMIZATION STUDY

Variable	Range	Optimum Value
Ruby Rod Diameter, in.	0.25 to 0.375	0.25
Ruby Rod Length, in.	6.625	6.625
Aperture Opening, d, mm	1.5 to 7	1.5
Focal Length of Lens, F, mm	12 to 26	16
Depth of Focal Point into Work Piece, t, mils	0 to 80	60
Energy per Pulse, joules	5 to 25	10*
Duration of Pulse, milliseconds	0.4 to 3	0.4

* Energy at surface of work piece equalled 0.6 joules.

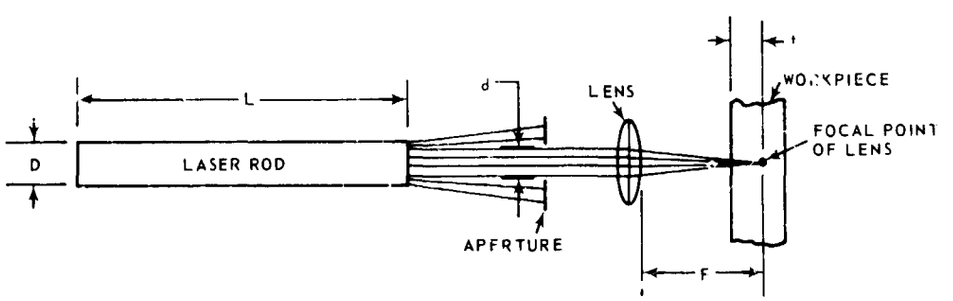

Figure 6 Schematic Diagram of Laser Hole-Drilling Equipment

NOFORN

3 ECID Development

(U) The ECID (electrochemical impingement drilling) process is a special application of the electrochemical machining process. In the ECM process, the cathode tube carrying the electrolyte moves through the work piece, and, therefore, the smallest hole that can be produced is limited by the outside diameter of the cathode tube. In the ECID process, this limitation is eliminated by releasing the electrolyte through a jet across a gap of 0.020 to 0.100 inch. The jet is produced by pumping the electrolyte into the nozzle at high pressure. A direct-current power supply is placed across the electrolyte and the work piece, which deplates material from the work piece. A schematic diagram of the equipment used for the process is shown in Figure 7. Figure 8 shows the appearance of the equipment at the start of the program, and Figure 9 shows the appearance of the equipment after modifications were made to permit three-dimensional positioning of the nozzle. A closeup view of a typical specimen being drilled is shown in Figure 10.

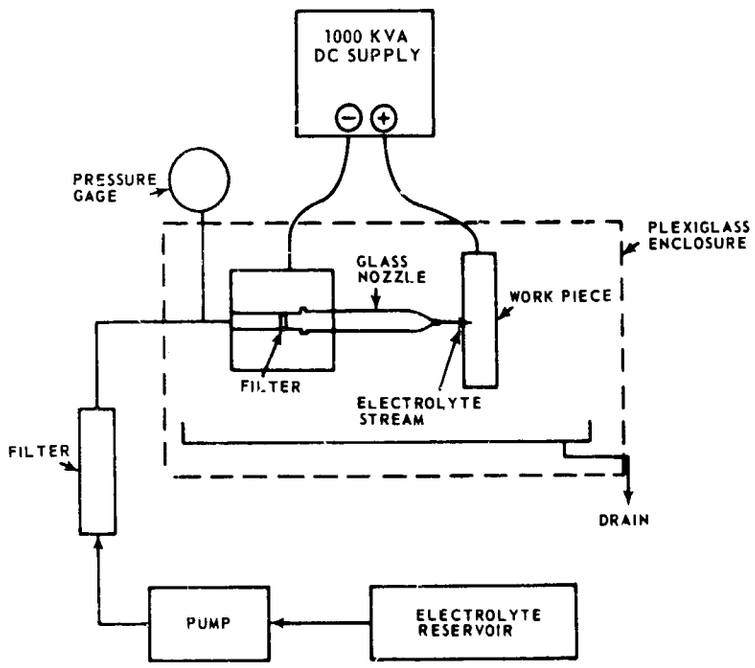

Figure 7 Schematic Diagram of ECID Hole-Drilling Equipment

NOFORN

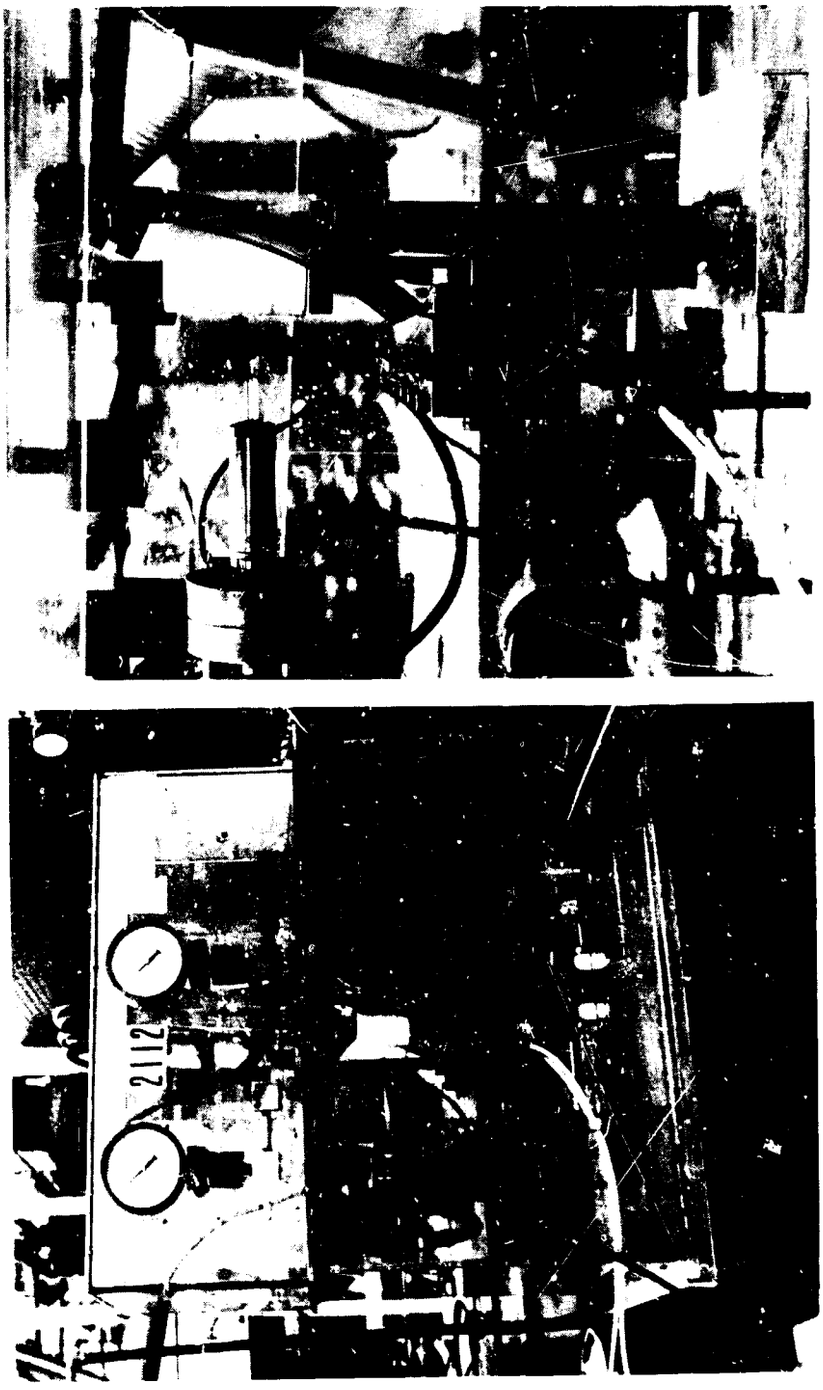

Figure 5 ECID Equipment Set up with 1.5-Mil Glass Nozzle to Produce 6- to 7-Mil Diameter Holes in 65-Mil Thick Waspaloy XP-68267/XP-68268

NOFORN

Figure 9 ECID Equipment Modified to Permit Three-Dimensional Nozzle Positioning

XP-73103

NOFORN

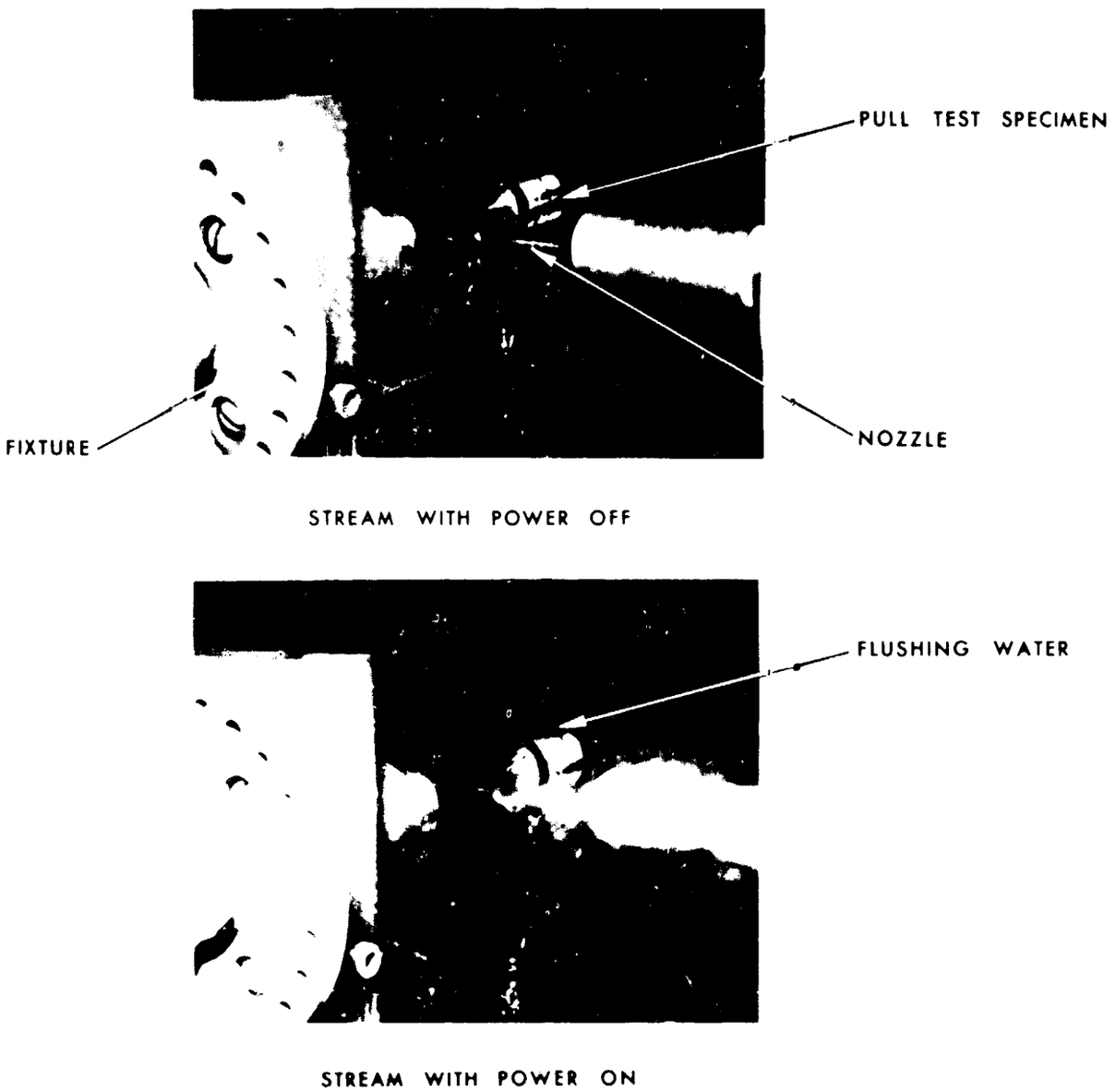

Figure 10 Closeup View of Push-Pull Low-Cycle Fatigue Specimen Being Drilled by ECID Process

NOFORN XP-78779

(U) In the early stages of the development of this process, drilling trials were continually hampered by plugging of the nozzle. The nozzles at the time had inside diameters between 0.5 and 2.5 mils which could be easily plugged by small particles from the air. The problem was solved by moving the nozzle drawing equipment into a clean room and keeping the resulting nozzles in plastic tubes except when actually being used for drilling. As an added precaution, a two-micron polyvinyl filter was added upstream of the nozzle to filter out any particles which passed through the main filter in the ECID apparatus.

(U) Considerable effort was expended to determine the optimum ECID operating parameters for obtaining the best hole surface finish and the shortest drilling time. Significant variables included nozzle design, nozzle-to-work piece gap, work piece material, electrolyte type and flow rate, voltage, and dwell time. Dwell time is the length of time that the drilling operation is continued after the electrolyte stream breaks through the material. Satisfactory values were determined for each of these variables. Investigations are continuing under another program to improve the ECID process further.

(U) To ensure that a particular hole size could be produced consistently, a method for producing a consistent nozzle shape and size had to be developed. The basic process developed involved pulling heated Pyrex tubing which initially had a 1/4-inch outside diameter and a 1/32-inch inside diameter. The process was standardized by using the equipment shown in Figure 11. In this device, the

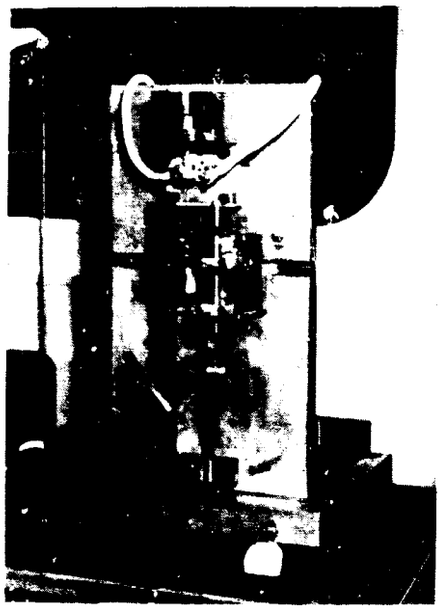

Figure 11 ECID Nozzle Forming Fixture XP-73102

NOFORN

glass tubing is heated by a Nichrome heating coil and then pulled by a weight. The power to the heating coil and the size of the weight can be varied to produce the desired results. The distance through which the tube was pulled was controlled by the length of time that power was supplied to the heating coil after the tubing started to yield. The heating coils had to be replaced periodically, and it was found that variations in the resistance of the coils significantly affected the results. Considerable care was required to ensure that consistent coils were used. Following drawing, the tubing was cut in the reduced section to form the nozzle. A clean cut was required, since any clipping at the nozzle tip permitted the electrolyte stream to disperse over too large an area. The flow characteristics and the diameter of the nozzles were checked in the apparatus shown in Figure 12. At the end of the program, approximately 65 percent of the nozzles produced were usable. Typical nozzles are shown in Figure 13.

(U) These nozzles suffered from two deficiencies. First, after several hundred holes had been drilled with a particular nozzle, erosion caused the nozzle's inside diameter to become enlarged, resulting in larger diameter holes. The hole size increased by approximately 0.5 mil for every 100 holes drilled with a particular nozzle. Second, the relatively large outside diameter of the nozzles limited the minimum possible spacing between holes during multiple drilling operations. Consequently, techniques for fabricating nozzles from quartz tubing with an outside diameter of 80 mils are being developed under another program. When successful, the developed techniques are expected to produce nozzles with significantly better resistance to erosion and with an outside diameter that will permit closer hole spacing during multiple drilling operations.

(U) The actual design of the nozzle was determined by trial and error. The inside diameter required to produce a three-mil diameter hole was determined to be between 0.5 and 1.0 mil. The length of the nozzle tip was determined experimentally on the basis of its effect on electrical and flow resistance. For a given voltage and pressure, the current and the electrolyte flow rate decrease as the tip length is increased, thereby increasing drilling time. However, the effects of the tip length and shape on the discharge stream diameter have not been determined precisely.

(U) The effect of the gap between the nozzle and the work piece was studied, and it was found that best results were obtained with a gap of approximately 60 mils. Increasing the gap increases the electrical resistance of the electrolyte stream, whereas decreasing the gap permits the return spray of electrolyte from the work piece to interfere with the impinging stream, thus causing enlargement of the hole being drilled.

NOFORN

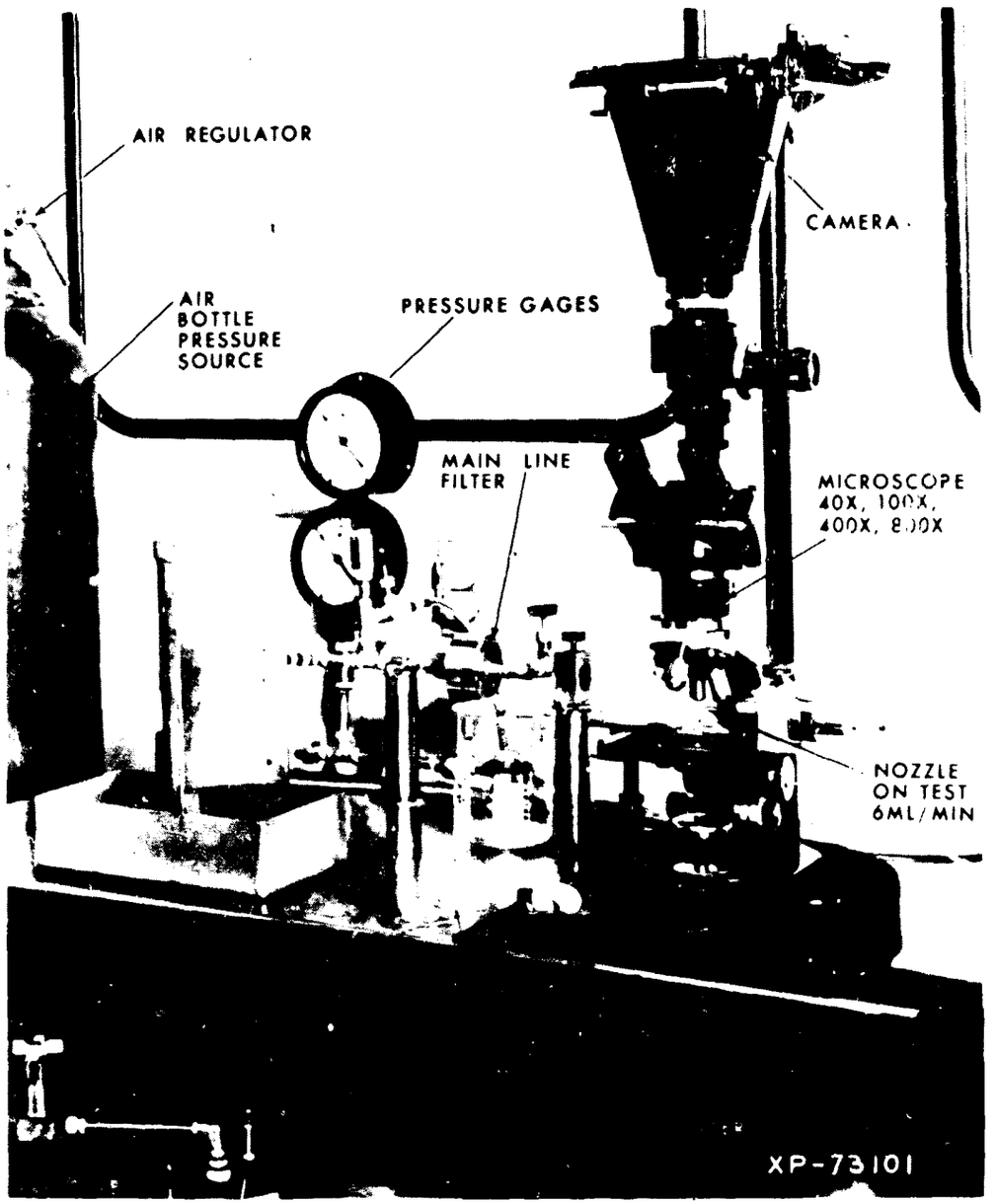

Figure 12 ECID Nozzle Flow Test and Inspection Bench XP-73101

NOFORN

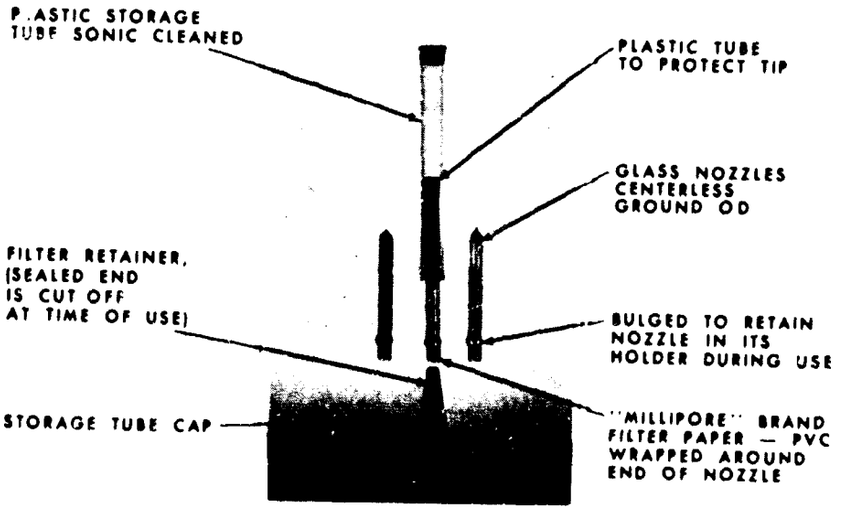

Figure 13 Typical ECID Nozzles Drawn From 1/4-Inch Outside Diameter Pyrex Tubing

(U) Drilling rate is a function of several parameters, including the type of material being drilled, the type of electrolyte used, the electrolyte flow rate, and the voltage across the electrolyte and the work piece. Material is removed from the work piece by electrolytic and, possibly, chemical action, and, therefore, the drilling time will be proportional to the valence of the work piece material. Since the valences of the base metals in the alloys drilled during the program were equal, the drilling times should be approximately equal in the absence of chemical reactions. Testing verified this theory for Mar-M-509 and Udimet-700 alloys. For other alloys, however, it is possible for complex reactions to occur which can vary both the drilling time and the surface finish, so actual drilling time must be determined experimentally for each material. During this program, 80-mil thick specimens were drilled in approximately 1.5 minutes.

(U) The type of electrolyte used affects the drilling time in two ways. First, it must produce the desired electrolytic reaction with the work piece material without detrimentally reacting with the material chemically. Secondly, it must have a high conductivity to provide a high current. Hydrochloric acid was found to meet both of these requirements for the materials drilled during this program.

(U) The electrolyte flow rate affects the drilling time since increased flow removes the products of electrolysis and chemical reaction more quickly, permitting fresh electrolyte to reach the work piece more rapidly.

NOFORN

(U) Another parameter affecting drilling rate is the voltage across the nozzle and the work piece. Increasing the voltage increases the electrolytic current and, therefore, the rate at which the electrolytic reaction occurs. The maximum voltage which can be used is limited, however, because at excessively high voltages arcing occurs between the nozzle and the work piece. The arcing probably occurs because of vaporization of the electrolyte as a result of the heat generated by the passage of current through the stream. If this is the case, higher voltages, and, therefore, higher currents, could be used by increasing the electrolyte flow rate, which would keep the electrolyte temperature below the critical vaporization point. A voltage just under the arcing voltage was used for all drilling operations during this program.

(U) The final parameter considered was dwell time. Dwell time is the length of time that the drilling operation is continued after the electrolyte stream breaks through the material. If drilling is stopped immediately after the electrolyte breaks through the work piece, a lip with sharp corners will remain at the exit side of the hole, and the diameter in this region will be substantially smaller than that of the remainder of the hole, as shown in Figure 14. Con-

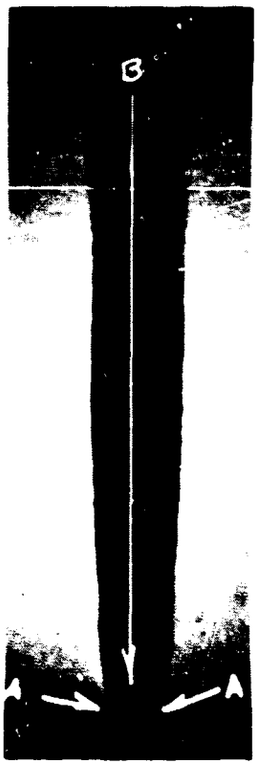

Mag: 100X

Figure 14 ECID Hole After Initial Electrolyte Penetration Showing Tip at Bottom of Hole.(A) Arrow (B) Shows Direction of Cutting Action

NOFORN

XP-7629

tinuing the operation several seconds longer removes the lip and rounds the corners at the exit of the hole. A dwell time of seven seconds was found to produce best results during this program. The time that the electrolyte breaks through the work piece is clearly indicated by a sharp drop in current.

(U) Once the nozzle design requirements and operating parameters were determined, it remained to determine to what extent the hole size was repeatable from one hole to the next and from one nozzle to the next nozzle. A large number of holes were drilled with ten different nozzles, and the holes were examined. For any single nozzle, the hole size was repeatable to within 0.1 mil, discounting the effects of nozzle tip erosion, which constituted a progressive increase in hole diameter at the rate of 0.5 mil per 100 holes. Between nozzles, the hole size was repeatable to within 0.5 mil for both 3-mil and 5-mil diameter holes.

4. Coating Trials

(U) In an effort to achieve maximum corrosion and erosion resistance, attempts were made to apply coatings to the inner surfaces of the holes to determine if such a process were feasible. Specimens with four-, six-, and ten-mil diameter holes produced by the ECID process were delivered to three vendors for coating. The process used by one of the vendors produced a uniform coating through all of the holes with a thickness equal to that of the coating on the external surface. Approximately one half of the coating inside the holes diffused into the base material, thereby decreasing the hole diameter by an amount approximately equal to the coating thickness. A typical coated specimen is shown in Figure 15.

Figure 15 Coated ECID Hole Drilled to 4-Mil Diameter at Exit in 80-Mil Thick Cast Udimet-700

NOFORN

Since it was found to be possible to apply a two- to three-mil thick coating to the inside of the holes, it was possible to relax the hole drilling requirements from a three-mil diameter hole to holes with diameters between five and six mils. The coating would then reduce the hole diameters to two to four mils, thereby meeting the original requirement.

5. EDM Development

(U) Following relaxation of the hole diameter requirement, holes were drilled by the EDM process using equipment specifically designed for small-diameter hole drilling. The vendor who performed the work claimed that by using specially designed equipment, drilling times would be shorter and the recast layer would be thinner than that obtained using the universal type of EDM equipment. The vendor produced five-mil diameter holes in 80-mil thick specimens including Udimet-700 and Mar-M-509 alloys in less than one minute. More conventional EDM equipment would require over an hour to produce equivalent holes. Further, the recast layer was essentially nonexistent. The equipment used is shown in Figure 16, and typical holes are shown in Figure 17.

6. Multiple-Hole Drilling

(U) Any process considered for producing small-diameter holes must be capable of producing several holes simultaneously if the process is to have practical value. Multiple-hole drilling trials, therefore, were conducted with the ECID process under another program. For these trials, nozzles were drawn from 80-mil tubing so that a spacing of 200 mils between adjacent nozzles could be achieved. A total of 230 holes were drilled in 55-mil thick material in groups of 10 requiring 23 minutes total time. Hole spacing in actual parts may need to be as close as 50 mils. It is not known at the present time if it is possible to produce holes by the ECID process with a 50-mil spacing, even if the problems of nozzle spacing can be resolved. With a 50-mil spacing between holes, interference may occur between adjacent electrolyte jets causing electrolysis or chemical reactions to occur on the surface between holes. If this is the case, the desired hole spacing can still be obtained, however, by drilling one set of holes with double the desired spacing, and then drilling a second set in the spaces between the holes in the first set.

C. LOW-CYCLE FATIGUE TESTING

1. Test Program Description

(U) Low-cycle-fatigue testing was performed to determine the cyclic life of candidate materials with and without holes. Two types of tests were performed: axial push-pull tests and strip bending tests. Both types of test were performed at 1500°F.

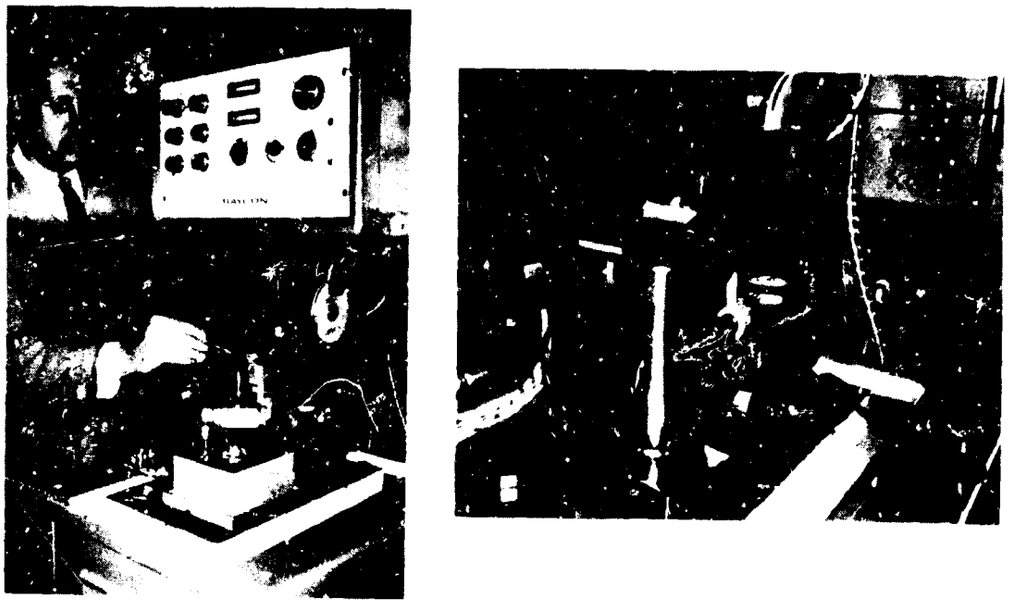

Figure 16 EDM Equipment Designed for Small-Diameter Hole Drilling

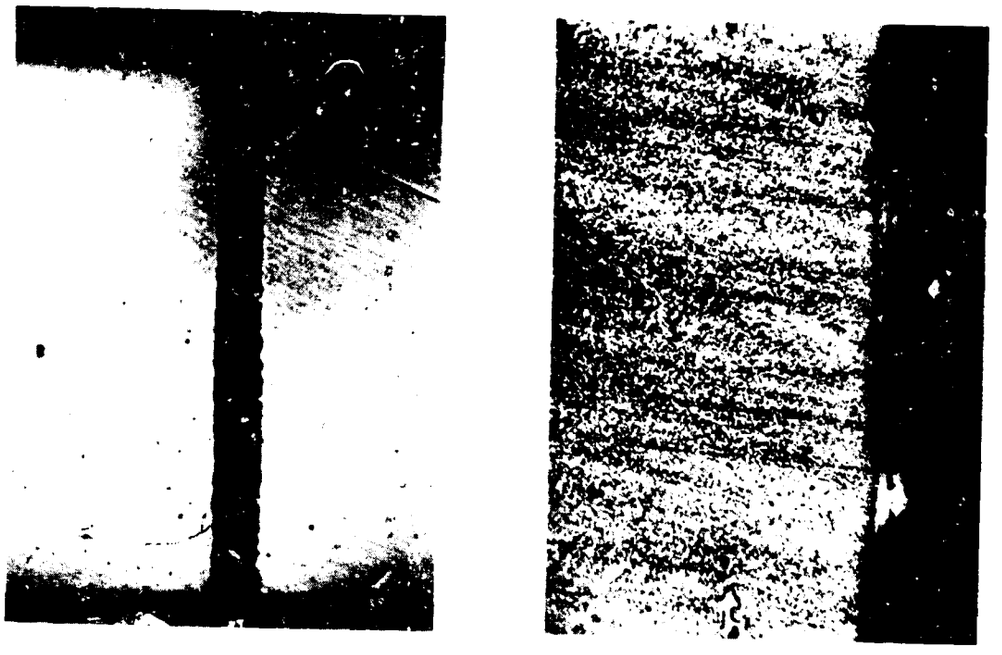

Figure 17 Seven-Mil Diameter Hole Drilled by EDM Process Through 80-Mil Thick Udimet-700 in Approximately 50 Seconds

NOFORN

(U) Axial push-pull testing was performed with the equipment shown in Figure 18. This rig loads the specimen through a hydraulic ram to a set strain level, which is maintained through a linear variable differential transformer (LVDT) extensometer attached to the inner surface of the specimen. With this arrangement, the strain level remains constant throughout the test regardless of strength changes in the specimen induced by the test. Most of the tests were performed with a maximum strain of one percent, although smooth specimens were tested at other strain levels for comparison purposes. The temperature of the specimen is raised to the desired level by induction heating.

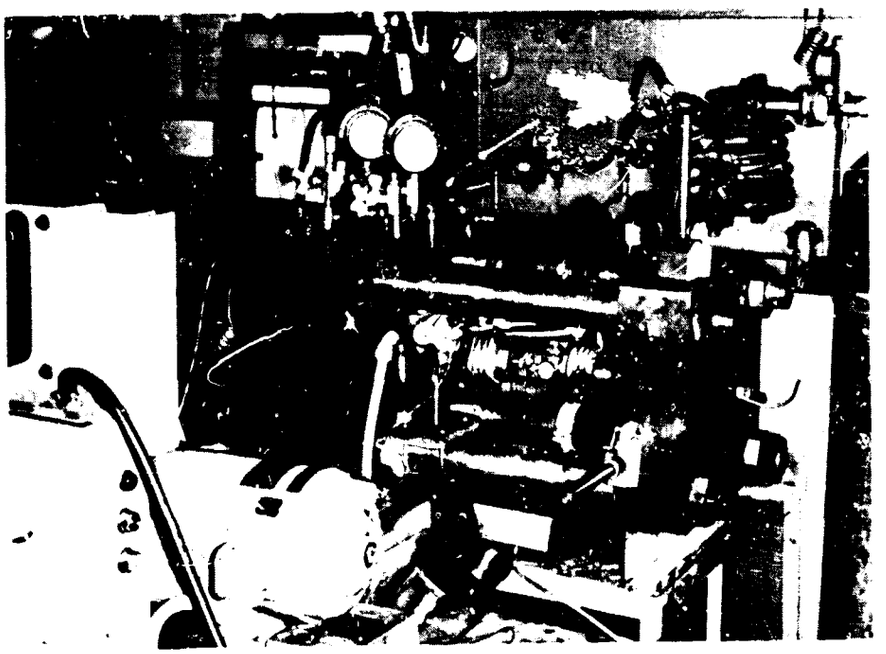

Figure 18 Hydraulically Operated Strain Cyclic Rig Used for Axial Push-Pull Testing

II-48610

(U) Bend testing was performed in the low-cycle fatigue test rig shown in Figure 19. This rig subjects the specimen to a pure bending load by applying equal and opposite moments to the ends of the specimen, as shown in Figure 20. During reversed bending, the ends of the specimen are displaced kinematically to maintain a circular arc. The maximum strain is maintained constant throughout the test regardless of strength changes in the specimen. Strain is determined

by the setting of the adjustable crank shown in Figure 20. Testing can be performed at elevated temperature by inserting the specimen in the furnace shown in Figure 19.

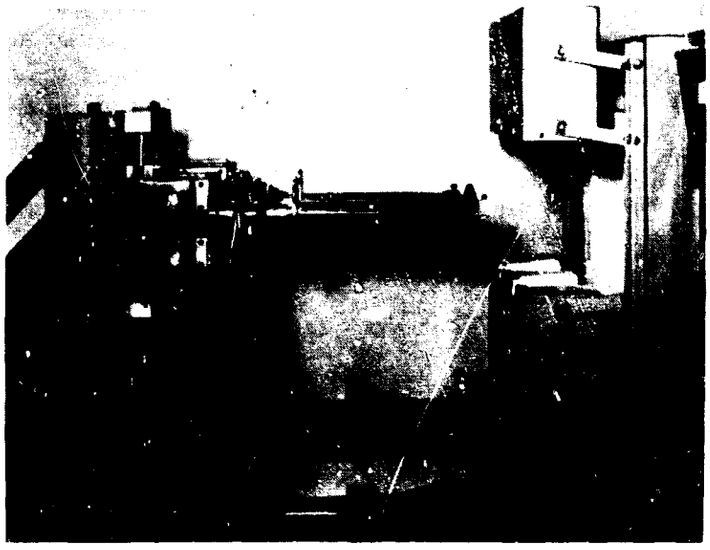

Figure 19 Pure Bending Low-Cycle Fatigue Rig

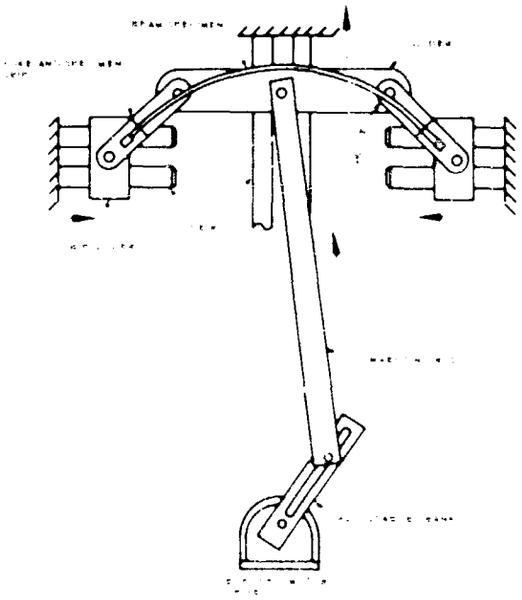

Figure 20 Operation of Pure Bending Low-Cycle Fatigue Rig

NOFORN

2. Specimen Preparation

(U) Four materials were tested during the program. These were conventionally cast U-700, wrought U-700, directionally solidified U-700, and conventionally cast Mar-M-509. These materials were formed into strip bend specimens, such as shown in Figure 21, and into tubular push-pull specimens, such as shown in Figure 22. Both types of specimens contained 100 holes spaced approximately 50 mils apart over an area measuring about 1/4 inch by 1 inch. The holes were produced by either the EDM or the ECID process. Specimens of each material without holes were tested to provide baseline data. Specimens were fabricated in two thicknesses, 0.040 inch and 0.080 inch.

(U) No heat treatment was required for cast Mar-M-509 material. The U-700 materials all received heat treatments before machining and drilling. The conventionally cast and directionally solidified U-700 materials both received the same heat treatment. These materials were solution heat treated at 2125 to 2150°F for four hours followed by furnace cooling at 100°F per hour to 1975°F and air cooling to room temperature. The wrought U-700 material was solution heat treated at 2125 to 2150°F for four hours, precipitation heat treated at 1975°F for four hours, and then air cooled. This was followed by treatment at 1550°F for 24 hours and air cooling and then treatment at 1400°F for sixteen hours with air cooling. Following heat treatment, the specimens were machined and drilled by the selected processes. They were then protected by a pack aluminum coating. The coating process included a diffusion heat treatment at 1975°F for four hours with air cooling. Following coating, the cast U-700 materials were precipitation heat treated at 1400°F for sixteen hours. The wrought U-700 material was precipitation heat treated at 1550°F for twenty-four hours and air cooled, followed by heat treatment at 1400°F for sixteen hours with air cooling. The Mar-M-509 material was precipitation heat treated at 1975°F for four hours following coating.

(U) The process selected for fabricating the specimens is one which would also be suitable for complete blade and vane fabrication. Heat treatment was performed before machining to prevent the surface recrystallization and contamination which otherwise might occur. In addition, the chosen heat treatment schedules tend to keep the grain boundaries clean, thereby enhancing the ductility of the part. The process was also compatible with a hard-facing process which would be required for the turbine blade parts. Hard-facing can be performed on U-700 material only when the material is in the as-cast condition or after it has received the complete heat treatment schedule. A temperature of 1975°F was selected for the diffusion treatment following the pack aluminizing process to ensure that recrystallization of the machined surface would not occur.

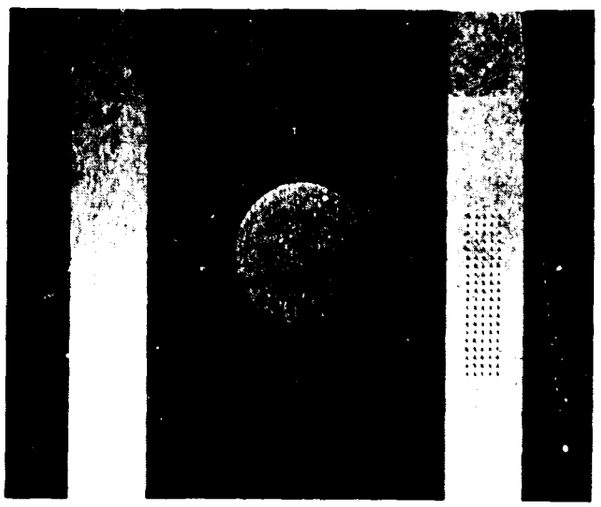

Figure 21 Typical Strip Bending Specimen with 5-Mil Diameter Holes Produced by the ECID Process. Hole Exit Surface is shown at Left and in the Center and Hole Entrance is shown at Right XP-76296

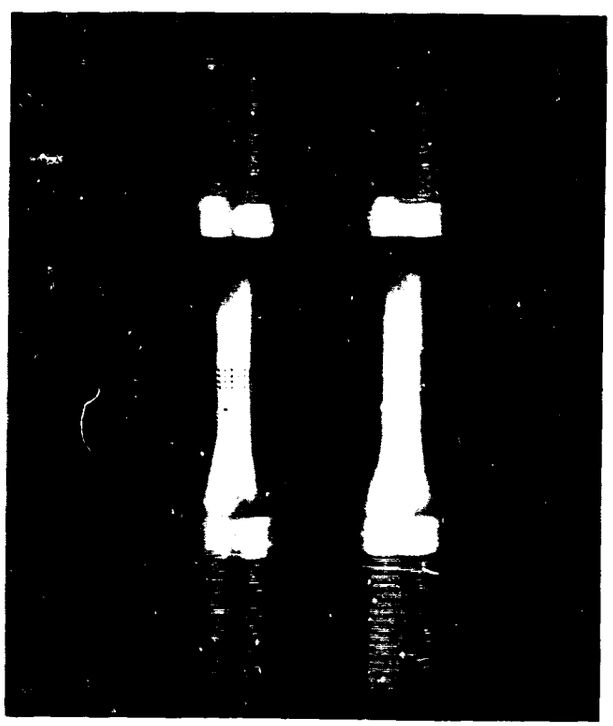

Figure 22 Typical Tubular Push-Pull Specimens with ECID Holes (Left) and EDM Holes (Right) H-65054

NOFORN

3. Test Results

(U) Detailed test results are presented in Figures 23 through 30, and average values for each material are presented in Table II. In general, the strip-bending low-cycle fatigue life was higher than the axial push-pull life. The thinner material tended to have the longer life in axial push-pull cycling, whereas the thicker material consistently had the longer life in strip bending.

(U) The directionally solidified U-700 material demonstrated the longest average strip bending low-cycle fatigue life in both material thicknesses with holes drilled by either the EDM or ECID processes. In fact, in strip bending, the drilled directionally solidified U-700 material had longer fatigue lives than any of the smooth specimens fabricated from other materials. Wrought U-700 material was slightly better than cast U-700 material in strip bending, but the fatigue life of Wrought U-700 material was significantly shorter than that of directionally solidified U-700 material for equal thicknesses and specimen conditions. Mar-M-509 material had the shortest life of the four materials for each specimen condition.

(U) In axial push-pull cycling, the directionally solidified U-700 material and the wrought U-700 material had comparable fatigue life for smooth specimens, but the fatigue life of the directionally solidified material with holes was significantly longer than that of the cast material with holes. A typical failed specimen of directionally solidified U-700 material is shown in Figure 31. For specimens with holes, the cast U-700 and wrought U-700 materials had comparable life. Mar-M-509 material again demonstrated the shortest life in axial push-pull cycling.

(U) The average fatigue life data presented in Table II clearly indicates the superiority of directionally solidified U-700 material with respect to fatigue life with and without holes at 1500°F. Study of the detailed data presented in Figures 23 through 30, however, indicates that the data for this material contains considerably more variation than that for the other materials. This indicates that more development effort should be applied to achieve consistent performance from this alloy.

D. CONCLUSIONS AND RECOMMENDATIONS

(U) The fabrication tests demonstrated that 5-mil-diameter holes can be drilled in 80-mil-thick alloys by either the ECID or the EDM process in less than 1 1/2 minutes and that 3-mil diameter holes can be drilled in 80-mil thick turbine alloys by the ECID process. Further development is required before multiple hole drilling will be feasible by either process.

NOFORN

(U) TABLE II

AVERAGE LOW-CYCLE FATIGUE LIFE FOR CANDIDATE TURBINE MATERIALS AT 1500°F WITH 1 PERCENT TOTAL STRAIN RANGE

Axial Push-Pull Test - Average Number of Cycles to Failure

	Cast U-700		Wrought U-700		Directionally Solidified U-700		Mar-M-509	
	40-Mil Thick	80-Mil Thick	40-Mil Thick	80-Mil Thick	40-Mil Thick	80-Mil Thick	40-Mil Thick	80-Mil Thick
Smooth	380	355	1460	1020*	1390	1190*	--	40**
ECID Holes	50	75	--	60*	585	320	--	10*
EDM Holes	110	150	195*	110	415	550	--	50*

Strip-Bending Test - Average Number of Cycles to Failure

	Cast U-700		Wrought U-700		Directionally Solidified U-700		Mar-M-509	
	40-Mil Thick	80-Mil Thick	40-Mil Thick	80-Mil Thick	40-Mil Thick	80-Mil Thick	40-Mil Thick	80-Mil Thick
Smooth	--	815	610	1150	4325*	17100	250	395*
ECID Holes	270	430	360	575	1940*	10700	90	150
EDM Holes	200	585	300	510	2300	5900	125	220

* Based on one test

** Interpolated

NOFORN

(U) Low-cycle fatigue testing demonstrated the superiority of directionally solidified U-700 material with respect to cyclic loading, both with and without ECID or EDM holes. The other materials tested demonstrated significantly shorter life and appeared to be more sensitive to the presence of ECID and EDM small-diameter holes than the directionally solidified U-700 material.

(U) Additional low-cycle fatigue testing should be performed to determine the effects of the type of cyclic strain, the thickness of the material, and the presence of the pack aluminum coating on fatigue life. The scatter in the data for the directionally solidified U-700 material indicates a need for achieving more consistent properties through development. However, the obvious superiority of this material at its current level is indicative of the potential of single-crystal U-700, and this material should be evaluated by a similar test program.

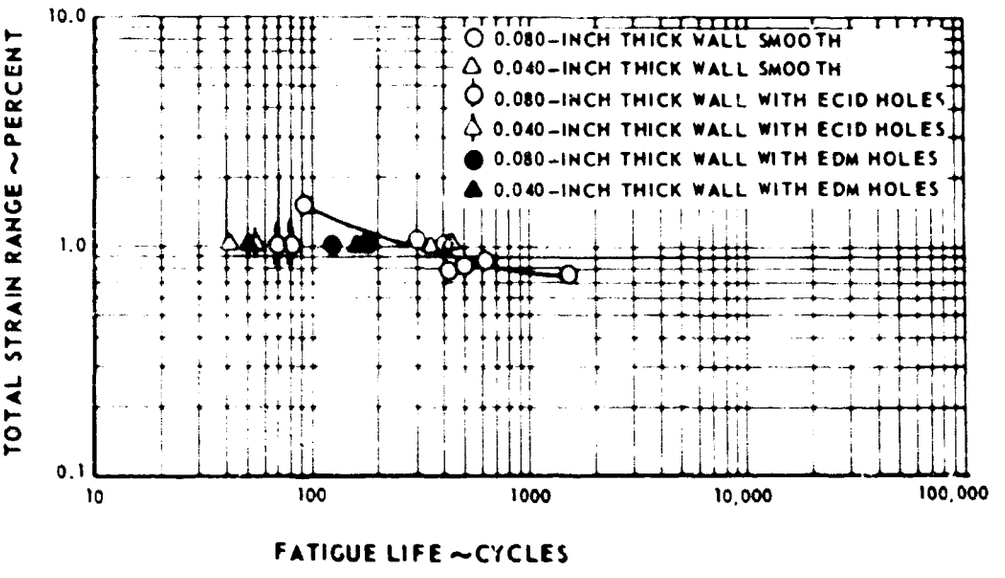

Figure 23 Axial Push-Pull Low-Cycle Fatigue Life of Cast U-700 (PWA 656) Material at 1500°F

NOFORN

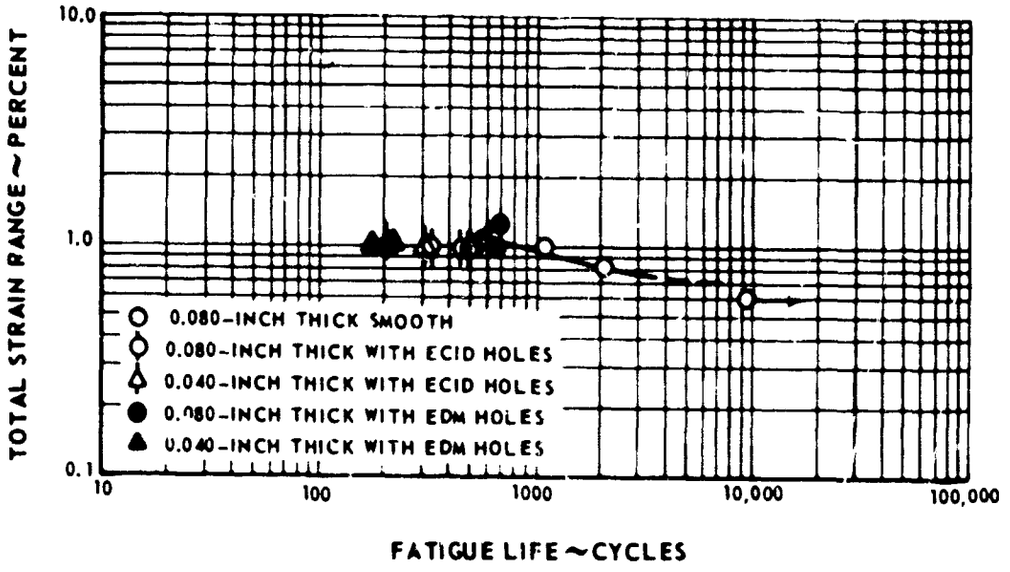

Figure 24 Strip Bending Low-Cycle Fatigue Life of Cast U-700 (PWA 655) Material at 1500°F

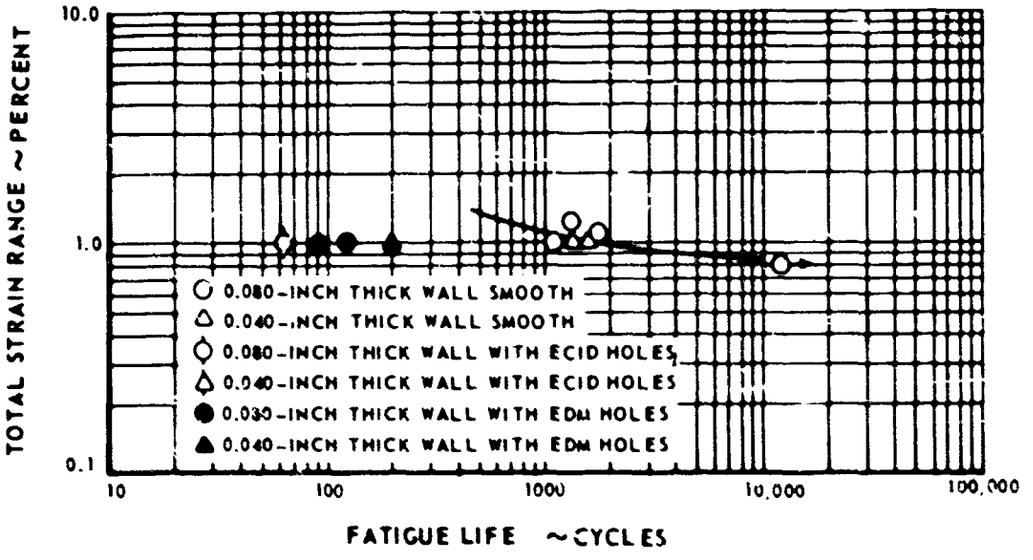

Figure 25 Axial Push-Pull Low-Cycle Fatigue Life of Wrought U-700 (PWA 689) Material at 1500°F

NOFORN

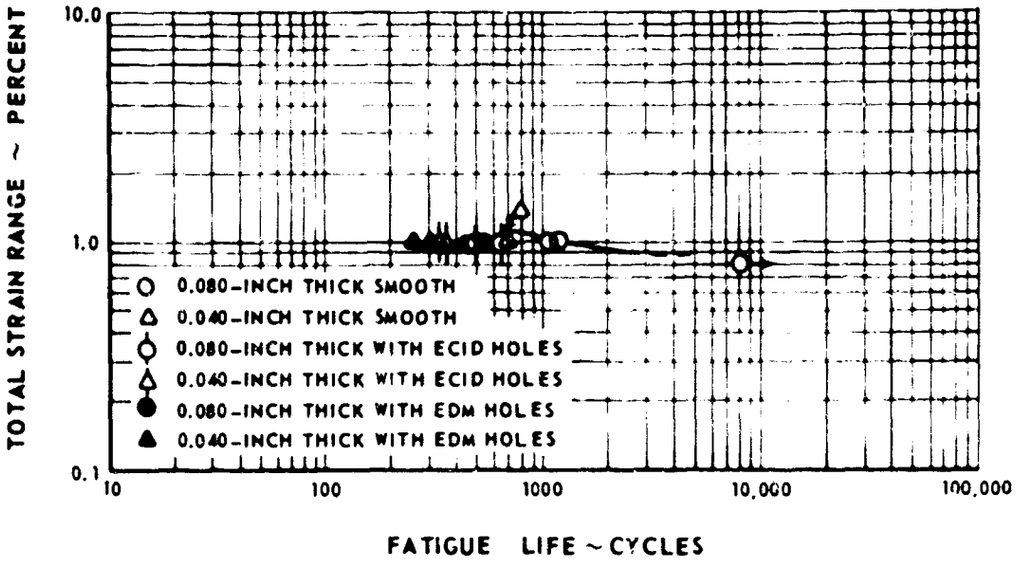

Figure 26 Strip Bending Low-Cycle Fatigue Life of Wrought U-700 (PWA 689) Material at 1500°F

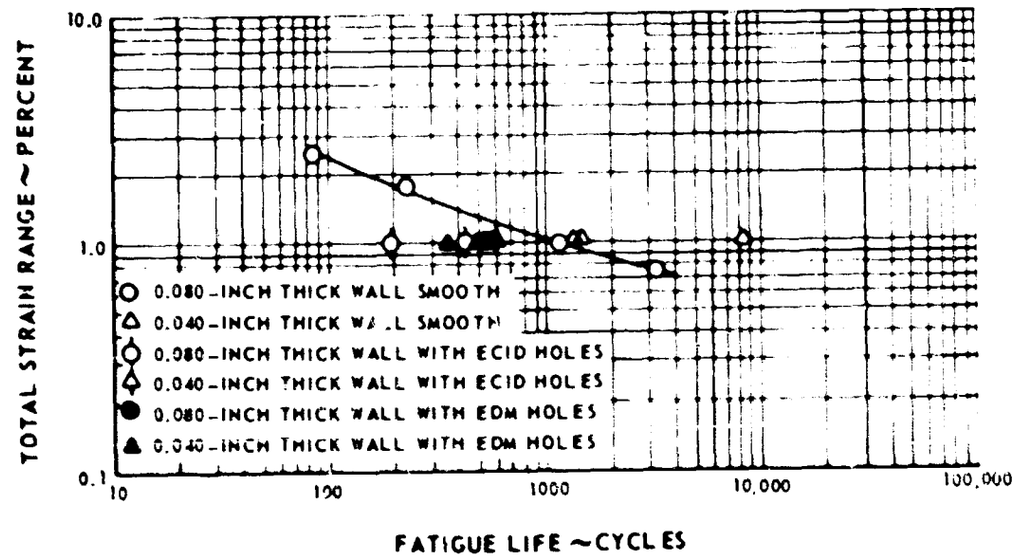

Figure 27 Axial Push-Pull Low-Cycle Fatigue Life of Directionally Solidified U-700 (PWA 1411) Material at 1500°F

NOFORN

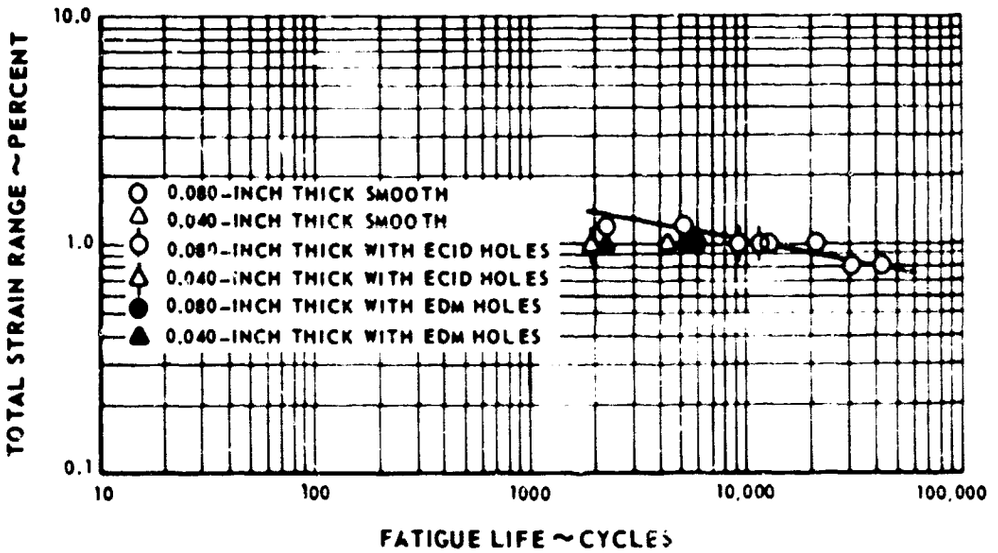

Figure 28 Strip Bending Low-Cycle Fatigue Life of Directionally Solidified U-700 (PWA 1411) Material at 1500°F

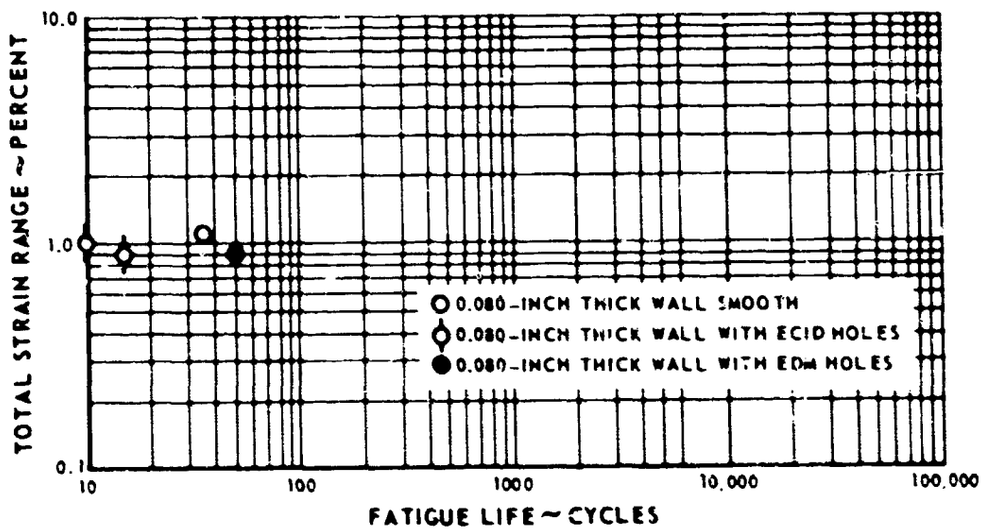

Figure 29 Axial Push-Pull Low-Cycle Fatigue Life of Cast Mar-M-509 (PWA 647) Material at 1500°F

NOFORN

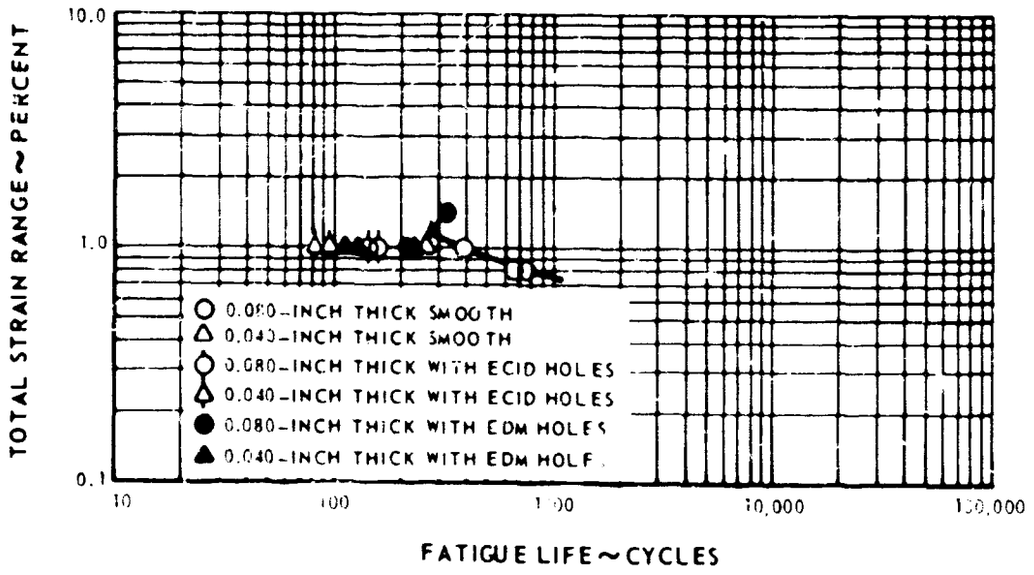

Figure 30 Strip Bending Low-Cycle Fatigue Life of Cast Mar-M-509 (PWA 657) Material at 1500°F

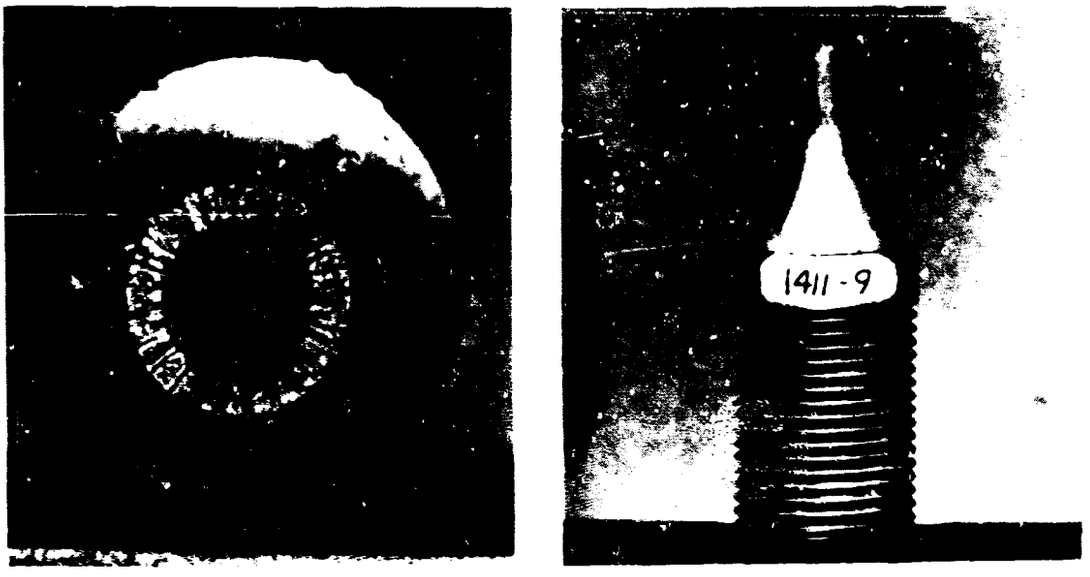

Figure 31 Directionally Solidified U-700 80-Mil Thick Push-Pull Fatigue Specimen with EDM Holes After 673 Cycles at 1 Percent Total Strain at 1500°F H-6932 H-6934

NOFORN

SECTION IV

ABRADABLE MATERIAL DEVELOPMENT

A. INTRODUCTION

(U) The objective of the abradable material development program was to select materials with good abradability for use in medium and high temperature environments.

(U) The program was conducted in several phases. Initially, a large number of materials were selected for study on the basis of literature surveys, experience, and assumed requirements for abradability. The second phase involved fabrication of the materials and bonding them to various materials. Subsequently, the resulting specimens were subjected to three types of tests. Static oxidation and aging tests were performed to determine the maximum service temperature in air for these specimens. Hot gas erosion tests were performed to determine the resistance of the materials to jet burner combustion gases or hot air at Mach 1.0 and Mach 0.8, respectively. Finally, dynamic abrasion tests were performed to evaluate the behavior of the candidate materials to abrasion from a spinning disk-and-blade assembly.

B. MATERIAL SELECTION

(U) At the start of the program, the characteristics of a material which enhance its abradability were not precisely known. It was assumed that relatively soft materials with low density would exhibit better abradability than tough materials with high density. It was also necessary, however, to select materials which would withstand the severe oxidation and erosion environment present in high-temperature environments. Literature surveys showed that, in general, nonmetallic materials would provide adequate life when used at temperatures up to 700°F. The more promising nonmetallic materials included silicone rubber, silicone foam rubber, Epoxy plastic, and inorganic binder materials. It was expected that the abradability of these base materials could be improved by the addition of filler materials such as chopped Fiberglas, hollow glass spheres, asbestos flakes, graphite, mica, and woven Fiberglas. Further literature search suggested that porous and fibrous high-temperature alloys as well as inorganic mica, graphite, and aluminum mixtures might be suitable for use in the intermediate range between 700°F and 1200°F.

(U) In a high-temperature environments it was assumed that abradability characteristics would have to be compromised somewhat to obtain a material with adequate resistance to high-temperature gas corrosion and erosion. Con-

sequently, high-temperature, high-strength nickel base alloys such as Hastelloy X and Incoloy 800 as well as type 410 stainless steel were chosen for evaluation. To enhance their abradability, these materials consisted of either a commercially produced hexagonal honeycomb structure or a drilled honeycomb structure. In addition, two feltmetals were tested. The complete list of the materials and material combinations selected for study is presented in Table III.

C. FABRICATION

(U) The fabrication of nonmetallic specimens involved the initial combining of the binder and the filler materials followed by specimen forming and curing. In some cases, specimens were formed by applying the mixed binder and filler directly to 0.045-inch thick backing plates. To promote bonding between the material and the backing plate, the plate was grit-blasted to provide a rough surface, and, when required, brushed with an adhesive sealant or bonding agent. In other cases, the material was formed into sheets without backing for subsequent fabrication into aging and erosion specimens. Following forming, the specimens were cured at room temperature or at a slightly elevated temperature to allow the material to harden. They were then cured at elevated temperatures to drive off excess volatile agents. Details of the fabrication process are shown in Table IV.

(U) Drilled metallic honeycomb material was fabricated from Hastelloy X, type 410 stainless steel, or Incoloy 800 materials by close-spaced drilling in 0.125- and 0.187-inch thick sheets. By varying the drill diameter, web thicknesses of 5, 8, and 20 mils were obtained. The holes were not drilled all the way through the material so that the equivalent of a solid backing plate remained. After drilling, the material was machined and formed to the dimensions of the backing plates, thereby eliminating the necessity of bonding the material to a separate plate. Details of the fabrication of metallic specimens are shown in Table V.

(U) It was necessary to bond the commercially obtained honeycomb materials to a backing plate, and this was performed with high-temperature braze alloy J8600 (Ni-33Cr-4Si-25Pd) at 2150°F in a hydrogen atmosphere.

(U) Difficulty was encountered in brazing the feltmetals to the backing strips because the feltmetal absorved the molten braze material. This resulted in inadequate braze coverage at the joint, and also drastically reduced the abradability of the feltmetal. In an attempt to eliminate the flow of braze material into the feltmetal (wicking), a 1-mil thick coating of nickel-aluminide coating was plasma sprayed onto the feltmetal prior to brazing. However, as shown in Figure 32, considerable wicking still occurred. Thicker coatings were applied and considerable reduction of braze penetration resulted, although some wicking still occurred. Finally, it was found that wicking could be essentially eliminated by

(U) TABLE III

MATERIALS STUDIED FOR ABRADABLE SEAL APPLICATIONS

Material Designation	
DC-325	Dow Corning white silicone ablative material
DC-93-004	Dow Corning aerospace sealant material
Chopped Fiberglas plus RTV Silicone Rubber	
Eccospheres plus DEN 438	Hollow silica microspheres in Dow Epoxy Novolac 438 resin
Molykote Z plus DEN 438	Molybdenum disulphide powder in DEN 438
Fiberglas plus DEN 438	Tricon number 101 weave Fiberglas in DEN 438
Fiberglas plus Polyimide	Alternate layers of number 108 and number 181 Fiberglas weaves in Polyimide binder
Fiberglas plus PBI	Fiberglas fabric impregnated with Polybenimidazole
SermeTel (PWA-7-3)	Mica, graphite, and aluminum added to SermeTel binder
Hastelloy X Feltmetal	
Haynes 25 Feltmetal	
Hastelloy X Drilled Honeycomb with 8-Mil Web	
Hastelloy X Commercial Honeycomb with 5-Mil Web	
Hastelloy X Commercial Honeycomb with 8-Mil Web	
Hastelloy X Commercial Honeycomb with 10-Mil Web	
410 Stainless Steel Drilled Honeycomb with 5-Mil Web	
410 Stainless Steel Drilled Honeycomb with 20-Mil Web	
Incoloy 800 Drilled Honeycomb with 20-MIL Web	
GE-757	RTV silicone rubber foam
GE Nichrome Foametal	

NOFORN

(U) TABLE IV

FABRICATION PROCEDURES FOR NONMETALLIC ABRADABLE SEAL MATERIALS

Material	Composition (Weight Percent)	Layup Procedure	Post-Lay Up Cure
DC-325	Vendor proprietary	Hand troweled and room-temperature vulcanized	4 hours at 250°F
DC-93-004	Vendor proprietary	Hand troweled and room-temperature vulcanized	24 hours at 400°F
Chopped Fiberglas plus RTV Silicone Rubber	50% chopped 1/4 inch diameter Fiberglas with heat-cleaned finish. 50% RTV silicone rubber	Hand troweled and room-temperature vulcanized	No cure cycle
Eccospheres plus DEN 438	17% Eccospheres and 83% DEN 438	Hand troweled and heated to 350°F for 4 hours	No cure cycle
Molykote Z plus DEN 438	50% MoS_2, and 50% DEN 438	Hand troweled and heated to 350°F for 4 hours	No cure cycle
Fiberglas plus DEN 438	60% Fiberglas and 40% DEN 438 (1 Layer Fiberglas 0.103 inch thick).	NMA Curing Agent, BDMA Accelerator, 250°F for 1.5 hours in "C" clamp-contained mold	4 hours at 400°F Finished material 0.065 inch thick after cure
Fiberglas plus Polyimide	45 to 50% Fiberglas and 50 to 55% Polyimide (Alternate layers of no. 108 and 181 Fiberglas weave)	Layup in mold 2 to 3 hours at 400°F then 5 to 15 minutes at 600°F. Compression laminated 1 to 5 minutes at 500 psi and 750 to 800°F	2 hours at 250°F, heated to 400°F over 2 hours and held at 400°F for 12 hours for 250 to 500°F test range. For higher test temperatures, place in cold oven and raise to temperature in 2 hours.
SermeTel (PWA 7-3)	100 ML SermeTel 2228 plus 20 gms Mica plus 15 gms Graphite plus 80 gms Aluminum	Hand troweled and air dried 12 hours or more prior to curing	Place in preheated oven and increase heat in increments: 2 hours at 140°F, 1 hour at 175°F, 1 hour at 200°F, 1 hour at 360°F, 1 hour at 615°F.
Fiberglas plus PBI	Narmco - Imidite 1850 Pre-Preg.	Layup in mold and compression laminated at 700°F for 3 hours. No adhesive used to bond material to back plate for rub strips	Oven purged to nitrogen atmosphere at room temperature for 1/2 hour, 600°F for 1 hour; 650°F for 1 hour; 700°F for 1 hour; 750°F for 1 hour; 800°F for 8 hours. Cooled to below 400°F in nitrogen before removal.
GE-757	Vendor proprietary	Hand troweled and room-temperature vulcanized	1 hour at 250°F

NOFORN

(U) TABLE V

FABRICATION PROCEDURES FOR METALLIC ABRADABLE SEAL SPECIMENS

Seal Material	As Received Condition	Fabrication Method	Material Preparation	Fabrication Procedure
Hastelloy X Feltmetal and Haynes 25 Feltmetal	30% density 0.060-inch thick metal fiber sheet	Brazing to backup strip	Seal material: Plasma spray coated with 0.005 inch thick Nickel-Aluminide coat, then Electroplated with 0.002-inch thick nickel plating over spray coat. Machined to 9-inch radius backing strip: Hastelloy X 1 1/2 x 6 x 0.045 inch 9 inch radius. Polish with 400-grit Silicon carbide paper.	Wash braze surfaces of seal material and backing strip with alcohol. Apply 0.005 inch-thich 82 Au-18Ni. Braze alloy slurry to seal material braze surface and clamp to backing strip in brazing fixture. Braze operation performed in Hydrogen atmosphere of Hayes Hamp Furnace at 1850°F for fixed cycle of furnace (about 15 minutes).
Hastelloy X Commercial Honeycomb	Honeycomb structure 0.125-inch cell size 0.110-inch height 0.005-inch, 0.008-inch, and 0.010-inch respective foil thicknesses.	Brazing to backup strip	All braze surfaces polished with 400-grit Silicon-Carbide paper. Backing strip is Hastelloy X Alloy 1 1/2 x 6 x 0.045-inch with 9-inch radius.	Wash braze surfaces of seal material and backing strip with alcohol. Apply 0.005-inch thick J-8690 braze alloy slurry to backing strip braze surface. Clamp seal material to backing strip in braze fixture. Braze in hydrogen atmosphere for 15 minutes at 2150°F J-8690 composition is Ni-33Cr-4Si-25Pd.
Hastelloy X, 410 Stainless Steel, and Incoloy 800 Drilled Honeycomb	Hastelloy X and 410 Stainless Steel Alloys: 0.187-inch thick; Incoloy 800: 0.125 inch thick	Drilling and machining	Material cut to rub strip dimensions per print.	Flanging and machining operations performed prior to drilling. Drilling operation performed with tape-controlled drilling machine using various drill sizes to produce required minimum web dimensions of 5, 8, and 20 mils. Strip then formed to 9-inch radius.

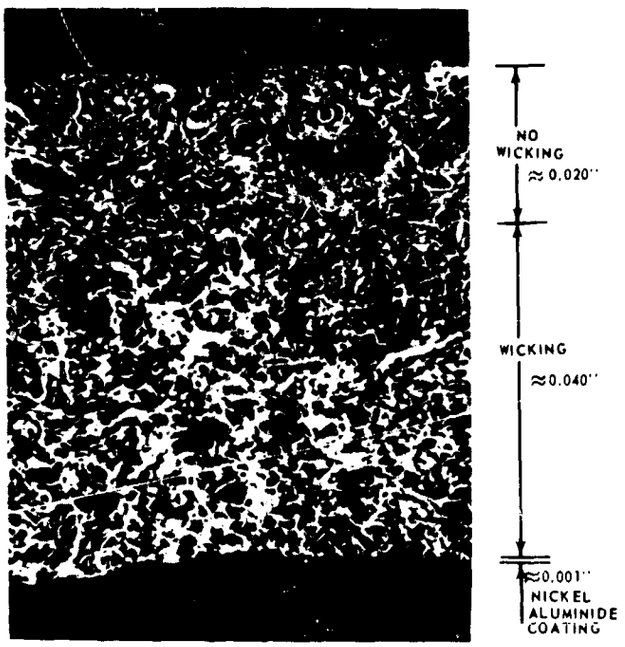

Figure 32 Photomicrograph of Feltmetal With 1-Mil Thick Plasma-Sprayed Coating of Nickel Aluminide Showing Extent of Wicking

applying a 5-mil thick plasma-sprayed coating of nickel aluminide and a 2-mil thick plated nickel coating (see Figure 33).

(U) The bond strengths obtained between the nonmetallic and metallic materials and the backing plates were initially evaluated by bend testing. A typical bend specimen is shown in Figure 34 after testing. Final evaluation of the bond strengths were made during the static oxidation and aging tests and during the dynamic abrasion tests. Bonds were considered to be satisfactory only when all failures of the material occurred outside of the interface between the specimen and the backing plate.

(U) In general, nonmetallic bonds failed because of loss of adhesion between the specimen and the backing plate as a result of thermal degradation of the bond during aging or because of insufficient strength to withstand blade impact during dynamic abrasion testing. Brazed bonds failed only in the feltmetal specimens and then only during dynamic abrasion testing. These failures were attributed to insufficient braze coverage during fabrication.

Figure 33 Photomicrographs of Feltmetal With 5-Mil Thick Plasma-Sprayed Coating of Nickel Aluminide With Nickel Plating Applied to Eliminate Wicking

NOFORN

Figure 34 Typical Specimen After Bending to Evaluate Bond Strength Between Abradable Material and Backing Plate XP-78405

D. TEST PROGRAM

1. Static Oxidation and Aging Tests

(U) Static oxidation tests were conducted for the metallic materials. These tests involved heating the specimens in electric resistance furnaces for 200 hours with thermal cycling to room temperature every four hours. The tests were performed to determine the maximum operating temperatures for each material for application in the range from 1000°F to 1900°F. Following testing, the specimens were examined for evidence of warpage, oxide sealing, and cracking. In addition, selected specimens were weighed to determine the gain in weight as a result of oxidation, and they were subjected to tensile and bend testing when the materials were suitable for such testing. All of the specimens were examined metallographically to determine the extent of oxide penetration. The temperature and duration of the static oxidation tests performed for each of the metallic materials are listed in Table VI.

(U) Examination of the Hastelloy X and Haynes 25 feltmetals following static oxidation revealed increasing oxide penetration with time and temperature, as shown in Figures 35 through 38. The change in weight associated with the oxide penetration is shown in Figures 39 and 40 for the two materials. In

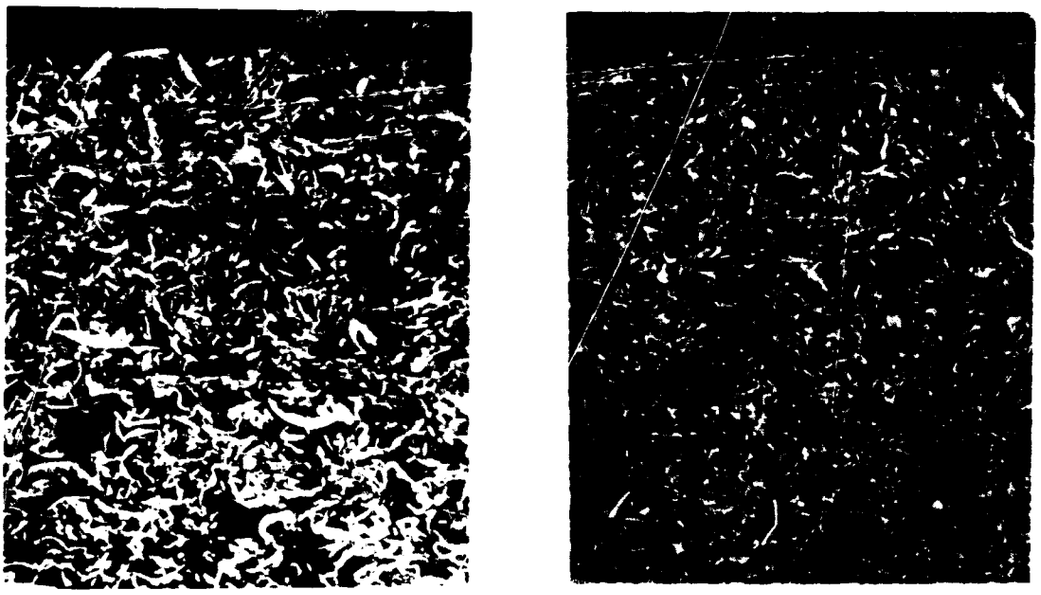

MAG: 50X

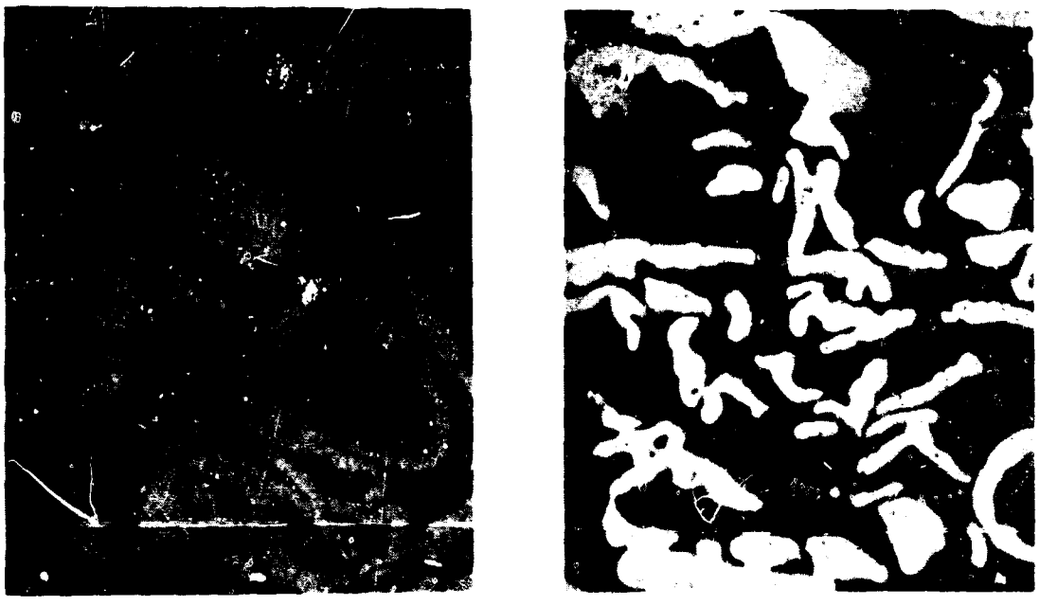

MAG: 500X

HASTELLOY X - 208.75 HOURS

HAYNES 25 - 198.00 HOURS

Figure 35 Photomicrographs of Hastelloy X and Haynes 25 Feltmetals After Static Oxidation Testing at 1000°F

NOFORN

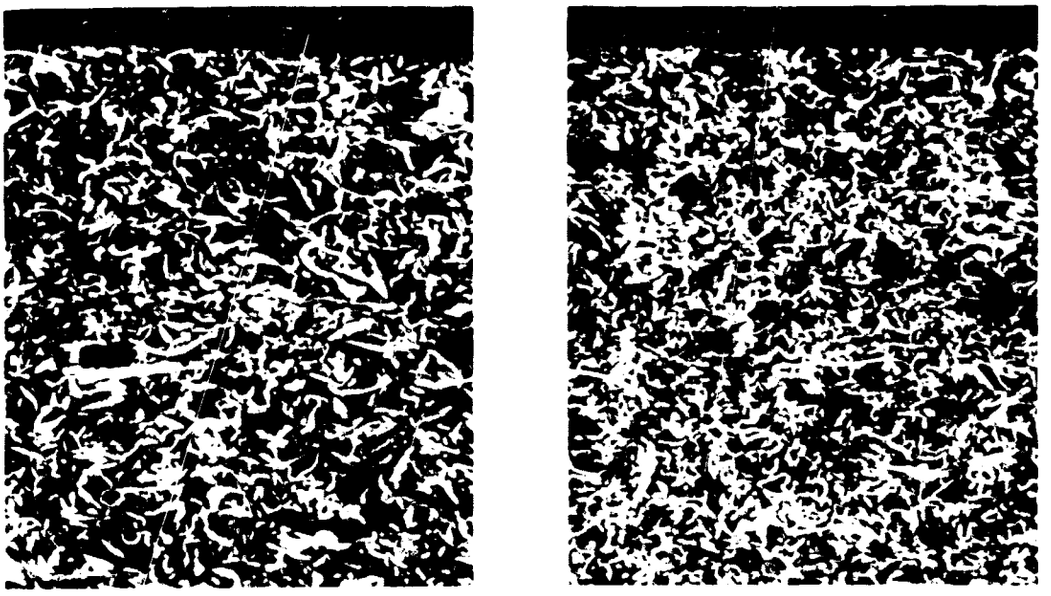

MAG: 50X

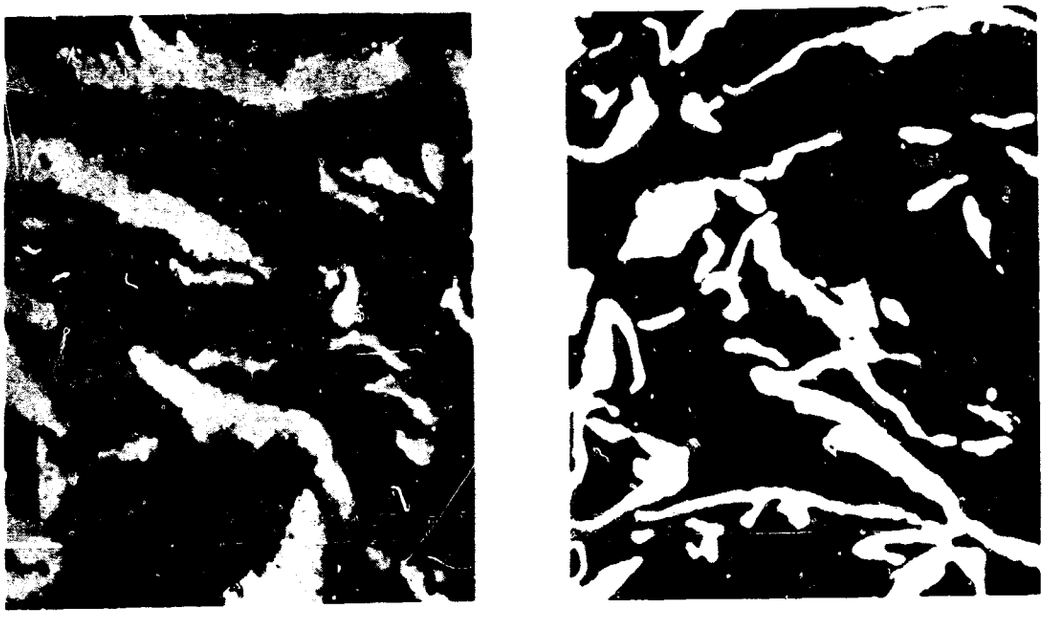

MAG: 500X

HASTELLOY X - 214.50 HOURS

HAYNES 25 - 200.00 HOURS

Figure 36 Photomicrographs of Hastelloy X and Haynes 25 Feltmetals After Static Oxidation Testing at 1200 F

NOFORN

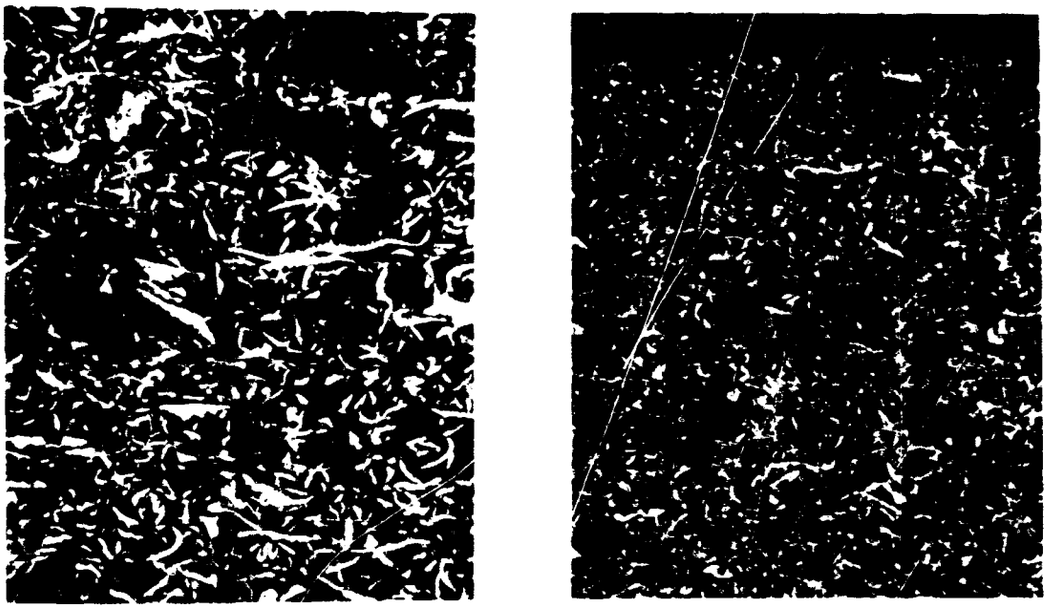

MAG: 50X

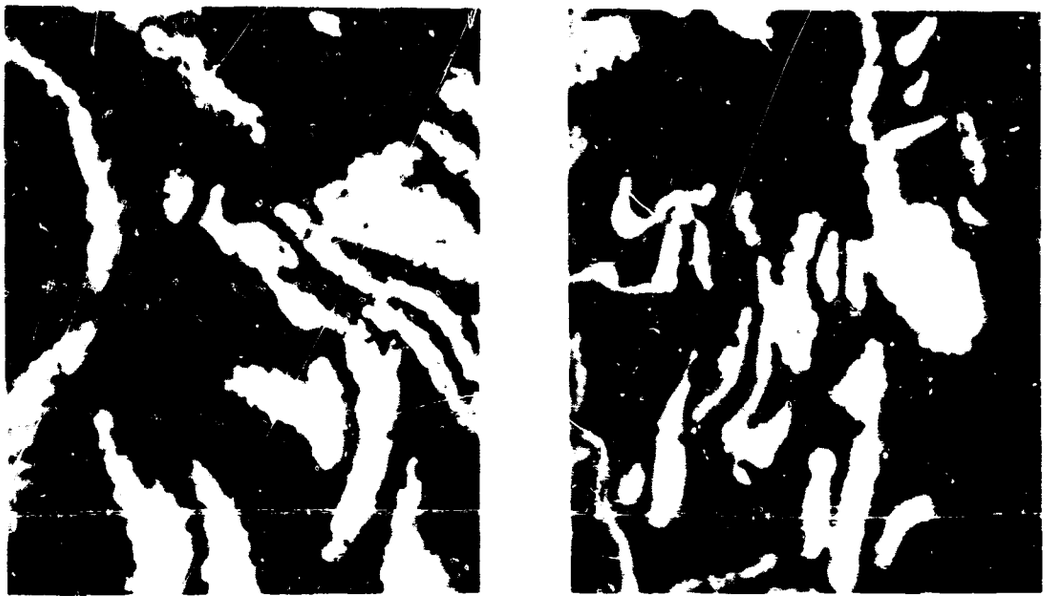

MAG: [illegible]

HASTELLOY X - [illegible] HOURS

HAYNES 25 - [illegible] HOURS

Figure 37 Photomicrographs of Hastelloy X and Haynes 25 Feltmetals After Static Oxidation Testing at 1400°F

NOFORN

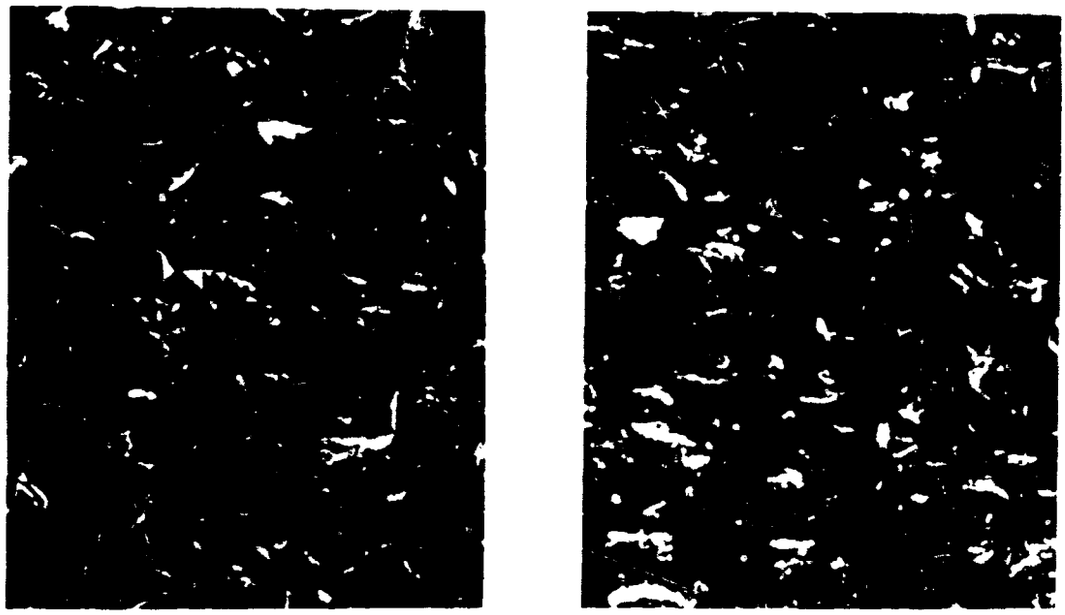

MAG: 50X

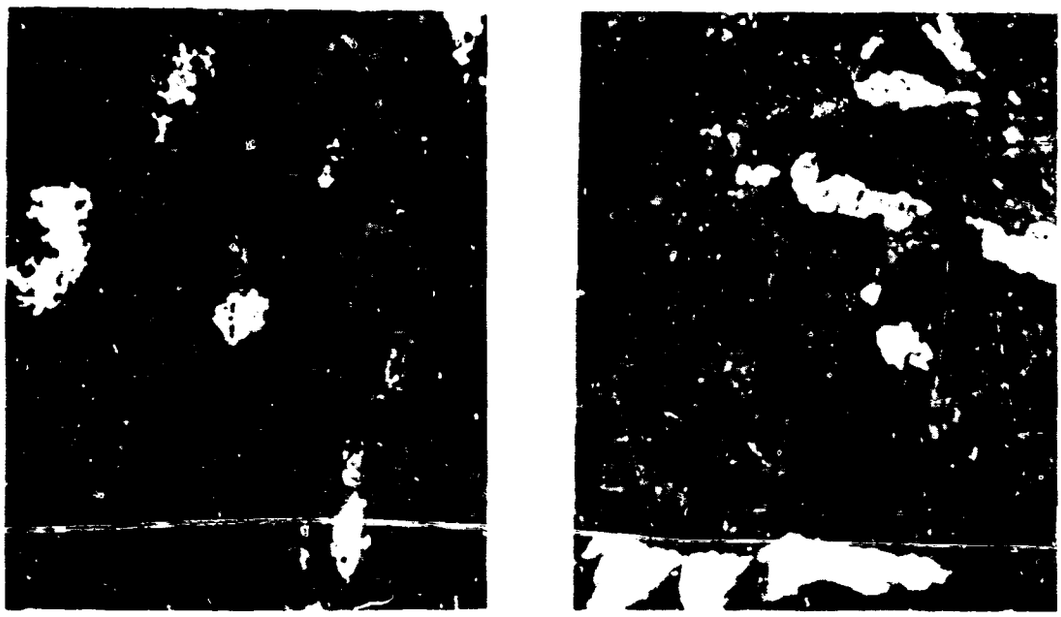

HASTELLOY X – [illegible] HOURS MAG: [illegible] HAYNES 25 – [illegible] HOURS

Figure 35 Photomicrographs of HastelHoy X and Haynes 25 Feltmetals After Static Oxidation Testing at 1600°F

NOFORN

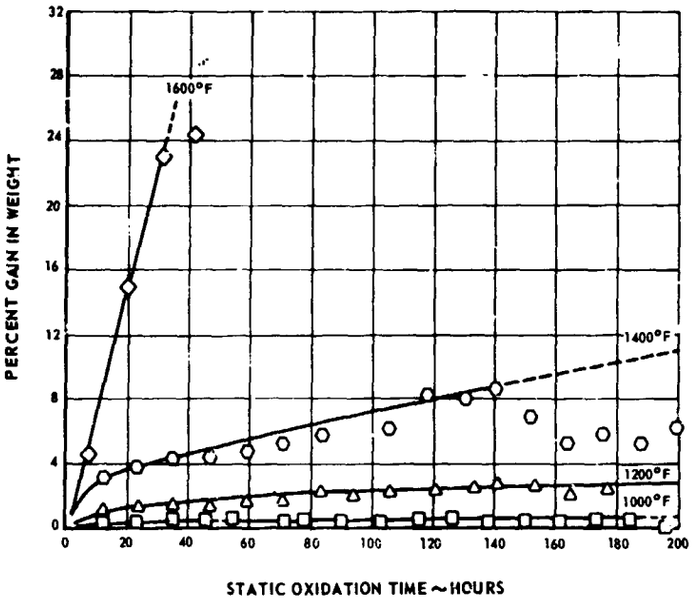

Figure 39 Percent Increase in Weight of Hastelloy X Feltmetal During Static Oxidation Testing

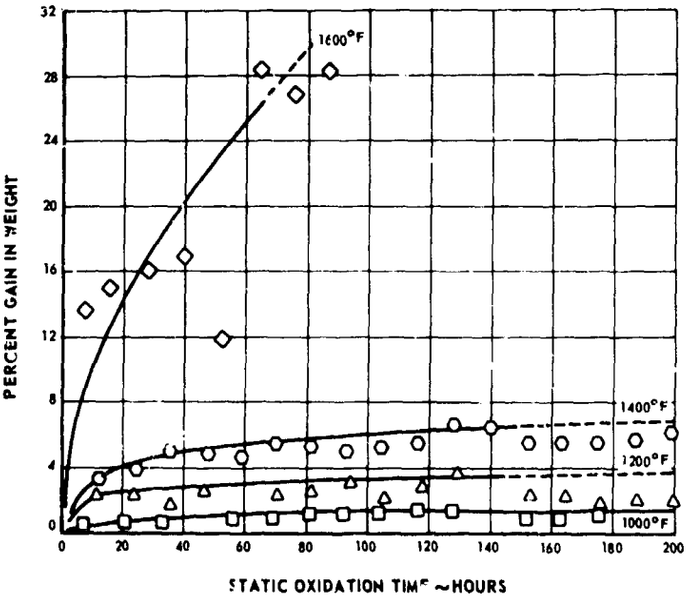

Figure 40 Percent Increase in Weight of Haynes 25 Feltmetal During Static Oxidation Testing

NOFORN

(U) TABLE VI

STATIC OXIDATION TESTS PERFORMED ON
METALLIC ABRADABLE SEAL SPECIMENS

	Oxidation Time (Hours) — Oxidation Temperature				
	1800°F	1600°F	1400°F	1200°F	1000°F
Hastelloy X Feltmetal	0	200	200	200	200
Haynes 25 Feltmetal	0	200	200	200	200
Hastelloy X Drilled Honeycomb with 8-Mil Web	200	200	200	0	0
Hastelloy X Commercial Honeycomb with 5-Mil Web	200	200	200	0	0
Hastelloy X Commercial Honeycomb with 8-Mil Web	200	200	200	0	0
Hastelloy X Commercial Honeycomb with 10-Mil Web	200	200	200	0	0
410 Stainless Steel Drilled Honeycomb with 5-Mil Web	0	200	200	0	0
410 Stainless Steel Drilled Honeycomb with 20-Mil Web	0	200	200	0	0
Incoloy 800 Drilled Honeycomb with 20-Mil Web	200	200	200	0	0

evaluating the data presented in these curves, it should be noted that the weight of the specimens after testing is a function of two factors, namely, the increase in weight as a result of oxidation, and the loss in weight resulting from separation of the oxide coating from the specimen. Consequently, the curves have generally been drawn through the maximum weight points, since, if no oxide separation occurred, the specimen weight would not decrease with time. Unfortunately, Figures 39 and 40 cannot be directly compared to determine the relative oxidation tendencies of the two materials. Although both materials were specified as having a density of 30 percent of the maximum theoretical density, the density of Hastelloy X material was actually 31.8 percent, and the density of the Haynes 25 material was actually 37.3 percent. Further, the fibers in the Haynes 25 material were considerably finer than those in the Hastelloy X material, resulting in more exposed surface area and a higher oxidation rate.

(U) The bend strength of the feltmetals after static oxidation testing was determined by bend testing. As shown in Figures 41 and 42, the bend strength of Hastelloy X feltmetal increased with oxidation time at 1000°F but decreased with oxidation time at higher temperatures, whereas the bend strength of Haynes 25

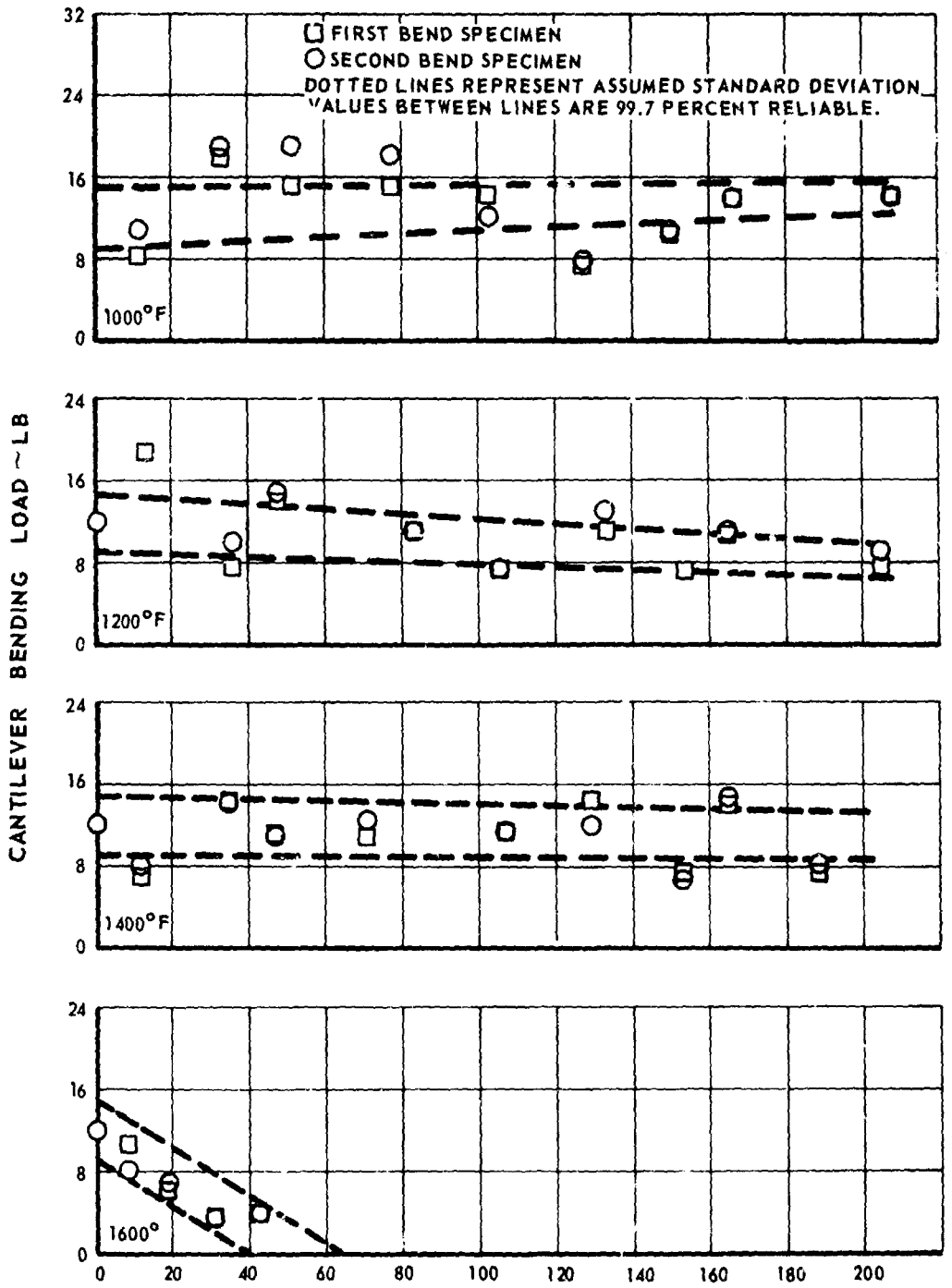

Figure 41 Effect of Oxidation Time and Temperature on Bend Strength of Hastelloy X Feltmetal

NOFORN

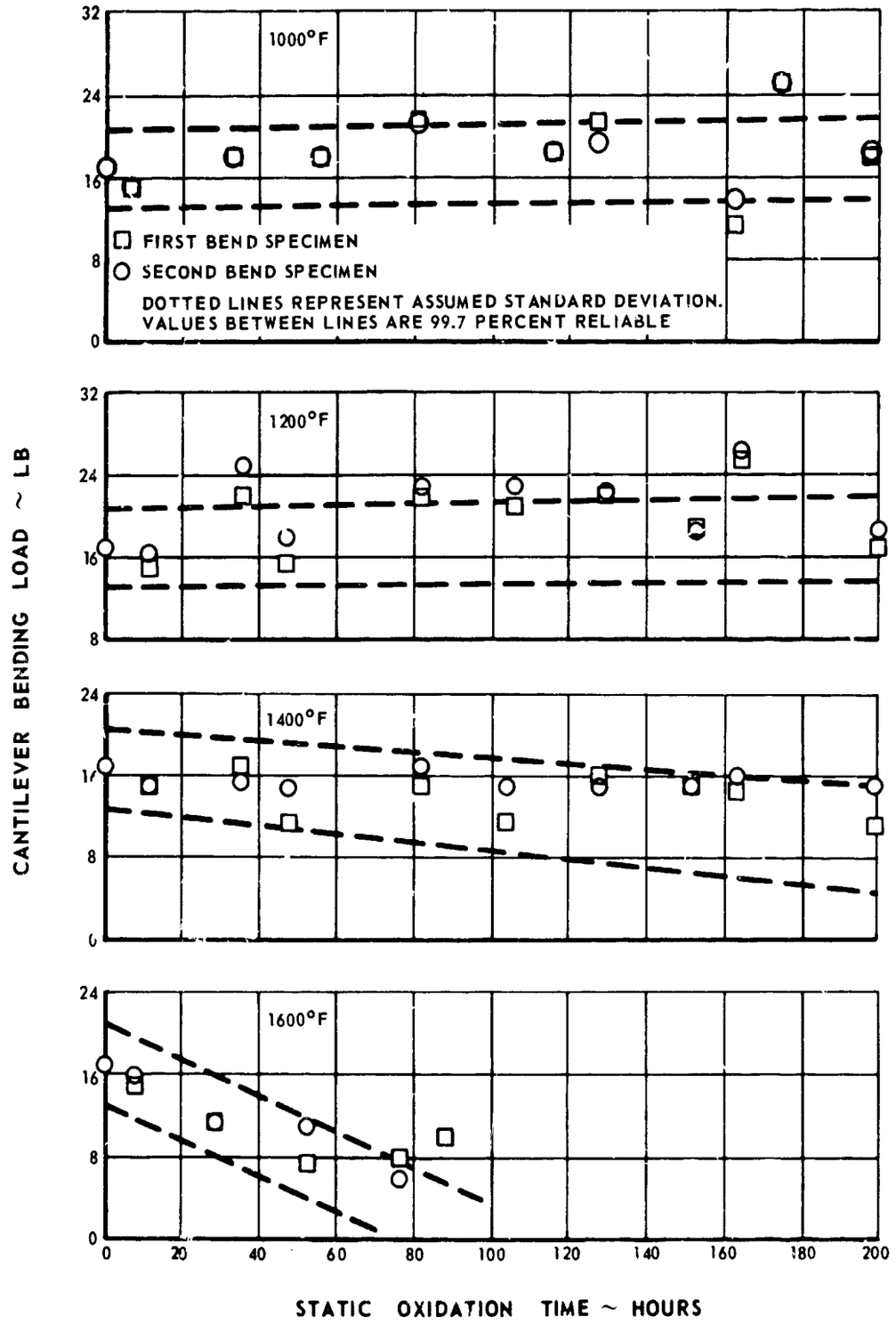

Figure 42 Effect of Oxidation Time and Temperature on Bend Strength of Haynes 25 Feltmetal

NOFORN

feltmetal increased with oxidation time at 1000°F and 1200°F, with a decrease occurring at higher temperatures. This behavior is attributed to the interaction of several mechanisms. The material strength is increased and the ductility is decreased by carbide and precipitation hardening and by the cementing effect of the oxide formation at the fiber intersections. Continued oxidation however, lowers the basic strength of the feltmetal fibers. Consequently, the strength of the material increases with oxidation time at the lower temperatures where the hardening effects predominate, and it decreases with oxidation time at the higher temperatures where the deterioration of the fiber strength from oxidation predominates. The extent to which this behavior influences the abradability of the feltmetals has not been determined, but, on the basis of the metallographic changes and the appearance of the specimens after static oxidation testing, it appears that both materials will provide a 200-hour life at 1200°F.

(U) The results of the static oxidation tests performed on the honeycomb materials are shown in Figures 43, 44, and 45. No significant difference was observed between the commercial and the drilled honeycombs when the same material was used. The behavior of the different materials differed significantly, however. After 200 hours at 1400°F, the Hastelloy X honeycomb showed negligible oxidation, whereas the Incoloy 800 material had surface oxidation penetration to a depth of about 0.25 mil, and the type 410 stainless steel had a loosely adhering oxide layer with penetration to a depth of about 0.5 mil. After 200 hours at 1600°F, minor oxide penetration was found in the Hastelloy X honeycomb, and a thin adhering oxide layer was found on the surface. A 0.1-mil thick oxide layer was found on the surface of the Incoloy 800 specimen with intergranular oxide penetration to a depth of about 0.5 mil. The stainless steel specimen was severely oxidized. After testing at 1800°F for 200 hours, the Hastelloy X specimen was oxidized and pitted on the surface to a depth of about 0.25 mil with about 1.0 mil of intergranular oxidation. The Incoloy 800 specimen was oxidized to a depth of about 3.0 mils. Because of the severe deterioration of the stainless steel specimen at 1600°F, stainless steel was not tested at 1800°F. It is apparent from these results that the Hastelloy X material is superior to the other materials with respect to oxidation resistance and that the Incoloy 800 material is superior to the stainless steel material.

(U) The nonmetallic materials were subjected to the aging tests shown in Table VII. Each material was tested initially at the maximum anticipated service temperature, and, normally, if satisfactory results were obtained, testing was not performed at lower temperatures. The test results obtained at the maximum qualifying temperatures for each material are shown in Table VIII. As shown, SermeTel material demonstrated an acceptable 200-hour life at 1200°F; Fiberglas plus Polyimide demonstrated a 200-hour life at 600°F; and the remaining nonmetallic materials demonstrated a 200-hour life at 400°F and 500°F. These results should be considered to be indicative of the capabilities of the binder material and independent of the particular filler material used.

NOFORN

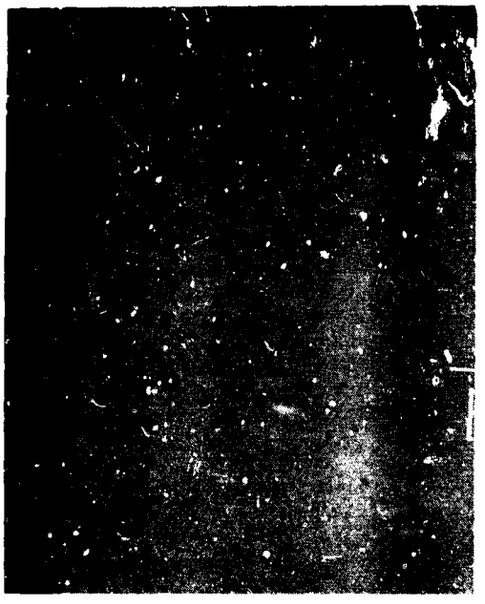

HASTELLOY X – DRILLED – 8-MIL WEB

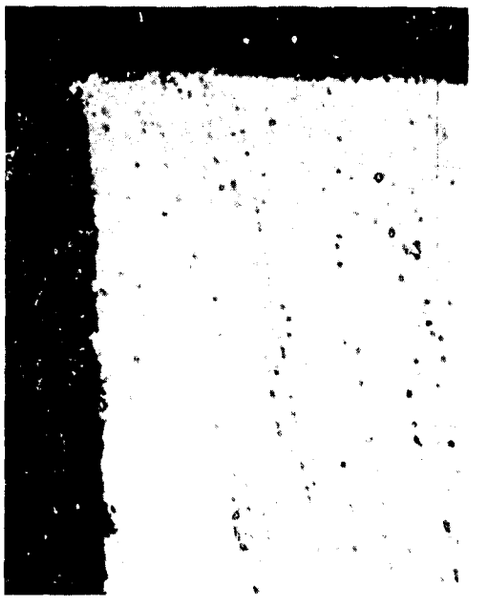

HASTELLOY X – COMMERCIAL – 5-MIL WEB

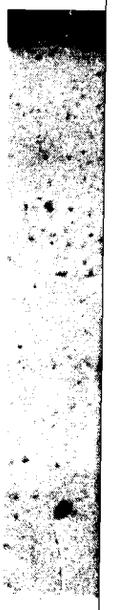

HASTEL

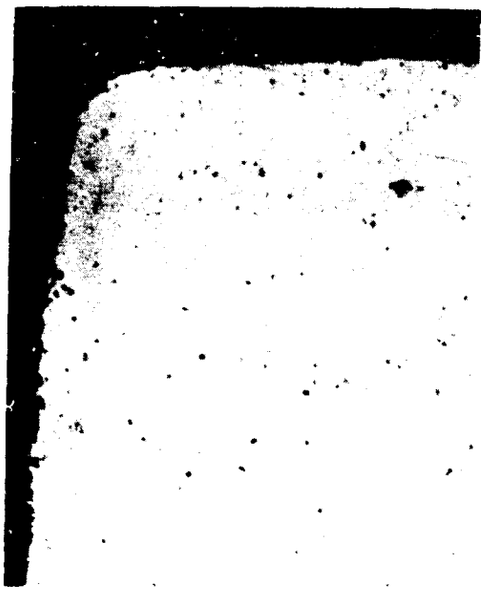

INCOLOY 800 – DRILLED – 20-MIL WEB

410 STAINLESS STEEL – DRILLED – 5-MIL

Figure 43 Photomicrographs of Honeycomb Materia
Testing at 1400°F for 200 Hours

NOFORN

UNCLASSIFIED

5-MIL WEB

HASTELLOY X - COMMERCIAL – 8-MIL WEB

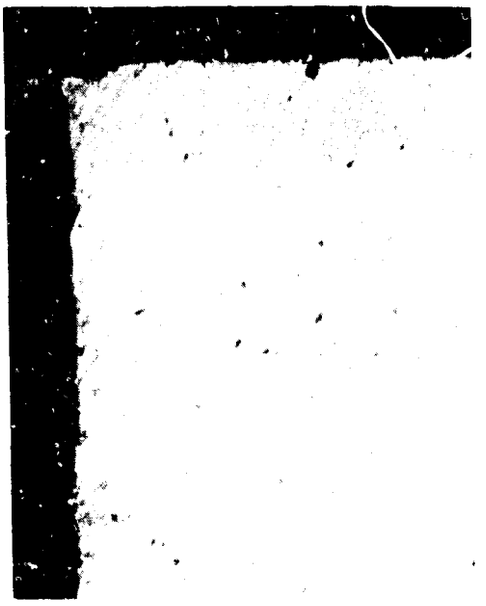

HASTELLOY X – COMMERCIAL – 10-MIL WEB

410 STAINLESS STEEL – DRILLED – 5-MIL WEB

410 STAINLESS STEEL – DRILLED – 20-MIL WEB

Mag: 500x

Micrographs of Honeycomb Materials After Static Oxidation at 1400°F for 200 Hours

2

HASTELLOY X – DRILLED – 8-MIL WEB

HASTELLOY X – COMMERCIAL – 5-MIL WEB

INCOLOY [illegible] DRILLED [illegible] MIL WEB

[illegible] STAINLESS STEEL [illegible] DRILL

Figure 11 Photomicrographs of Honeycomb Testing at 1600 F for 200 Hours

NOFORN

UNCLASSIFIED

1

B

HASTELLOY X - COMMERCIAL - 5-MIL WEB

HASTELLOY X - COMMERCIAL - 5-MIL WEB

NLESS STEEL - DRILLED - 5-MIL WEB

STAINLESS STEEL - DRILLED - 5-MIL WEB

Mag: 500X

phs of Honeycomb Materials After Static Oxidation
1 for 200 Hours

HASTELLOY X - DRILLED - 8-MIL WEB

HASTELLOY X - COMMERCIAL

HASTELLOY X - COMMERCIAL - 10-MIL WEB

Figure 3a. Photomicrographs of Honeycomb S
Testing at 1800°F for 200 Hours

NOFORN

UNCLASSIFIED

HASTELLOY X - COMMERCIAL – 5-MIL WEB

HASTELLOY X - COMMERCIAL – 8-MIL WEB

WEB

INCOLOY 800 – DRILLED – 20-MIL WEB

Mag: 500x

omicrographs of Honeycomb Materials After Static Oxidation
ng at 1800°F for 200 Hours

(U) TABLE VII

STATIC AGING TESTS PERFORMED ON NONMETALLIC ABRADABLE SEAL SPECIMENS

	Aging Time (hours)				
	Aging Temperature				
	1200°F	600°F	500°F	400°F	250°F
DC-325	0	0	200	200	200
DC-93-004	0	0	200	200	200
Chopped Fiberglass plus RTV Silicone Rubber	0	0	200	0	0
Eccospheres plus DEN 438	0	0	100	0	0
Molykote plus DEN 438	0	0	100	0	0
Fiberglas plus DEN 438	0	0	100	200	200
Fiberglas plus Polyimide	0	200	0	0	200
Fiberglas plus PBI	0	0	200	0	200
SermeTel (PWA 7-3)	200	0	0	0	0

(U) TABLE VIII

STATIC AGING TEST RESULTS FOR NONMETALLIC ABRADABLE SEAL SPECIMENS

Binder Material	Filler Material	Aging Temperature (°F)	Aging Time (Hours)	Remarks
DEN 438	Fiberglas	400	200	Accepted: binder appears dark and somewhat embrittled.
DEN 438*	Fiberglas	500	200	Failed: binder separated from filler. Severely charred and cracked.
DEN 438*	Molykote Z	500		Failed: material severely warped brittle and cracked.
DEN 438*	Eccospheres	500		Failed: material severely warped brittle and cracked.
DC-325	Proprietary	500		Accepted: material slightly hardened.
DC-93-004	Proprietary	500		Accepted: material slightly hardened.
RTV Silicon Rubber	Chopped Fiberglas	500		Accepted: material slightly hardened
PBI	Fiberglas	500		Accepted: negligible change.
PBI	Fiberglas	600	100	Failed: complete loss of binder
Polyimide	Fiberglas	600	200	Accepted: negligible change
SermeTel (PWA 7-3)	Mica, Graphite, Aluminum.	1200	200	Accepted: some surface hardening noted. Some spalling of material at sharp edge noted

*The 200-hour service temperature for these materials may be assumed to be 400°F on the basis of the first test results listed above.

NOFORN

(U) The results of the tensile tests performed during the program are shown in Figure 46. Both the Haynes 25 and the Hastelloy X feltmetals showed a marked decrease in tensile strength after static oxidation testing at 1200°F for 200 hours. The strength of the nonmetallic materials generally increased with aging at the lower temperatures, but decreased at higher temperatures. This behavior is attributed to additional curing of the binder material at the lower temperatures and to deterioration of the binder at higher temperatures. The filler material used affects the nominal strength of the material, but it does not appear to affect the rate of deterioration.

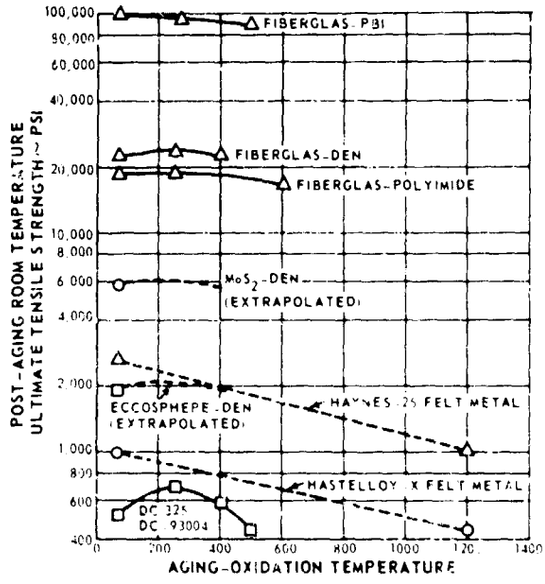

Figure 46 Room Temperature Tensile Strength of Abradable Materials After Aging for 200 Hours at Various Temperatures

2. Hot-Gas Erosion Tests

(U) The maximum temperature at which each material could be expected to demonstrate a 200-hour useful life was determined on the basis of the static oxidation and aging tests. To evaluate the materials further, each material was exposed to a high velocity gas stream for 100 hours at this temperature. Materials for use at medium temperatures were tested in the equipment shown in Figure 47, and the materials for high temperature use were tested in the equipment shown in Figures 48 and 49.

(U) All of the materials which are candidates for use in the medium temperature range demonstrated an ability to resist erosion from a Mach 0.8 gas stream

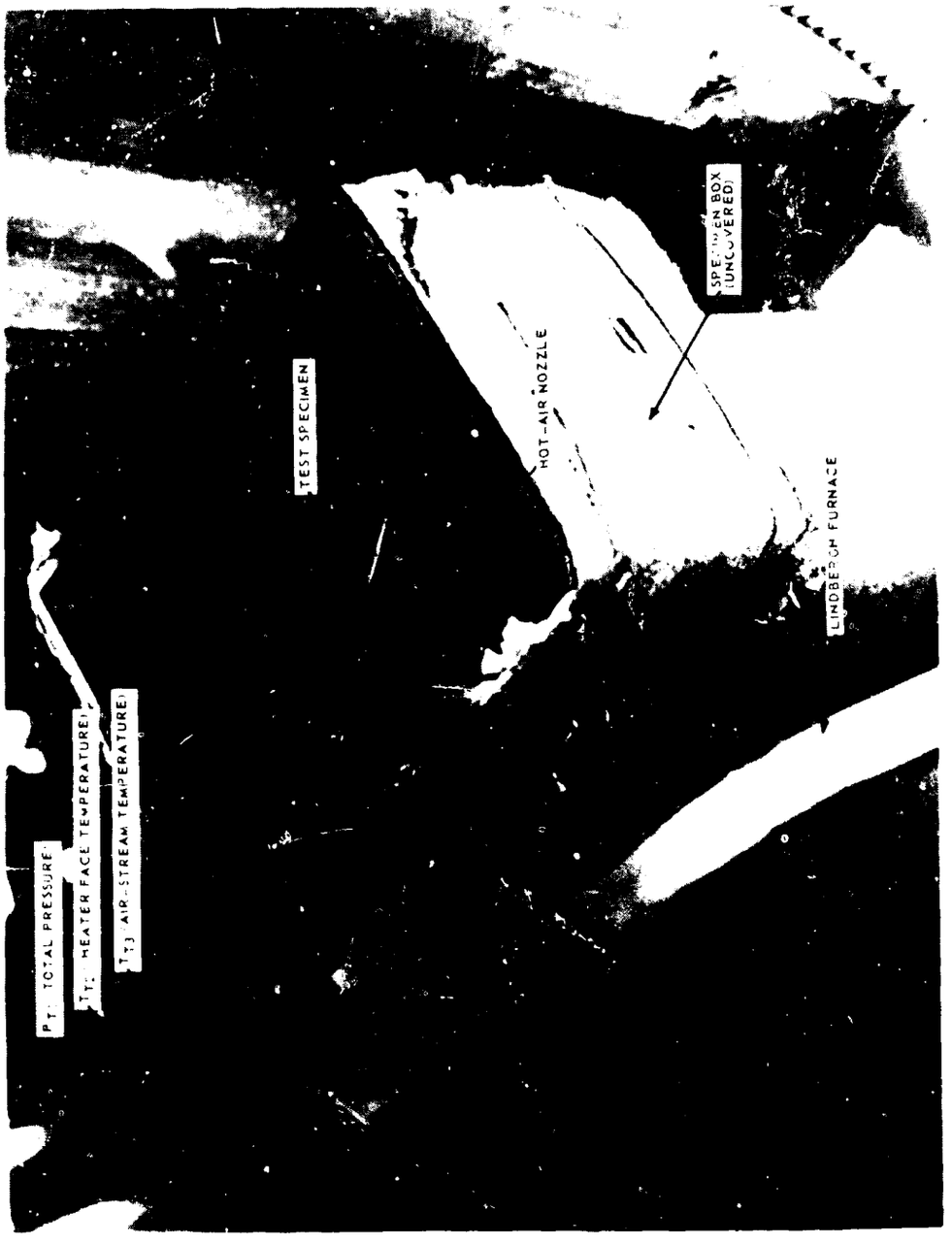

Figure 47 Hot Gas Erosion Test Equipment for Abradable Materials for Medium-Temperature Use X025057

NOFORN

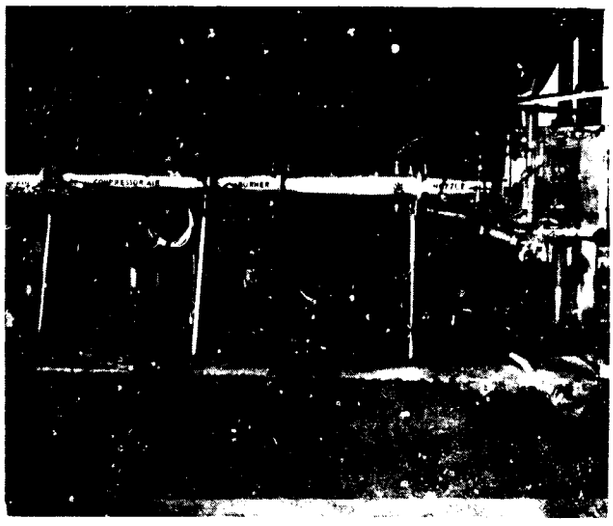

Figure 48 Hot Gas Erosion Test Equipment for Abradable Materials for High-Temperature Use X-23639

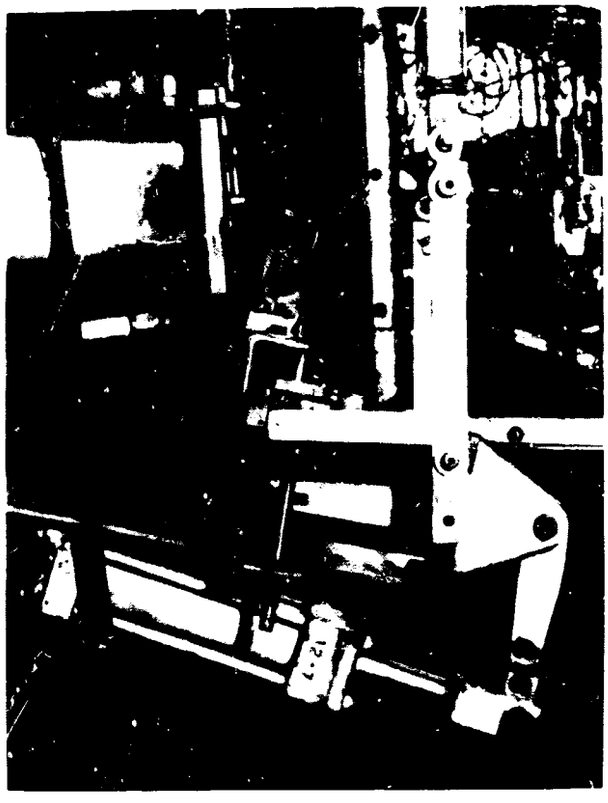

Figure 49 Closeup View of Hot Gas Erosion Test Equipment for Abradable Materials for High-Temperature Use

NOFORN

for 100 hours at the temperature determined on the basis of the static aging tests (see Table IX). As shown in Table IX, some of the tests were terminated before a complete 100 hours had been accumulated since the erosion properties are limited by the binder material used, and many of the materials had identical binders. When initial results were the same as those for a material which had already been tested and which had the same binder, it was assumed that the results for the remainder of the test would also be the same. The conditions of all of the specimens is shown in Figure 50.

(U) The materials which were candidates for use in the high temperature range were exposed to combustion exhaust products at Mach 1.0. The results of the tests on Hastelloy X honeycomb materials are shown in Figures 51 through 54. All of these specimens contained an adherent oxide coating approximately 0.5 mil thick after testing. Intergranular oxidation extended from 4.0 mils beneath the surface for the specimen tested at 1800°F for 100 hours to 2.0 mils for the specimen tested at 1600°F for 100 hours. The other Hastelloy X specimens were tested for shorter periods of time and, therefore, had proportionately less oxide penetration. It should be noted, however, that the surfaces exposed directly to the gas stream suffered somewhat from erosion. For example, the hot gas impingement area of the Hastelloy X drilled honeycomb specimen tested at 1800°F for 100 hours suffered a loss of approximately 25 percent of the web width as a result of erosion.

(U) The results of the test on Incoloy 800 specimens are shown in Figures 55, 56, and 57. After 47 hours of exposure to a Mach 1 gas stream at 1800°F, considerable erosion had occurred. The remaining oxide coating was 2 mils thick, and intergranular oxide penetration extended approximately 4 mils beneath the surface. One hundred hours of exposure to a Mach 1 gas stream at 1600°F resulted in essentially all of the oxide layer being eroded away with a reduction in web thickness of about 5 percent. Intergranular oxidation penetrated about 4 mils beneath the surface. Testing with a gas stream at 1400°F for 100 hours resulted in essentially the same conditions, as shown in Figure 57.

(U) Hot gas erosion results of the test on type 410 stainless steel are shown in Figure 58. Exposure for 100 hours to a Mach 1 gas stream at 1400°F resulted in significant oxide surface erosion which reduced the web thickness by about 10 percent.

(U) On the basis of the static oxidation and the hot-gas erosion tests, it appears that Hastelloy X drilled or commercial honeycomb would provide a 200-hour service life at 1800°F. The Incoloy 800 material would be marginal at 1600°F, although it would be satisfactory at 1400°F, as would the type 410 stainless steel. Neither the web thickness or the method by which the honeycomb was produced appeared to affect the service lives of these materials.

NOFORN

(U) TABLE IX

HOT-GAS EROSION TEST RESULTS FOR CANDIDATE MATERIALS FOR FAN AND COMPRESSOR SEALS

Material	Test Temperature (°F)	Time in Test (Hours)	Remarks
DC-325	500	100	Local hardening; negligible surface erosion.
DC-93-004	500	100	Local hardening; negligible surface erosion.
Chopped Fiberglas plus RTV Silicone Rubber	500	14	Test terminated after 14 hours; material showed results similar to DC-325 after 14 hours.
Eccospheres plus DEN 438	500	12	Severe charring; negligible erosion.
Molykote Z plus DEN 438	500	100	Minor surface cracking and blistering; moderate charring; negligible erosion.
Fiberglas plus DEN 438	400	100	Minor surface cracking; negligible erosion.
Fiberglas plus Polyimide	600	100	Negligible surface erosion.
Fiberglas plus PBI	600	100	Binder completely eroded from filler (Fiberglas).
SermeTel (PWA 7-3)	1200	100	Negligible surface erosion.
Hastelloy X Feltmetal	1200	100	Negligible surface erosion; negligible oxidation.
Haynes 25 Feltmetal	1200	100	Negligible surface erosion; negligible oxidation.

NOFORN

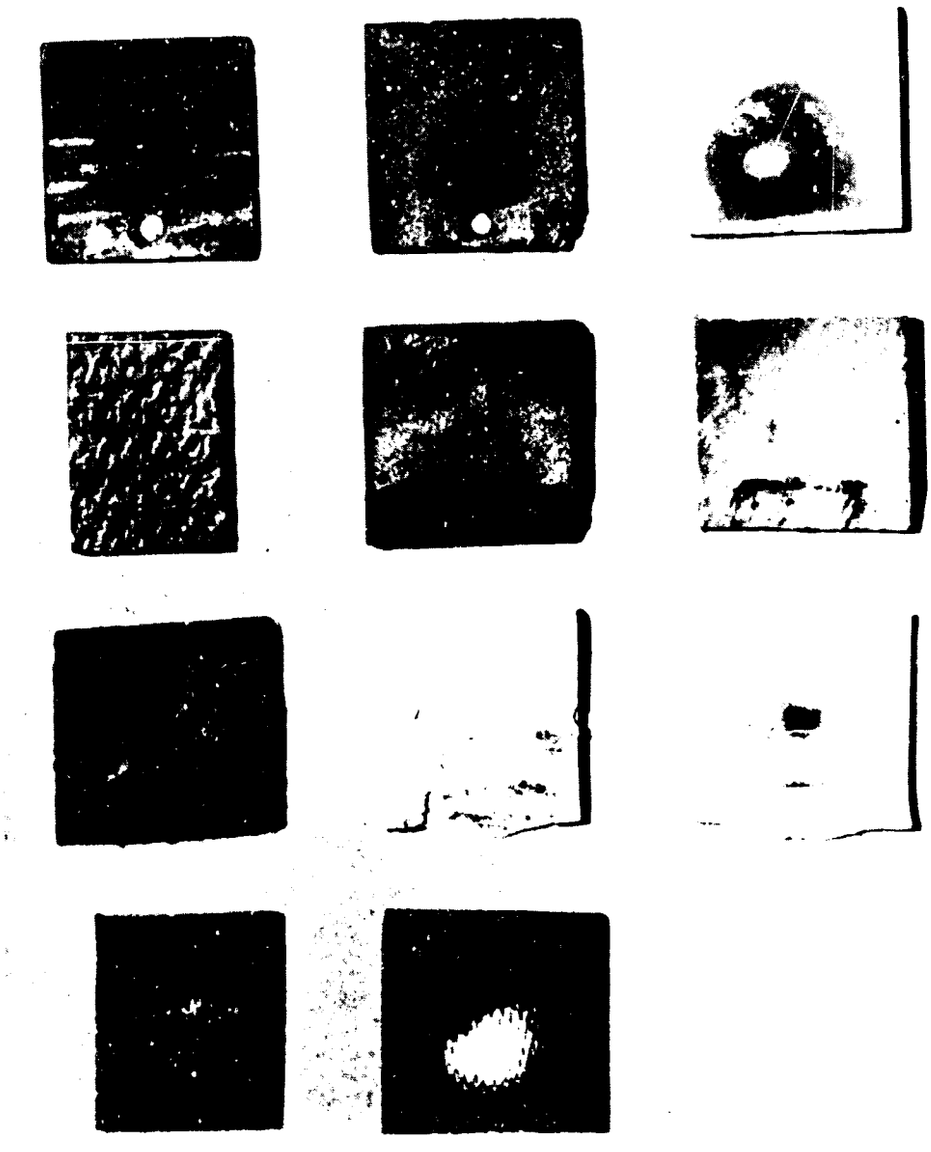

Figure 50 Hot Gas Erosion Specimens After Testing CN-5586

A. Haynes 25-Refmetal, 100 Hours at 1200°F
B. Hastelloy X-Refmetal, 100 Hours at 1200°F
C. Sermetel [illegible], 100 Hours at 1200°F
D. Fiberglas plus Epoxy Novolac, 100 Hours at 400°F
E. Eccospheres plus Epoxy Novolac, 12 Hours at 500°F
F. MoSi$_2$ plus Epoxy Novolac, 100 Hours at 500°F
G. Fiberglas plus RTV Silicone Rubber, 14 Hours at 500°F
H. [illegible], 100 Hours at 600°F
I. [illegible], 100 Hours at 600°F
J. Fiberglas plus Polyimide, 100 Hours at 600°F
K. Fiberglas plus PBI, 100 Hours at 600°F

All specimens tested in Mach 0.8 gas stream at 45-degree incidence angle.
Indentations caused by specimen clamp.

NOFORN

MAG: 100X

MAG:

Figure 51 Photomicrographs of Hastelloy X Drilled Honeycomb With .5-Mil Web After Exposure to Mach 1 Gas Stream at 1800 F for 100 Hours

NOFORN

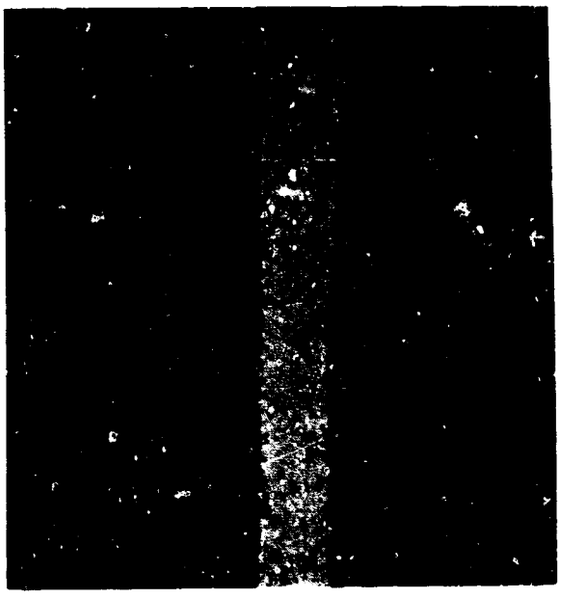

MAG: 100X

MAG: [illegible]

Figure 52 Photomicrographs of Hastelloy X Commercial Honeycomb With 5-Mil Web After Exposure to Mach 1 Gas Stream at 1500 F for 57 Hours

NOFORN

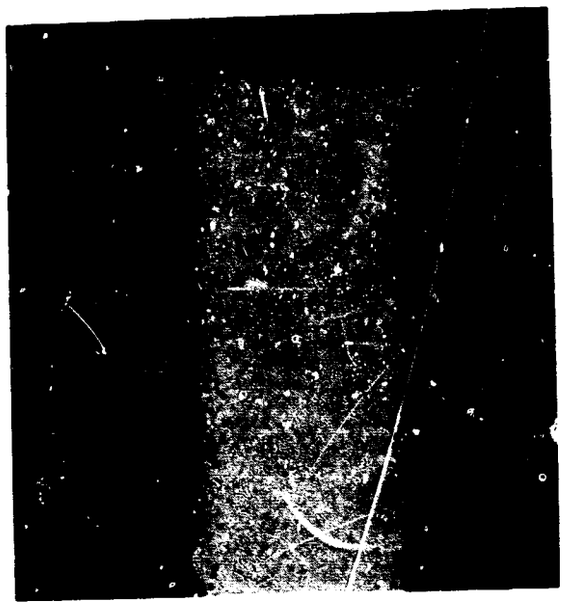

MAG: 100X

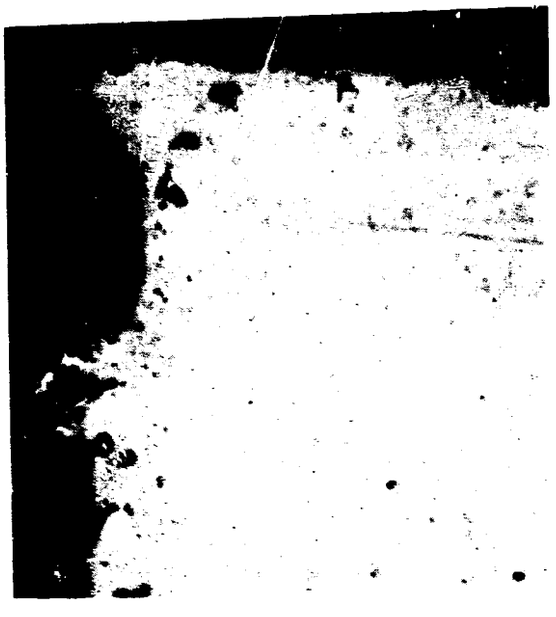

MAG: 50X

Figure 53 Photomicrographs of Hastelloy X Commercial Honeycomb With 10-Mil Web After Exposure to Mach 1 Gas Stream at 1800 F for 13 Hours

NOFORN

MAG: 75X

MAG. 500

Figure 34 Photomicrographs of Hastelloy X Commercial Honeycomb With 5-Mil Web After Exposure to Mach 1 Gas Stream at 1600°F for 100 Hours

NOFORN

MAG: 75X

MAG: 500X

Figure 55 Photomicrographs of Incoloy 800 Drilled Honeycomb With 20-Mil Web After Exposure to Mach 1 Gas Stream at 1800°F for 17 Hours

NOFORN

MAG: 75X

MAG: 500X

Figure 56 Photomicrographs of Incoloy 800 Drilled Honeycomb With 20-Mil Web After Exposure to Mach 1 Gas Stream at 1600 F for 100 Hours

NOFORN

MAG: 75X

MAG: 500X

Figure 57 Photomicrographs of Incoloy 800 Drilled Honeycomb With 20-Mil Web After Exposure to Mach 1 Gas Stream at 1400°F for 100 Hours

NOFORN

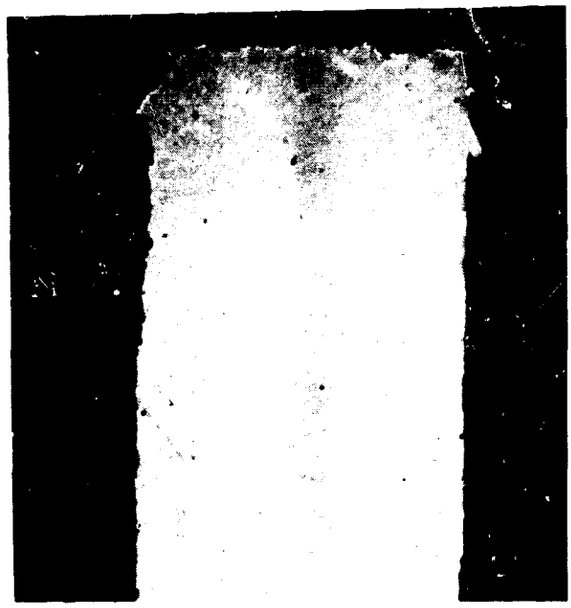

MAG. 75X

MAG. 500X

Figure 58 Photomicrographs of Type 410 Stainless Steel Drilled Honeycomb With 20-Mil Web After Exposure to Mach 1 Gas Stream at 1400°F for 100 Hours

NOFORN

3. Dynamic Abrasion Tests

(U) The dynamic abrasion tests simulated the actual mechanical and thermal conditions that the abradable specimens would be expected to sustain. The specimens were mounted on a brake-shoe block, heated, and moved into a bladed-disk spinning assembly. The test equipment is shown in Figures 59 and 60. All of the specimens were aged at the temperature for which they were qualified as a result of the aging and erosion tests. However, a number of the specimens failed during aging because of inadequate bond strength between the abrasive material and the backup plate. The condition of the specimens before and after exposure to the maximum static oxidation of aging temperature is shown in Table X and Figure 61. The specimens which were in satisfactory condition were used in the dynamic abrasion tests. Unaged specimens were substituted for the failed aged specimens to provide additional information for calculations of the abradability index and to determine the unaged abradability of these materials in the event that future work improves the bonding techniques and permits these materials to withstand the aging treatment.

(U) The abrasion test results were evaluated on the basis of a semiquantitative abradability index developed for the purpose during this program. The index was developed on the basis of several considerations. First, no blade tip wear, W_t, was to be tolerated, nor could bond failure in the abradable material be tolerated. Further, the drag force produced when the specimen contacts the blades, F_d, should be as small as possible. A large drag force indicates undesirably strong resistance to abrasion. The penetration time, T_p, which represents the time for the drag force to return to zero, should be as short as possible, since the least reduction in blade tip speed is desired, and since a short penetration time indicates ease of abrasion. Finally, the depth of penetration, D_p, should be as large as possible for a given groove drag force and penetration time. It was assumed that penetration time and drag force would be inversely proportional to the depth of penetration in establishing the abradability index. The requirement for no tip wear resulted in weighing this parameter by a factor of 1000. The resulting equation for abradability index is:

$$\text{Abradability Index} = T_p \left(\frac{F_d}{D_p} \right) (1 + 1000\, W_t)$$

(U) It should be noted in considering this equation that sufficient data is not available to verify the relative weights assigned to the various parameters. However, it is felt that the equation provides sufficient reliability to indicate the comparative abradability of the materials evaluated. In using the abrada-

NOFORN

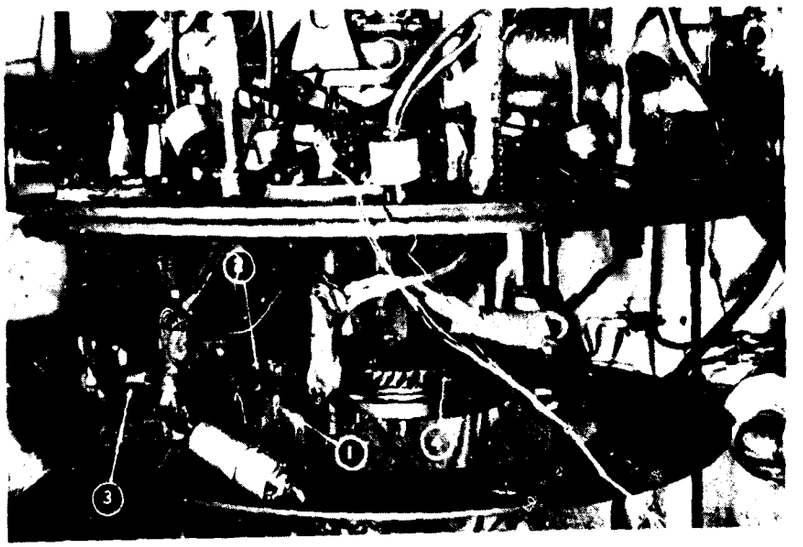

Figure 59 Dynamic Abrasion Test Rig H-65345

1. Strain Gage Transducer Link
2. 220-Volt Heaters
3. Air Actuator
4. Compressor Rotor
5. Steam Drive Turbine

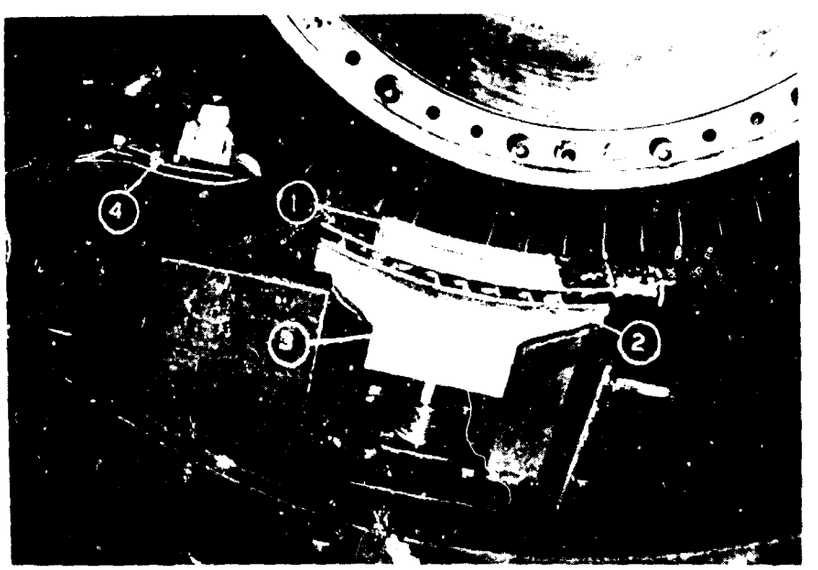

Figure 60 Closeup View of Dynamic Abrasion Test Rig X-24740

1. Abradable Seal Sample
2. Abradable Seal Heater
3. Actuator Head
4. Transducer and Thermocouple Lead Wires

NOFORN

(U) TABLE X

ABRASION TEST SPECIMEN BOND CONDITION
BEFORE AND AFTER AGING

Material	Bond Condition	
	As Fabricated	After Test Exposure
DC-325	Good with minor cracking of material when bent but negligible bond failure.	Marginal with some cracking and localized separation of seal from back-up plate after aging.
DC-93-004	Same as DC-325	Poor: seal separated from back-up plate during aging.
Chopped Fiberglas plus RTV Silicone Rubber	Marginal with some separation of seal from back-up plate when bent.	Marginal
Eccospheres plus DEN 438	Poor since brittle material shatters when bent.	Poor
Molykote Z plus DEN 438	Good: Material and bond withstood normal bending.	Poor: seal cracked and separated from backup plate during aging.
Fiberglas plus DEN 438	Good	Poor: bond failure due to aging.
Fiberglas plus Polyimide	Good	Good
Fiberglas plus PBI	Marginal with some separation of laminate noted after fabrication.	Poor: Seal separated from backup plate during aging.
SermeTel (PWA 7-3)	Good	Poor: seal cracked and separated from backup plate during aging.
Hastelloy X Feltmetal	Good	Fair: localized bond failure due to braze "wicking."*
Haynes 25 Feltmetal	Same as Hastelloy X	Same as Hastelloy X
Hastelloy X Commercial Honeycomb	Good: strength of honeycomb braze prevented normal bend test.	Good
Hastelloy X Drilled Honeycomb	Integral specimen: no bond required.	Integral specimen: no bond required.
410 Stainless Steel Drilled Honeycomb	Integral specimen: no bond required.	Integral specimen: no bond required.
Incoloy 800 Drilled Honeycomb	Integral specimen: no bond required.	Integral specimen: no bond required.
GE-757	Same as DC-325	Marginal: local separation from backup plate in rub area. (Specimen not aged)
GE Nichrome Foametal	Good	Specimen not aged

*Wicking: absorption of braze alloy by feltmetal by capillary action which starves bond interface.

NOFORN

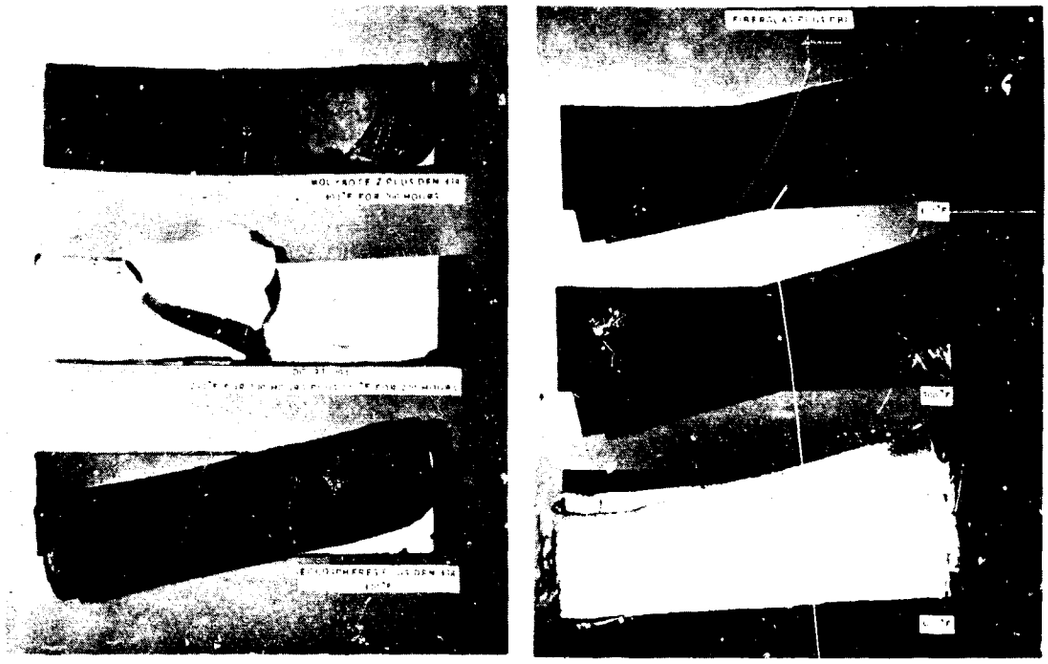

Figure 61 Typical Nonmetallic Abradable Specimens After Aging for Various Periods at Various Temperatures XP-77923/XP-77926

bility index, it was necessary to determine a value which would separate materials with acceptable and unacceptable abrasion characteristics. Study of the equation and the material requirements resulted in selection of the index value of 71.4 with F_d expressed in pounds, T_p in seconds, and D_p and W_t expressed in inches. Index values of 71.4 and below, therefore, were considered to be acceptable, and values above 71.4 were considered to be unacceptable.

(U) Results of the abrasion tests are shown in Table XI. As shown, the only qualifying material is DC-325. All other materials had excessively high abradability indices, failed to surve the mandatory aging treatment, or physically failed during the abrasion test. The conditions of typical specimens after dynamic abrasion testing are shown in Figures 62 through 75.

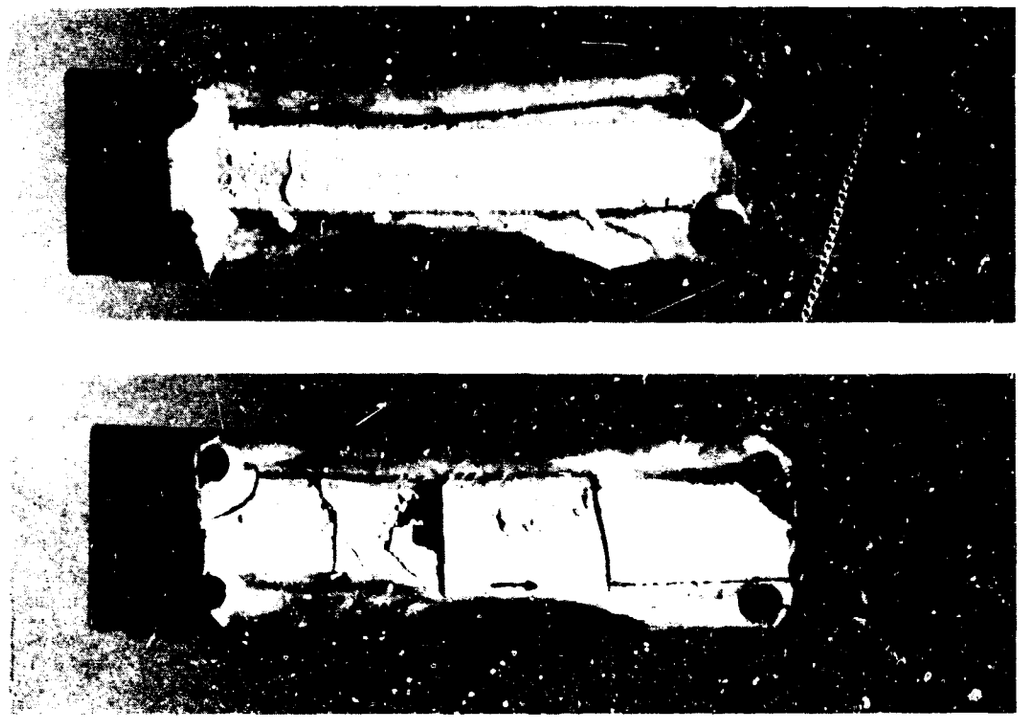

Figure 62 DC-325 Unaged (Top) and Aged (Bottom) Rub-Strip Specimens After Dynamic Abrasion Testing at 525°F and 500°F, Respectively
XP-77925

Figure 63 DC-93-004 Unaged Rub-Strip Specimens After Dynamic Abrasion Testing at 525°F
XP-77925

NOFORN

(U) TABLE XI

DYNAMIC ABRASION TEST RESULTS

Material	Prerub Condition	Blade Speed	Contact Time (Seconds)	Time For Penetration (Seconds)	Depth of Penetration (Inch)	Drag Force (lb)	Drag Penet Dept (lb/
DC-325	Unaged	13,990	5	0.2	0.080	6.6	82
DC-325	Aged 100 Hours at 250° F and 200 Hours at 500°F.	13,986	5	0.2	0.040	1.3	32
DC-93-004	Unaged	14,000	6	0	0.064	0	
Chopped Fiberglas plus RTV Silicone Rubber	Unaged	14,000	4 3/4	0	Bond Ruptured	0	
Chopped Fiberglas plus RTV Silicone Rubber	Aged	14,000	5	0	Bond Ruptured	0	
Fiberglas plus DEN 438	Unaged	13,996	5	0.15	0.13	1.5	1
Fiberglas plus DEN 438	Aged slightly loose due to drilling	14,000	6 1/2	0.3	0.050 (Rubbed through seal)	15.1	23
Molycote Z plus DEN 438	Unaged	13,956	5 3/4	0.15	0.068	4	5
Fiberglas plus PBI	Unaged	14,056	5	0.7	0.045	13.0	20
Fiberglas plus Polyimide	Aged	14,000	5	0.5	0.024	5.5	22
SermeTel (PWA-7-3)	Unaged	14,000	5 1/2	0.3	0.021	5	2
Hastelloy X Feltmetal	Aged	13,866	4 3/4	0.5	0.037	9	2
Haynes 25 Feltmetal	Aged	14,016	6	0.5	0.037	14	3
Hastelloy X Commercial Honeycomb with 10-Mil Web	Aged	13,769	6	0.2	0.044	11.2	3
410 Stainless Steel Drilled Honeycomb with 20-Mil Web	Aged	14,050	4 3/4	1.4	0.026 to 0.009	23	
GE-757 Rubber Foam	Unaged	13,920	5	0	0.060	0	
GE Nichrome Foametal	Unaged	13,993	4	1.5	0.026	28	

* Index not determined, bond failure during test

** Index not determined, blades contacted backup plate

NOFORN

UNCLASSIFIED

(U) TABLE XI

DYNAMIC ABRASION TEST RESULTS

Contact Time (Seconds)	Time For Penetration (Seconds)	Depth of Penetration (Inch)	Drag Force (lb)	Drag Force Penetration Depth (lb/in)	Initial Temperature (°F)	Temperature Rise (°F)	Blade Tipwear (Inches)	Abradability Index
5	0.2	0.080	6.6	82.5	525	0	0	6.5
5	0.2	0.040	1.3	32.6	500	0	0	16.5
6	0	0.068	0	0	525	0	0	0
4 3/4	0	Bond Ruptured	0	0	505	0	0	*
5	0	Bond Ruptured	0	0	500	0	0	*
5	0.15	0.13	1.5	11.5	410	5	0	17.3
6 1/2	0.3	0.060 (Rubbed through seal)	15.1	252	410	56	Not applicable	**
5 3/4	0.15	0.068	4	59	90	20	0	8.9
5	0.7	0.045	13.0	289	115	15	0.002	606
5	0.5	0.024	5.5	229	600	0	0.002	342.0
5 1/2	0.3	0.021	5	238	120	16	0	71.4
4 3/4	0.5	0.037	9	243	1005	30	0.003	444.0
6	0.9	0.037	14	380	920	0	0.004	1520.0
6	0.2	0.044	11.2	266	1025	0	0.001	212.0
4 3/4	1.4	0.026 to 0.009	20	952	1145	50	0.006	9445.0
5	0	0.060	0	0	560	0	0	0
4	1.5	0.026	29	1076	1040	330	0.005	**

PAGE NO 75

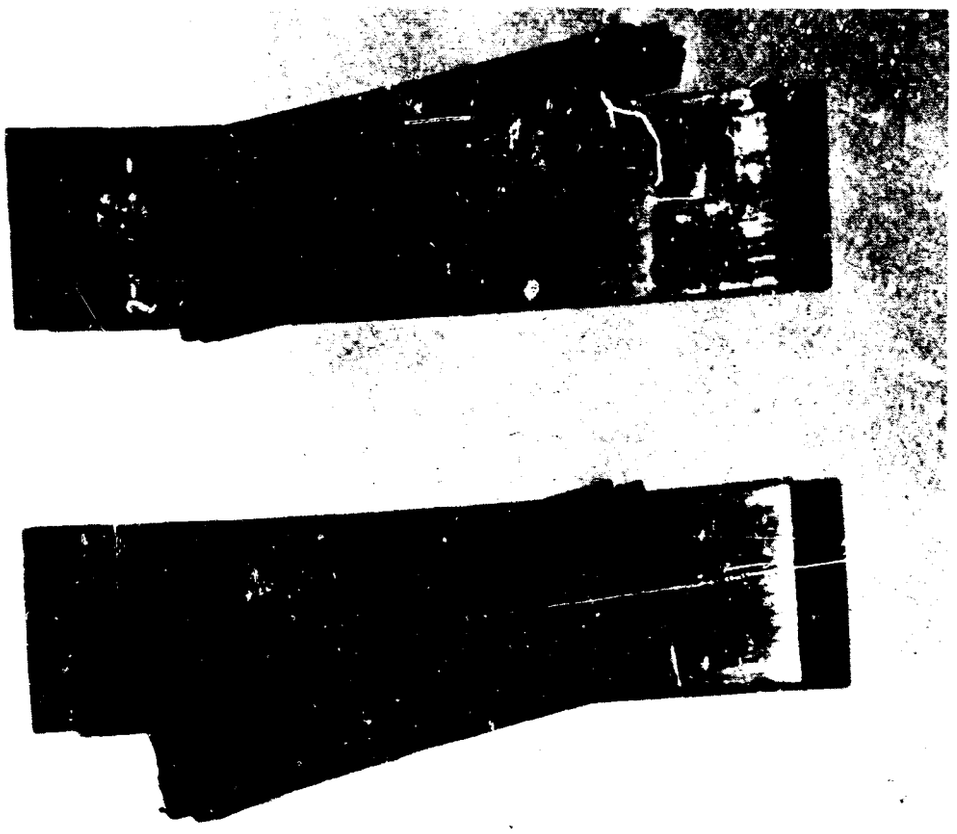

Figure 64 Chopped Fiberglas Plus RTV Silicone Rubber Unaged (Top) and Aged (Bottom) Rub-Strip Specimens After Dynamic Abrasion Testing at 505°F and 500°F, Respectively XP-77924

Figure 65 Eccospheres Plus DEN 438 Unaged Rub-Strip Specimen After Bond Failure During Dynamic Abrasion Test XP-77925

NOFORN

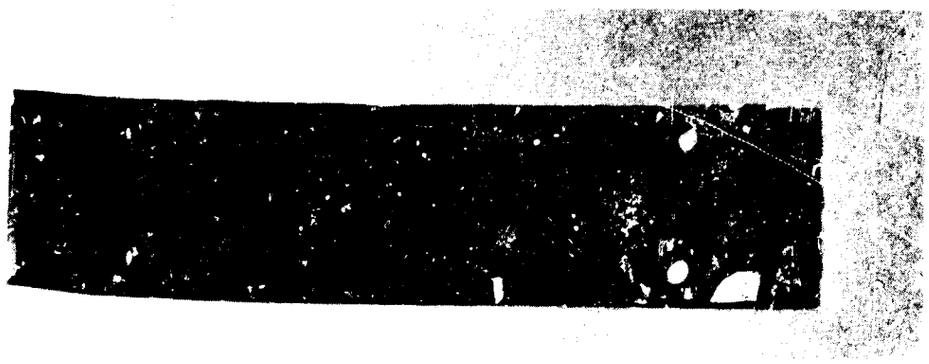

Figure 66 Molykote Z Plus DEN 438 Unaged Rub-Strip Specimen After Dynamic Abrasion Testing at Room Temperature XP-77928

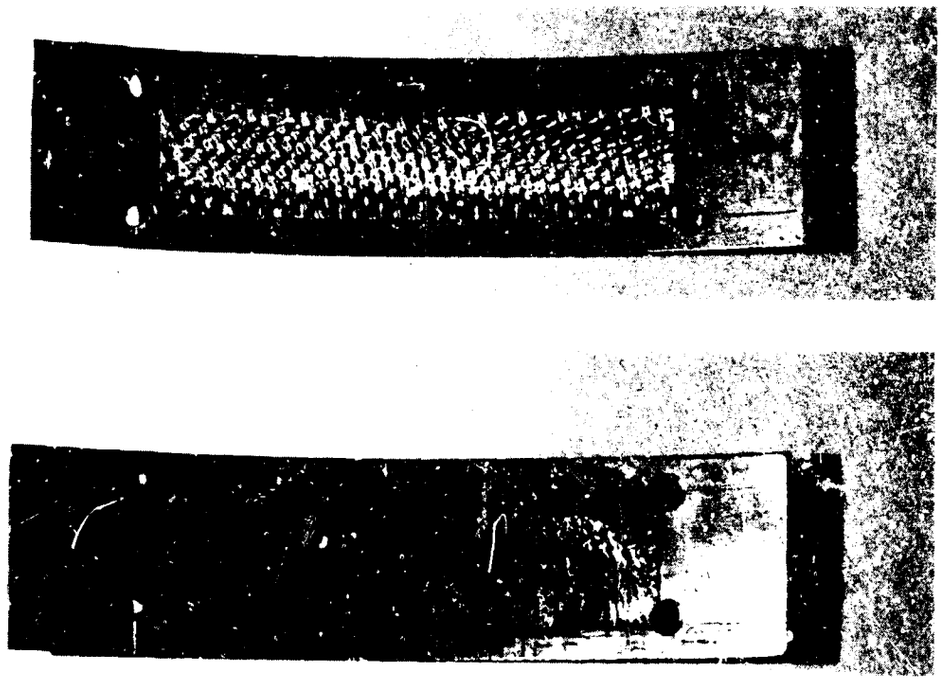

Figure 67 Fiberglas Plus DEN 438 Unaged (Top) and Aged (Bottom) Rub-Strip Specimens After Dynamic Abrasion Testing at -110°F XP-77929

NOFORN

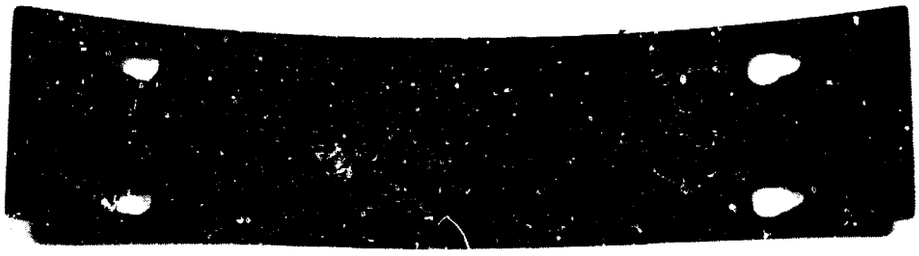

Figure 68 SerineTel (PWA 7-3) Unaged Rub-Strip Specimen After Dynamic Abrasion Testing at 120°F XP-78511

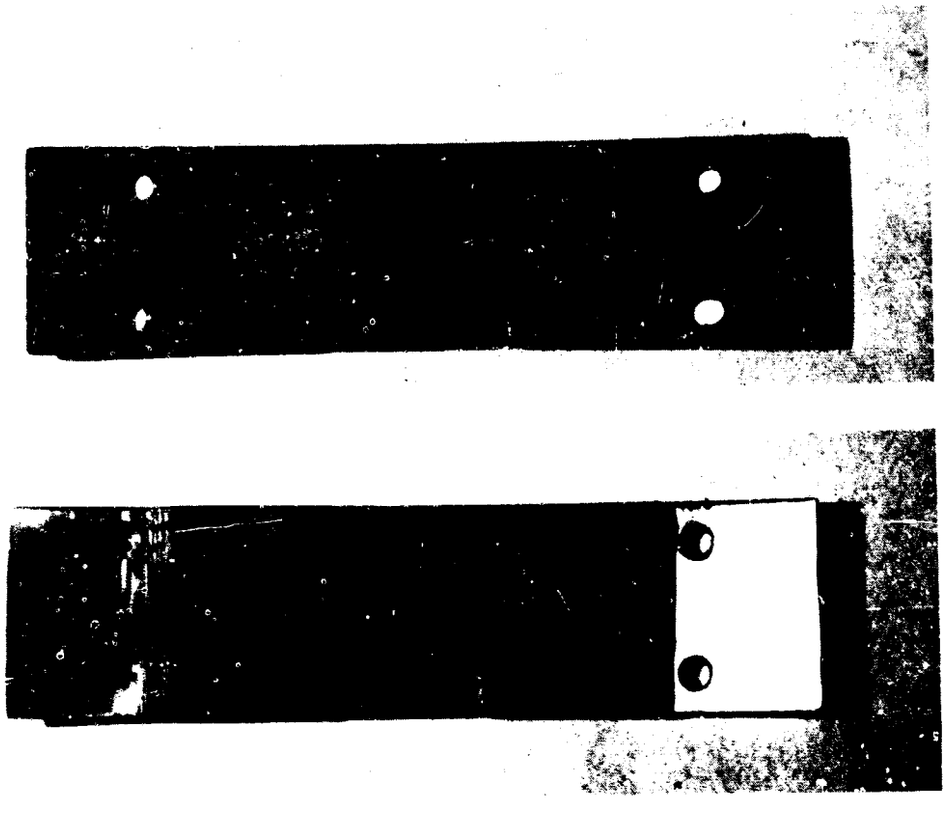

Figure 69 Fiberglas Plus PBI Unaged (Top) and Aged (Bottom) Rub-Strip Specimens After Dynamic Abrasion Testing at 135 F and 600 F, Respectively XP-77929

NOFORN

Figure 70 Hastelloy X Feltmetal Aged Rub-Strip Specimen After Dynamic Abrasion Testing at 1005°F XP-78511

Figure 71 Haynes 25 Feltmetal Aged Rub-Strip Specimen After Dynamic Abrasion Testing at 920°F XP-77927

Figure 72 Hastelloy X Commercial Honeycomb Aged Rub-Strip Specimen After Dynamic Abrasion Testing at 1025°F XP-77927

NOFORN

Figure 73 Type 410 Stainless Steel Drilled Honeycomb Aged Rub-Strip Specimen After Dynamic Abrasion Testing at 1145°F XP-77927

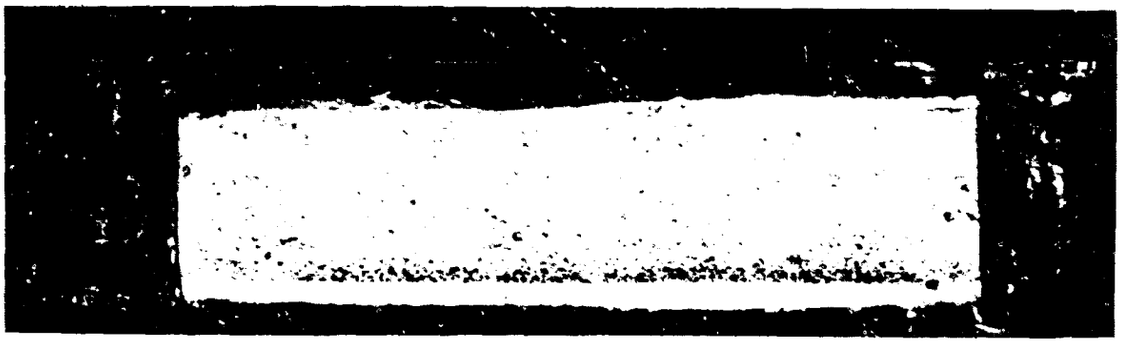

Figure 74 GE-757 Unaged Rub-Strip Specimen After Dynamic Abrasion Testing at 580°F XP-78913

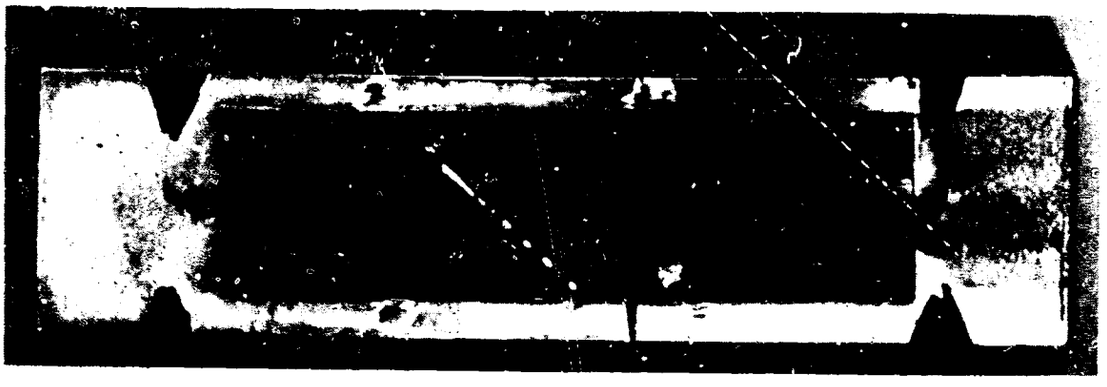

Figure 75 GE Nichrome Foametal Unaged Rub-Strip Specimen After Dynamic Abrasion Testing at 1080°F XP-78913

NOFORN

E. CONCLUSIONS AND RECOMMENDATIONS

(U) None of the materials successfully completed all of the evaluation tests. However, as shown in Table XII, none of the materials evaluated satisfied this requirement. Only one material was considered to be even marginal, and this was DC 325 material, which has good characteristics except for bond strength and service life, both of which are marginal

(U) The metallic honeycomb materials failed to qualify primarily because of their toughness and abrasive qualities which caused blade tip wear. Insufficient bond strength was the chief cause of failure for the nonmetallic materials. In view of these results, it is evident that further study is required to determine a geometry which will reduce the toughness of the metallic specimens to eliminate the problem of tip wear. Additional study of nonmetallic materials is also recommended.

(U) This program attempted to demonstrate the capability of a number of nonmetallic materials to withstand the conditions existing in medium temperature environments. These materials did not qualify, however, because of the abrasive qualities of the filler materials, which resulted in blade tip wear. Consequently, future work with nonmetallic materials should be concentrated on an extensive investigation of a number of filler materials in combination with a limited number of proven high-temperature binding materials.

(U) Several useful trends were established. A measure of abradability was developed which is useful for comparing the relative abrasion qualities of materials. In addition, it was found that abradability appears to be inversely proportional to the tensile strength of the material. Finally, a number of materials were found which are capable of withstanding high temperature corrosion and erosion conditions. The outstanding problem is finding a material which is capable of withstanding operating environmental conditions and which also has sufficiently low toughness and abrasive characteristics to preclude blade tip wear.

NOFORN

(U) TABLE XII

SUMMARY OF ABRADABLE SEAL MATERIAL TEST PROGRAM

Material	Component Application	Fabrication Bond Strength	Static Oxidation and Aging	Hot Gas Erosion	Dynamic Abradability	Abradable Seal Application At Maximum Temperature	Qualifying Remarks
DC-325	Fan plus low-temperature compressor	Marginal	Good	Good	Good	Marginal	Less than 200 hour life
DC-93-004	Fan plus low-temperature compressor	Poor	Good	Good	Good	Unacceptable	Bond failure
Chopped Fiberglas plus RTV 60 Silicone Rubber	Fan plus low-temperature compressor	Poor	Good	Good	Good	Unacceptable	Bond failure
Eccospheres and DEN 438	Fan plus low-temperature compressor	Poor	Poor	Good	Poor	Unacceptable	Brittle bond and seal material
Molykote Z plus DEN 438	Fan plus low-temperature compressor	Poor	Good	Good	Good	Unacceptable	Brittle bond
Fiberglas plus DEN 438	Fan plus low-temperature compressor	Poor	Good	Good	Good	Unacceptable	Bond failure
Fiberglas plus Polyimide	Fan plus low-temperature compressor	Good	Good	Good	Poor	Unacceptable	Blade tip wear
Fiberglas plus PBI	Fan plus low-temperature compressor	Poor	Good	Good	Poor	Unacceptable	Bond failure and blade tip wear
SermeTel (PWA 7-3)	Fan and Compressor	Poor	Good	Good	Good	Unacceptable	Bond failure
Hastelloy X Feltmetal	Compressor and Turbine	Poor	Good	Good	Poor	Unacceptable	Bond failure and blade tip wear
Haynes 25 Feltmetal	Compressor and Turbine	Poor	Good	Good	Poor	Unacceptable	Bond failure and blade tip wear
Hastelloy X Drilled Honeycomb	Compressor and Turbine	Good	Good	Good	Poor	Unacceptable	Blade tip wear
Hastelloy X Commercial Honeycomb	Compressor and Turbine	Good	Good	Good	Poor	Unacceptable	Blade tip wear
410 Stainless Steel Drilled Honeycomb	Compressor and Turbine	Good	Good	Good	Poor	Unacceptable	Blade tip wear
Incoloy 800 Drilled Honeycomb	Compressor and Turbine	Good	Good	Good	Poor	Unacceptable	Blade tip wear
GE-757	Fan and low-temperature compressor	Marginal	-	-	Good	-	Performance similar to DC-325 with some material cracking
GE Nichrome Foametal	Fan and compressor	Good	-	-	Poor	Unacceptable	Blade tip wear

NOFORN

SECTION VI

EVALUATION OF MATERIALS FOR USE IN A HIGH-TEMPERATURE CORROSIVE AND EROSIVE ENVIRONMENT

A. INTRODUCTION

(U) A number of materials were evaluated for use in a high-temperature corrosive and erosive combustion environment. The program involved four distinct tasks. Initially, materials were selected for study on the basis of experience and a literature survey. This was followed by the fabrication of specimens for testing. During the fabrication effort, data on the formability and coating of the materials was obtained, and welding requirements were determined. The third task was low-cycle fatigue testing, and the fourth task consisted of two series of thermal endurance tests.

B. MATERIAL SELECTION

(U) The materials for evaluation were selected on the basis of high-temperature strength and good oxidation-corrosion resistance. A literature search resulted in the selection of nine basic materials, including high-temperature nickel-base super-alloys, dispersion strengthened alloys in coated and uncoated form, and coated refractory alloys. Hastelloy X was also included to provide baseline data. The complete list of the materials evaluated is shown in Table XIII, together with nominal compositions and suppliers.

C. SPECIMEN FABRICATION

(U) The specimens were fabricated to a design which simulated a louvered section of a typical combustion liner. The specimen design is shown in Figure 76. No difficulty was encountered in forming any of the materials except thoriated L-605 alloy and coated TD nickel-chrome alloy. Several attempts were made to form L-605 alloy to the required geometry, but each attempt resulted in cracks in the specimen. Various attempts to heat treat the material to improve its formability were unsuccessful. The heat treatments attempted are shown in Table XIV.

(U) The formability of coated TD nickel-chrome alloy was found to be significantly poorer than that of the uncoated material. Specimens were successfully fabricated, however, by using a hot forming process.

(U) Resistance welding was used for all of the materials except Cb-129Y, which was electron-beam welded because of its high melting point. Welding did not cause any difficulties during fabrication.

(U) TABLE XIII

MATERIALS SELECTED FOR EVALUATION
IN COMBUSTOR LINER PROGRAM

Material	Base Material	Weight Percent of Alloying Elements									Others	Vendor
		Cr	Fe	C	Mn	Si	S	Ti	Al	Cu	Mo	
TD Nickel*	Ni	0.01	1.05	0.006	-	-	0.003	0.001	-	0.003	-	2.1 (Volume) ThO_2 0.01 C_o	Pigment Dept. - Metal Products E.I. duFont deNemours & Co., Inc. 10419 Nemours Bldg. Wilmington, Delaware
TD Nickel-Chrome*	Ni	21.20	-	0.018	-	-	0.005	-	-	-	-	2.8 (Volume) ThO_2 0.002N	Same as for TD Nickel
	Ni	21.30	-	0.006	-	-	0.005	-	-	-	-	2.8 (Volume) ThO_2 0.002N	
Mar-M-Boy X	Ni	21.33	18.22	0.06	0.61	0.50	0.006	-	-	-	9.01	0.64W 0.016P, 1.40 Co	Union Carbide Corp. Stellite Division Kokomo, Indiana
Inconel 625	Ni	22.15	2.26	0.02	0.04	0.18	0.01	0.13	0.21	0.01	9.62	3.66 Cb and Ta	Huntington Alloy Products Division The International Nickel Company Huntington, West Virginia
Inconel 718	Ni	15.6	0.35	0.04	0.05	0.20	0.007	0.70	3.40	0.10	-	-	Same as Inconel 625
Incoloy 804	Ni	29.3	25.4	0.06	0.85	0.50	0.007	0.40	0.25	0.40	-	-	Same as Inconel 625
DS Nickel-Chrome**	Ni	20.0	-	-	-	-	-	-	-	-	-	2.4 (Volume) ThO_2	Research & Development Division Sherritt-Gordon Mines, Limited Fort Saskatchewan, Alberta, Canada
Cb-129Y**	Cb	-	-	-	-	-	-	-	-	-	-	10.0W, 10.0Hf, 0.1Y	Wah Chang, Albany Division P.O. Box 460, Albany, Oregon
L-605 (Modified)	Co	20.0	-	-	-	-	-	-	-	-	15.0	11.0Ni, 4 (Volume) ThO_2	Sylvania Electric Chemical-Metallurgical Division Towanda, Pennsylvania

* Tested coated and uncoated
** Tested coated only

TABLE XIV

Heat Treatments Applied to Thoriated
L-605 Sheet Prior to Forming

Temperature (°F)	Atmosphere	Time at Temperature (hr)	Cooling Rate
2250	Hydrogen	1.00	Air quench
2250	Hydrogen	0.25	Oil quench
2250	Hydrogen	0.25	Water quench
2300	Hydrogen	2.00	Cooled in H_2

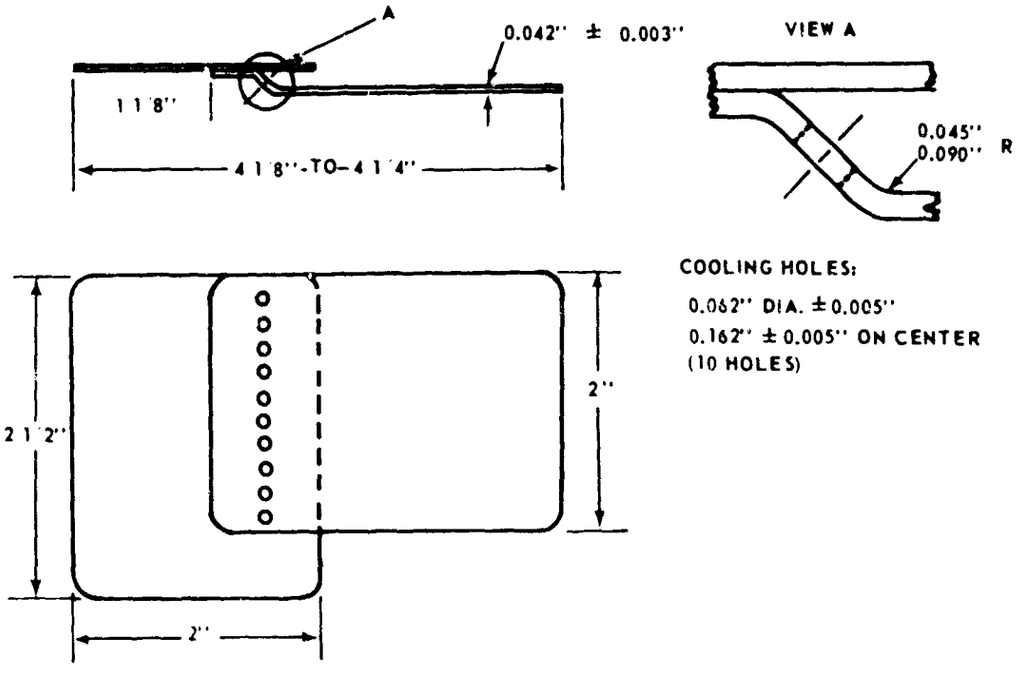

Figure 76 Test Specimen Design

(U) Two coatings were used to provide oxidation protection for the material. A coating of Cr-Ti-Si material was applied to the refractory alloy, Cb-129Y by a two-cycle vacuum process. Prior to coating, all edges were ground to a minimum radius of 0.050 inch, and fillet welds were added to joined pieces to provide the minimum 0.050-inch radius at all interfaces. The radii were required to ensure coating integrity at all joint interfaces and edges. Thoriated nickel and thoriated nickel-chrome alloys were coated with a duplex chromized-aluminized process. All edges of these specimens were ground to a full radius to prevent unequal coating buildup. Photomicrographs showing the coating produced are presented in Figures 77, 78 and 79.

NOFORN

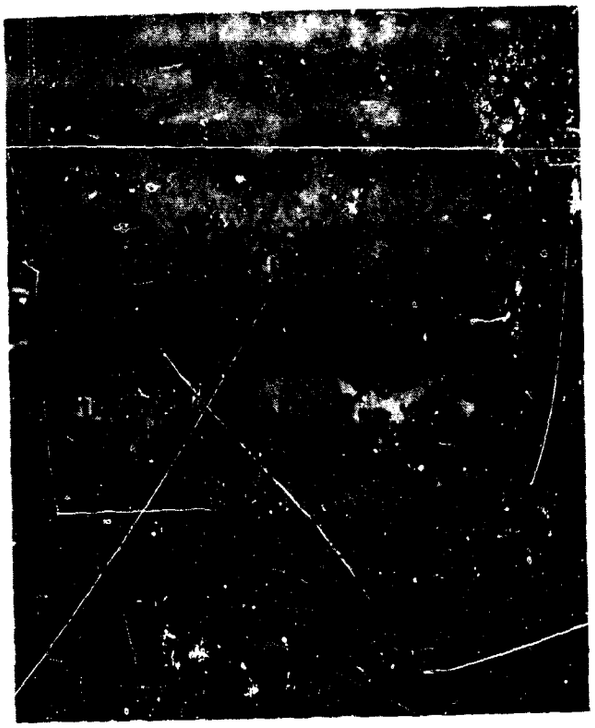

Etchant: 33 % HF, 33 % HNO_3, 34 % H_2O Mag: 500X

Figure 77 Photomicrograph of Co-129Y Specimen With Cr-Ti-Si Coating

Unetched Mag: 1000X

Figure 78 Photomicrograph of TD Nickel Specimen With Duplex Chrome-Aluminide Coating

NOFORN

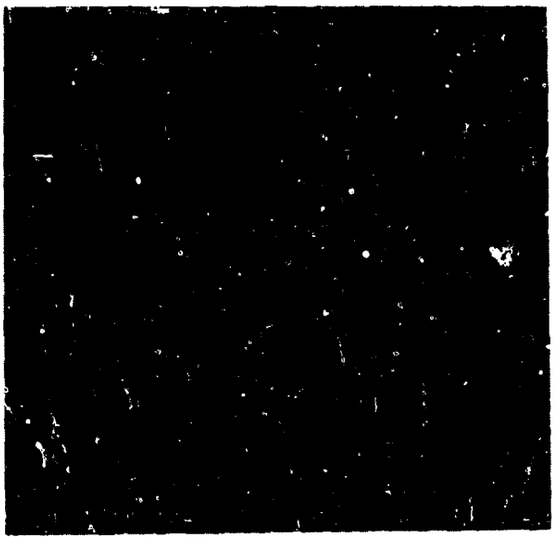

Unetched Mag: 1000X

Figure 79 Photomicrograph of TD Nickel-Chrome Specimen With Duplex Chrome-Aluminide Coating

D. LOW-CYCLE FATIGUE TESTING

(U) Low-cycle fatigue testing was performed on selected materials using the true reverse-bending rig shown in Figures 80 and 81. The materials tested were uncoated Hastelloy X, uncoated TD nickel, chrome-aluminde-coated TD nickel-chrome, and uncoated Inconel 625. Each material was tested at five strain levels, 1.2, 0.87, 0.68, 0.55, and 0.38 percent. These strain levels were chosen to simulate the environmental strains imposed by thermal cycling during engine operation. Testing was performed at 1650 and 1800°F.

(U) The fatigue data obtained was correlated by fitting an analytically determined equation to the data. This equation was developed using the principles presented by Tavernelli and Coffin[1] and Manson[2]. Construction of the analytical curve is

[1]J. F. Tavernelli and L. F. Coffin, Jr., "Experimental Support for Generalized Equation Predicting Low Cycle Fatigue," Journal of Basic Engineering, December 1962.

[2]S. S. Manson, "Fatigue: A Complex Subject - Some Simple Approximations," Experimental Mechanics, July 1965.

NOFORN

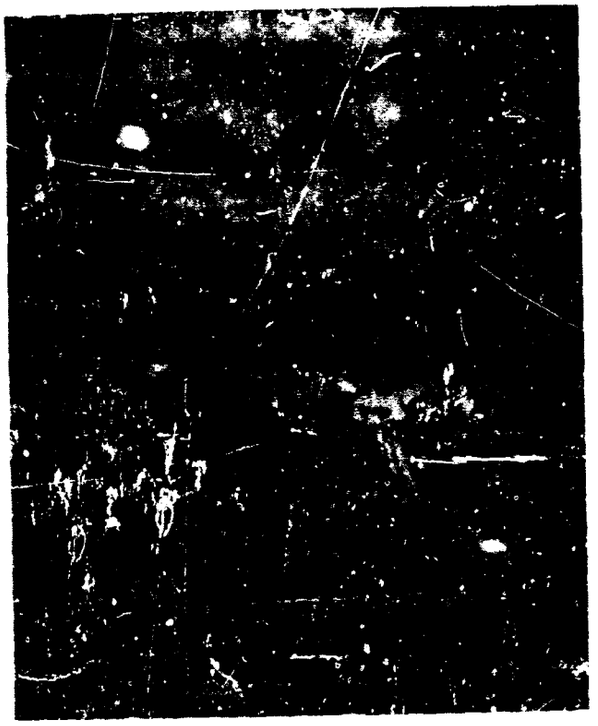

Etchant: 33% HF, 33% HNO_3, 34% H_2O Mag: 500X

Figure 77 Photomicrograph of Co-129Y Specimen With Cr-Ti-Si Coating

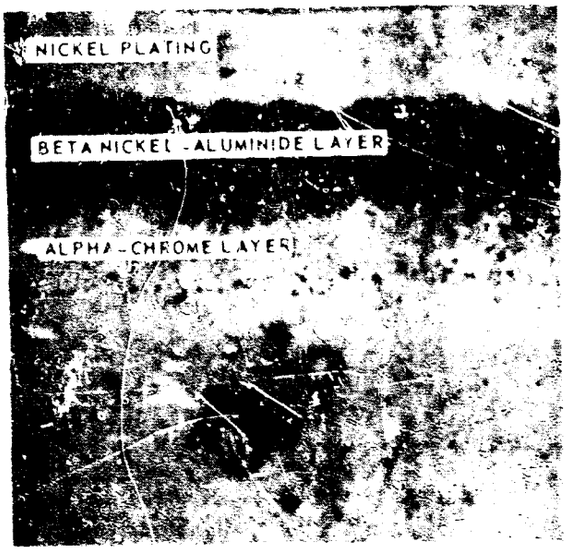

Unetched Mag: 1000X

Figure 78 Photomicrograph of TD Nickel Specimen With Duplex Chrome-Aluminide Coating

NOFORN

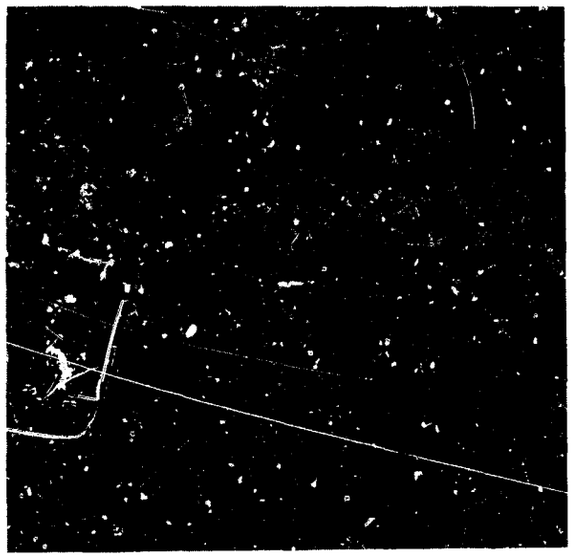

Unetched Mag: 1000X

Figure 79 Photomicrograph of TD Nickel-Chrome Specimen With Duplex Chrome-Aluminide Coating

D. LOW-CYCLE FATIGUE TESTING

(U) Low-cycle fatigue testing was performed on selected materials using the true reverse-bending rig shown in Figures 80 and 81. The materials tested were uncoated Hastelloy X, uncoated TD nickel, chrome-aluminde-coated TD nickel-chrome, and uncoated Inconel 625. Each material was tested at five strain levels, 1.2, 0.87, 0.68, 0.55, and 0.38 percent. These strain levels were chosen to simulate the environmental strains imposed by thermal cycling during engine operation. Testing was performed at 1650 and 1800°F.

(U) The fatigue data obtained was correlated by fitting an analytically determined equation to the data. This equation was developed using the principles presented by Tavernelli and Coffin[1] and Manson[2]. Construction of the analytical curve is

[1]J. F. Tavernelli and L. F. Coffin, Jr., "Experimental Support for Generalized Equation Predicting Low Cycle Fatigue," Journal of Basic Engineering, December 1962.

[2]S. S. Manson, "Fatigue: A Complex Subject - Some Simple Approximations," Experimental Mechanics, July 1965.

NOFORN

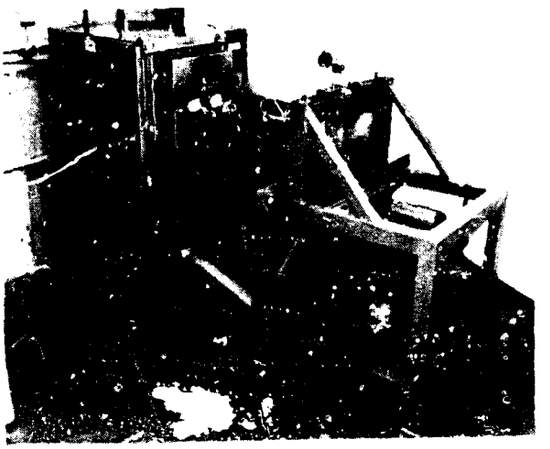

Figure 80 True Reverse-Bending Low-Cycle Fatigue Rig X-22621

Figure 81 Closeup View of True Reverse-Bending Low-Cycle Fatigue Rig X-22620

NOFORN

shown in Figure 82. As shown, construction of the curve depends on the values of the fracture elongation, the ultimate tensile strength, the endurance strength, and the modulus of elasticity. By using static properties, it is possible to construct the fatigue curve without obtaining experimental fatigue data.

(U) The plastic portion of the curve consists of an intercept and a slope which are dependent on the relationship between the plastic strain and the total strain of the material. This relationship must be known for any given level of strain and may be determined from tensile test plots of stress versus strain, since total strain equals the sum of the plastic strain and the elastic strain. The elastic portion of the curve is proportional to the ultimate and endurance strengths of the material. The equation used for this program was:

$$\epsilon_{tr} = 2\frac{(\epsilon_f - \epsilon_m)}{(4N)^{2a}} + 2\frac{\sigma_{uts}}{E}(4N)\frac{\ln(\sigma_{uts}/\sigma_e)}{\ln(0.25 \times 10^{-3})}$$

where:

ϵ_{tr} = Total strain range

ϵ_f = Fracture elongation

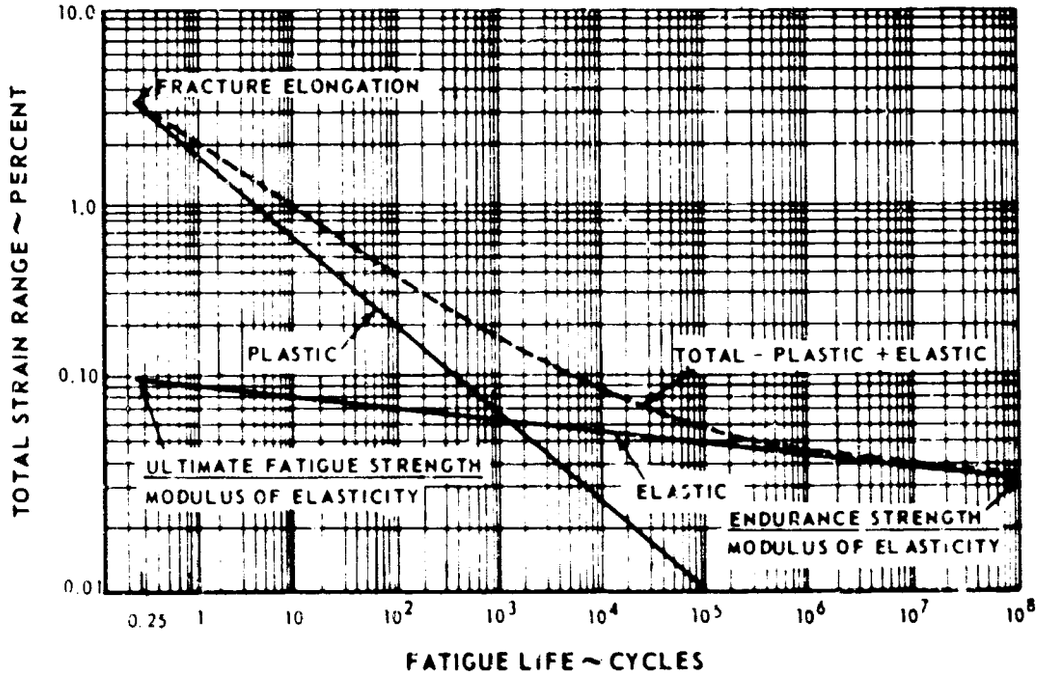

Figure 82 Analytical Construction of Fatigue Curve

NOFORN

ϵ_m = Mean applied strain

a = Material constant

σ_{uts} = Ultimate tensile strength

E = Modulus of elasticity

σ_e = Endurance strength

(U) For this program a minimum of experimental fatigue data was used to determine a "best fit" curve. This was done by substituting the values of fatigue test data into the analytical equation to determine the correlation with the known static properties.

(U) Low-cycle fatigue test results, based on the correlation method described above, are presented for each of the materials in Figures 83 through 88. No data is presented for Hastelloy X or Inconel 625 materials for fatigue life at 1800°F because plastic deformation occurred during testing which resulted in "hinging" of the specimen. A typical hinged specimen is shown in Figure 89 together with a normal low-cycle fatigue fracture. In reviewing the curves, it should be recognized that some error is probably present at the high-life range since no fatigue data was obtained at strain ranges below 0.38 percent.

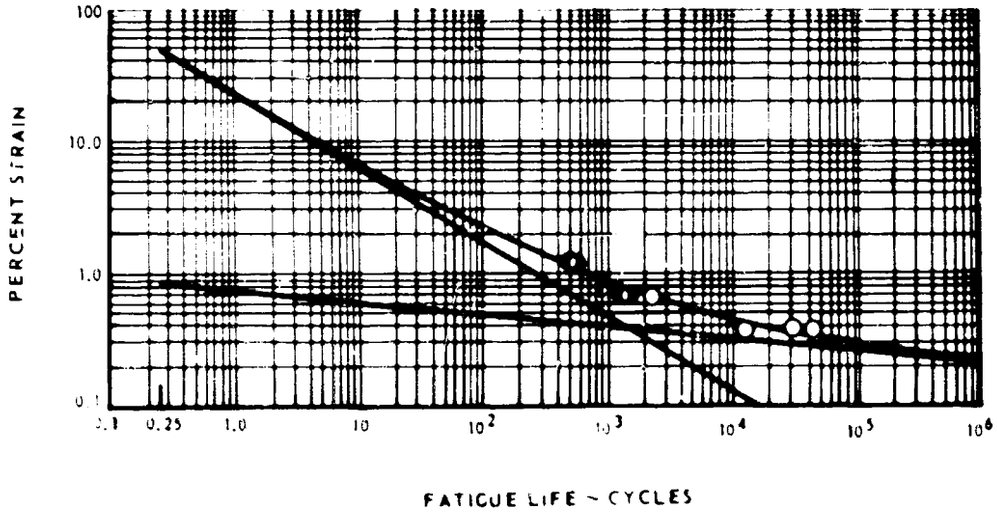

Figure 83 Low-Cycle Fatigue Test Results for Hastelloy X Material at 1650°F

NOFORN

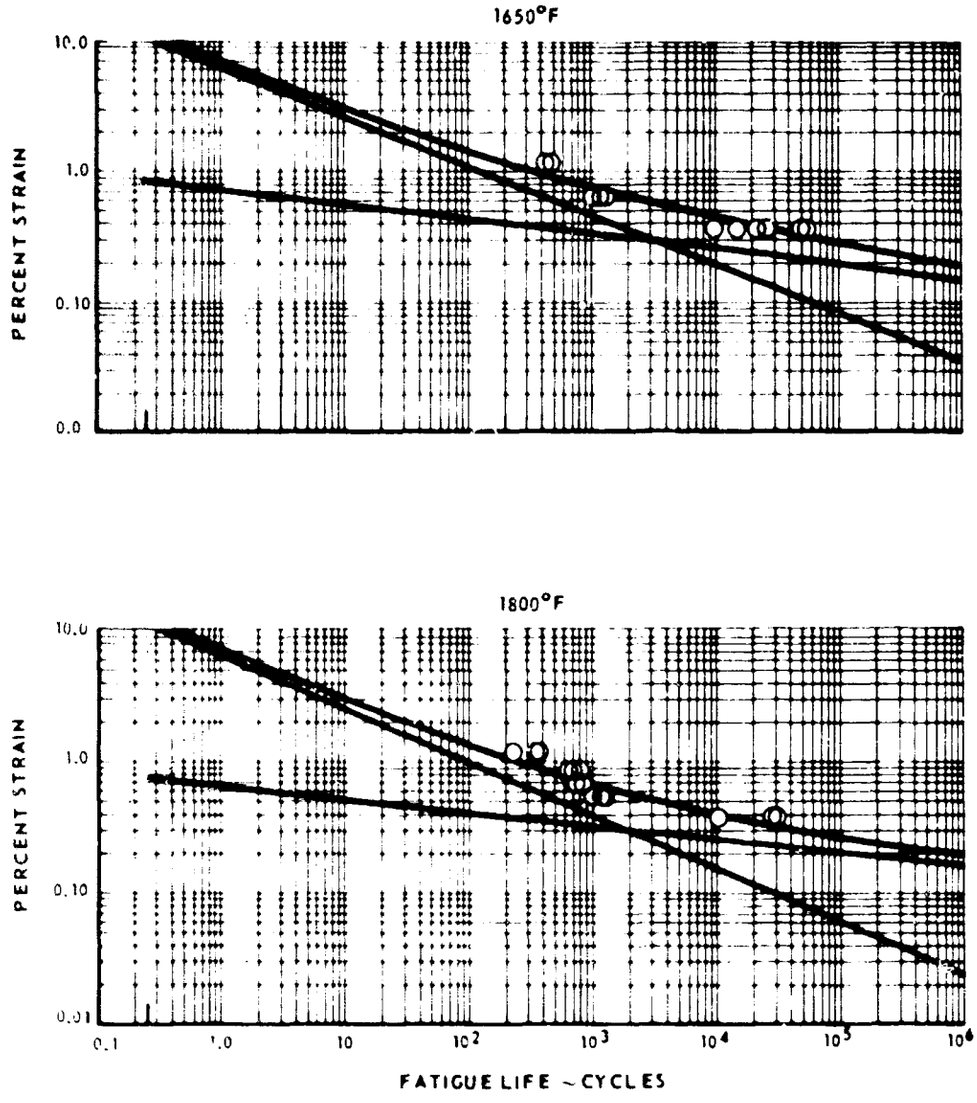

Figure 84 Low-Cycle Fatigue Test Results for TD Nickel Alloy at 1650°F and 1800°F

NOFORN

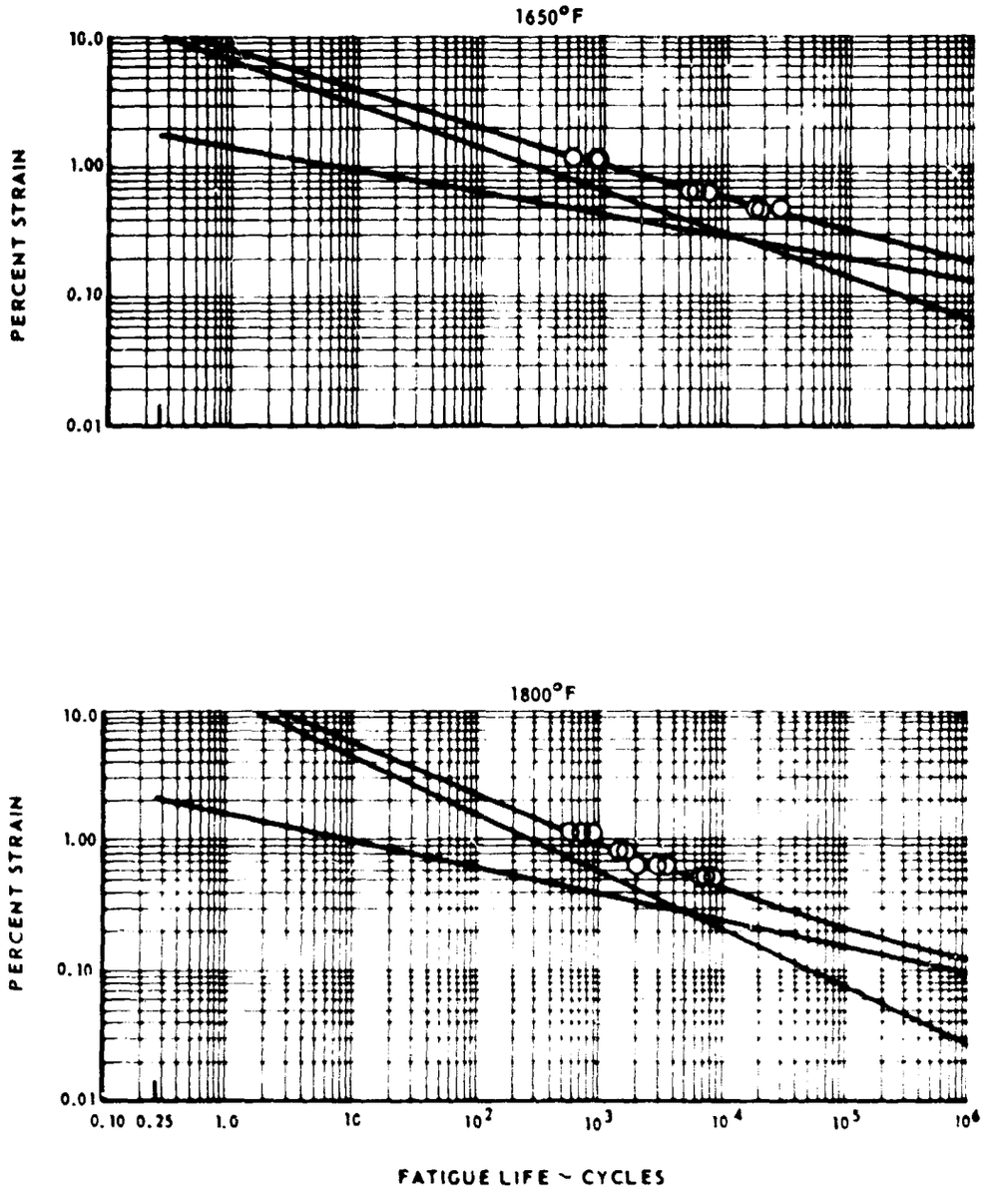

Figure 85 Low-Cycle Fatigue Test Results for TD Nickel Alloy With Chrome-Aluminide Coating at 1650°F and 1800°F

NOFORN

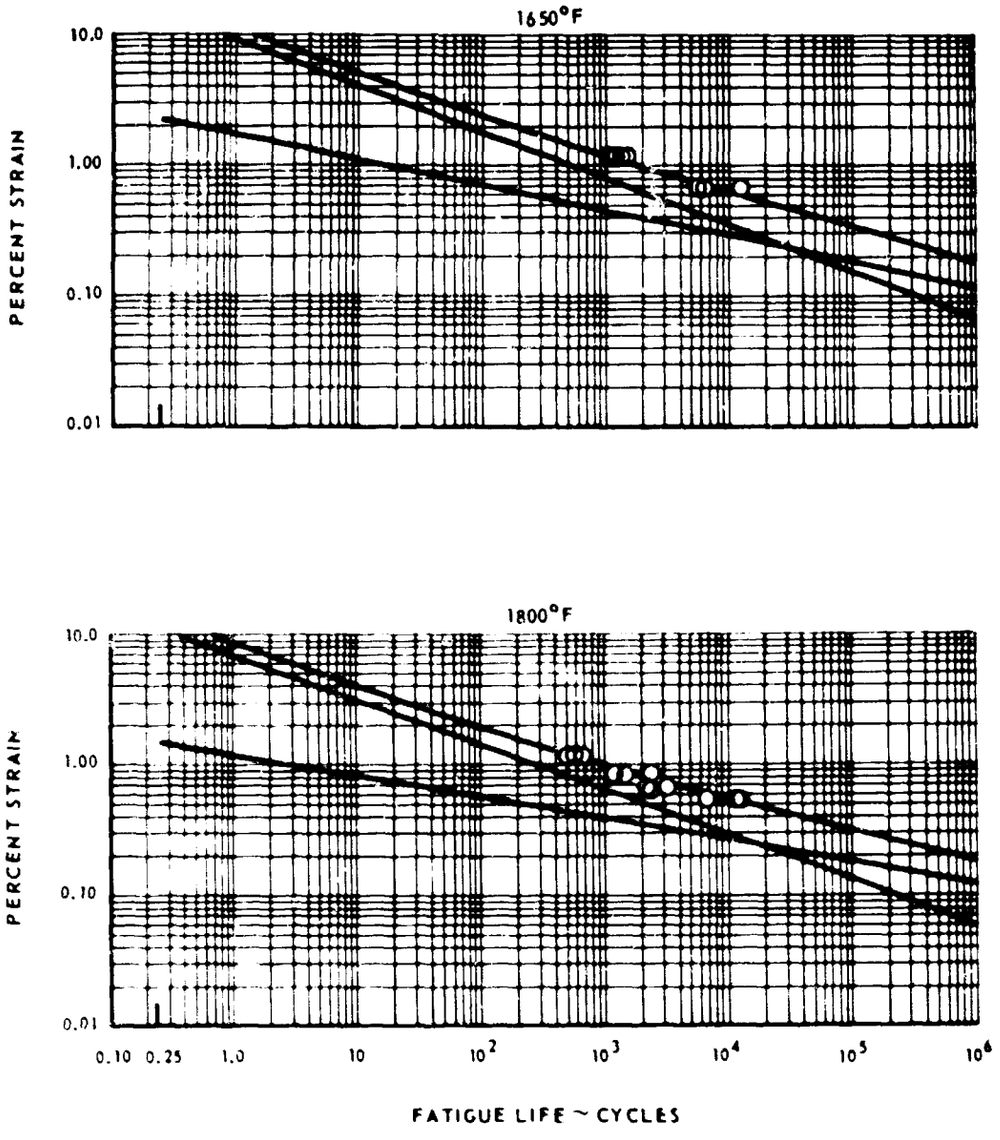

Figure 86 Low-Cycle Fatigue Test Results for TD Nickel-Chrome Alloy at 1650°F and 1800°F

NOFORN

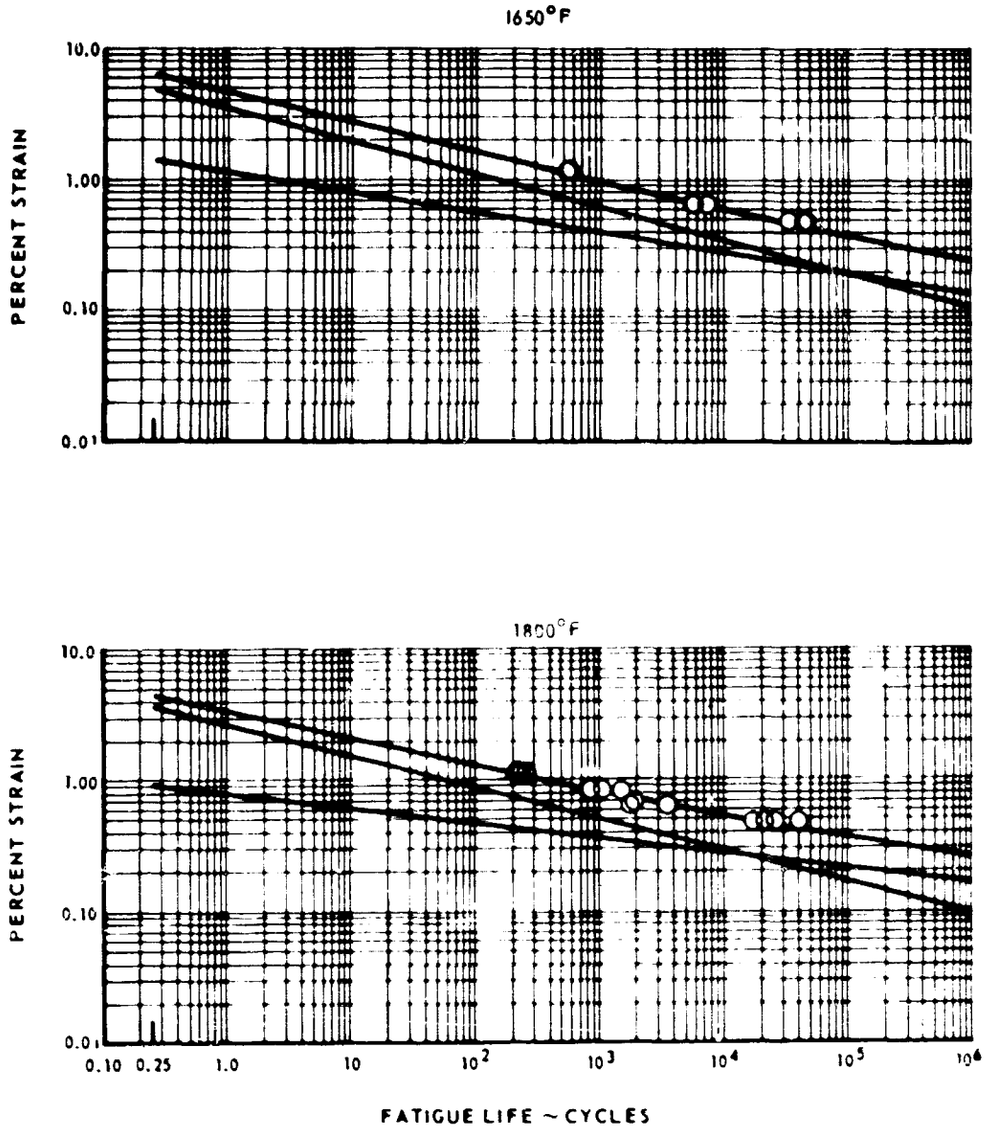

Figure 87 Low-Cycle Fatigue Test Results for TD Nickel-Chrome Alloy Coated With Chrome-Aluminide Coating at 1650°F and 1800°F

NOFORN

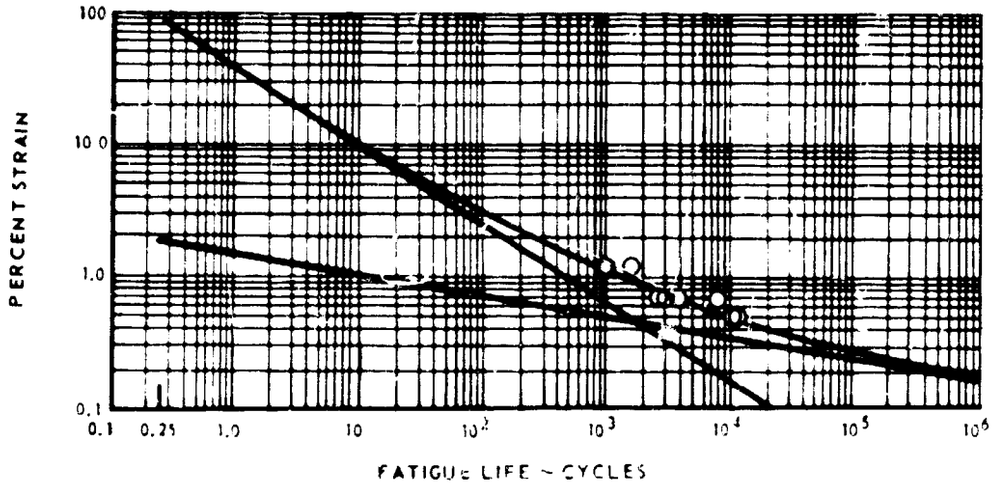

Figure 88 Low-Cycle Fatigue Test Results for Inconel 625 Alloy at 1650°F

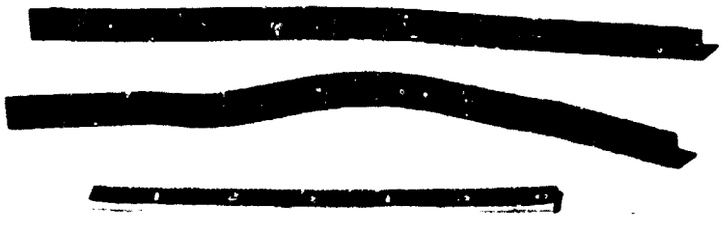

Figure 89 Normal Low-Cycle Fatigue Specimen After Failure (Top) and Hinged Specimen (Bottom)

NOFORN

(U) Comparison of the curves shows that for a 1000-cycle life at 1650°F, coated TD nickel, Inconel 625, and uncoated TD nickel-chrome posses the best fatigue characteristics. These are followed by coated TD nickel-chrome, Hastelloy X, and uncoated TD nickel. At 1800°F for the same cyclic life, the order is the same except the Inconel 625 and Hastelloy X must be eliminated entirely since both of these materials underwent plastic deformation at this temperature. If the materials are evaluated for cyclic lives of about 10^5 cycles, however, the relative order of the materials with respect to their fatigue characteristics differs. For a life of about 10^5 cycles at 1650°F, coated TD nickel chrome has the best fatigue characteristics, followed by coated TD nickel and uncoated TD nickel chrome and then by Hastelloy X, Inconel 625, and uncoated TD nickel. At 1800°F, the order is coated TD nickel chrome, uncoated TD nickel chrome, coated TD nickel and uncoated TD nickel. The change in order for the two cyclic lives is not really anomalous since varying the composition of a material to produce a better ultimate and endurance strength usually causes some loss in fracture elongation, and these parameters govern opposite ends of the fatigue curve.

(U) The data for a cyclic life of 1000 cycles indicates that uncoated TD nickel-chrome alloy has better fatigue characteristics than coated TD nickel-chrome alloy. This behavior was not expected since the coating was added to improve the cyclic fatigue life. It appears that the coating process had detrimental effects on the base material properties which were not completely offset by the expected improvement in properties produced by the coating. Further development of the coating composition and application procedure could be expected to improve the fatigue properties.

E. ENDURANCE TESTING

(U) The selected materials were exposed to combustion gases for extended periods. The gas stream velocity was about Mach 0.3 to 0.4, and test temperatures ranged from 1800°F to 2200°F. These tests were performed in two phases. Phase I consisted of ten-hour cyclic endurance tests with ten minutes of exposure to the hot gas stream and one minute out of the gas stream. All of the materials except thoriated L-605, for which a specimen could not be fabricated, were tested during Phase I. The specimens were tested in pairs at 2200°F, 2000°F, and 1800°F, using the equipment shown in Figures 90 and 91. The two materials which showed the least deterioration at the maximum temperature were tested during Phase II. The Phase II test was a 100-hour cyclic endurance test with the specimens positioned in the gas stream for one hour and out of the gas stream for one minute during each cycle. The gas stream temperature was 2000°F, and the specimens cooled to approximately 500°F during the one minute when they were removed from the gas stream. The specimens were inspected periodically for general condition during both phases of the program, and, at the completion of the tests, all materials were thoroughly examined for general condition and microstructure.

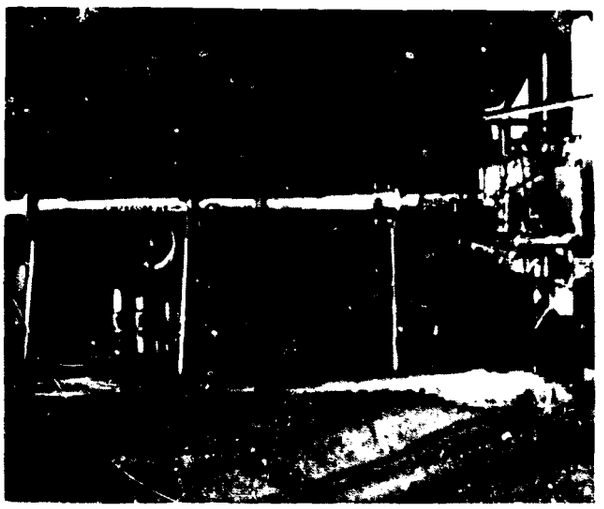

Figure 90 High-Temperature Material Cyclic Endurance Test Rig X-23642

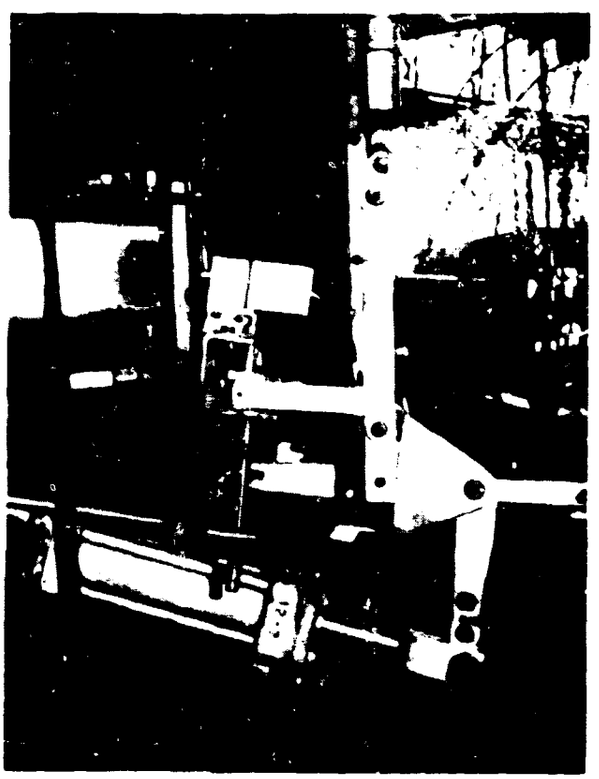

Figure 91 Closeup View of High-Temperature Material Cyclic Endurance Test Rig Showing Specimens in Test Position X-23611

NOFORN

1. Phase I Test Results

(U) The condition of the Hastelloy X and the nickel-base alloys Incoloy 804, Inconel 702, and Inconel 625 after testing is shown in Figures 92 through 95. As shown, each of these materials suffered from excessive surface oxidation, spalling, and warpage, with the effects becoming more pronounced as the test temperature was increased. None of these materials are considered to be suitable for the intended application.

(U) The condition of uncoated TD nickel and uncoated TD nickel-chrome specimens is shown in Figures 96 and 97. As shown, the depth of oxidation penetration increased as the test temperature was increased, and cracking occurred parallel to the rolling direction in the TD nickel specimens tested at 2000°F and 2200°F.

(U) Figures 98 and 99 show the results for the chrome-aluminide-coated TD nickel and TD nickel-chrome specimens respectively. After 10 hours at 1800°F, neither specimen showed significant deterioration. After testing at 2000°F, both materials showed evidence of oxidation in limited areas of the outer layer, with the oxide attack being somewhat more advanced in the coated TD nickel-chrome material than in the coated TD nickel material. In addition, the coated TD nickel specimen contained some aligned porosity at the coating-substrate interface, which was attributed to diffusion by the Kirkendall effect[1]. At 2200°F, both specimens suffered from blistering and peeling of the coating and subsequent oxidation of the base metal.

(U) The last two materials tested during Phase I were DS (dispersion strengthened) nickel-chrome alloy and Cr-Ti-Si-coated Cb-129 Y alloy. The condition of specimens is shown in Figures 100 and 101 respectively. The DS nickel-chrome specimen showed negligible deterioration after testing at 1800°F, but severe warping occurred during testing at 2000°F. Limited oxide penetration occurred during testing at 1800°F, but the oxide penetrated down to the chrome layer during testing at 2000°F, and it reached the base metal during testing at 2200°F. In evaluating the results for this material, it should be noted that the specimen used was only 20 mils thick, whereas other specimens were 42 mils thick. This was the only specimen thickness available at the time. The small thickness definitely contributed to the inability of this specimen to withstand Mach 0.3 to 0.4 gas velocities at elevated temperatures. The coated Cb-129 Y specimen showed evidence of coating failure at all test temperatures. Initially, craze cracking occurred in the outer layers. Subsequent crack growth penetrated the underlying

[1] Seventh Quarterly Progress Report to AFML Development of Coatings for Protection of Dispersion Strengthened Nickel from Oxidation, Contract AF33 (615)-1704, E. I. Dupont de Nemours & Co., Inc., October 10, 1966.

NOFORN

laves phase and then invaded the solution and parent-metal regions. Oxidation followed the cracks into the base metal, where rapid deterioration of the CB-129 Y alloy occurred.[2] Incomplete coating in weld areas contributed to the catastrophic oxidation of the base metal observed after testing at 2200°F.

(U) In summary, all of the materials tested during Phase I showed a similar type of deterioration after testing at 1800°F, with the amount of deterioration being least for the coated TD nickel and the coated TD nickel-chrome specimens. At 2000°F, all of the materials suffered from oxide penetration into the base metals except for the coated TD nickel and the coated TD nickel-chrome specimens, on which the coatings remained uniformly attached to the substrates with only limited areas of oxidation in the outer layer. At 2200°F, all of the specimens suffered from considerable deterioration. The relative amounts of warpage for the specimens tested are shown in Figure 102. Warpage was measured at the location shown in Figure 103. Oxide penetration for all of the uncoated specimens is shown in Figure 104.

(U) On the basis of the Phase I test results, chrome-aluminide-coated TD nickel chrome and chrome-aluminide-coated TD nickel were selected for Phase II testing at 2000°F.

2. Phase II Test Results

(U) During the 100-hour test of the coated TD nickel specimen, cracking occurred parallel to the rolling direction after 40 hours of testing followed by oxidation in the cracks and in areas around the cooling holes where the coating spalled from the specimen. However, after 100 hours of testing, the over-all coating was still protective except for the same area noted above. This is shown in Figure 105.

(U) Initial examination of the specimen indicated that the coating was intact, although a light green highlight was present in the area exposed to the maximum temperature, whereas the material originally had a silver-gray metallic luster. Metallographic examination verified that the coating was intact. It also revealed that surface oxide and oxide penetration of the coating occurred, with some porosity present at the coating-substrate interface.

(U) The coated TD nickel-chrome specimen suffered severe deterioration during the 100-hour test, as shown in Figure 106. Initial coating deterioration was observed after 15 hours of testing. The deterioration continued as the test pro-

[2] H. A. Hauser and J. F. Holloway, Jr., Evaluation and Improvement of Coatings for Columbium Alloy Gas Turbine Engine Components, AFML-TR-66-186, Pratt & Whitney Aircraft Division of United Aircraft Corporation, East Hartford, Connecticut, July 1966.

NOFORN

1800°F
10 HOURS

2000°F
10 HOURS

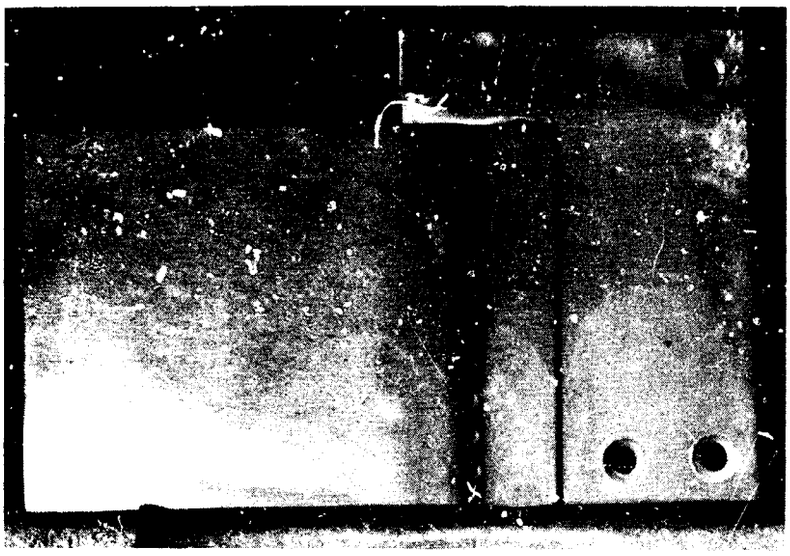

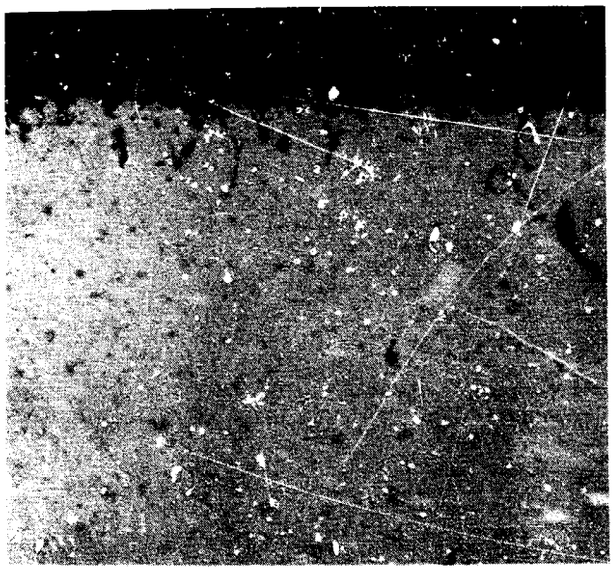

MAG: 500X

Figure 92 Phase I Endurance Test Results

NOFORN

UNCLASSIFIED

2000°F
10 HOURS

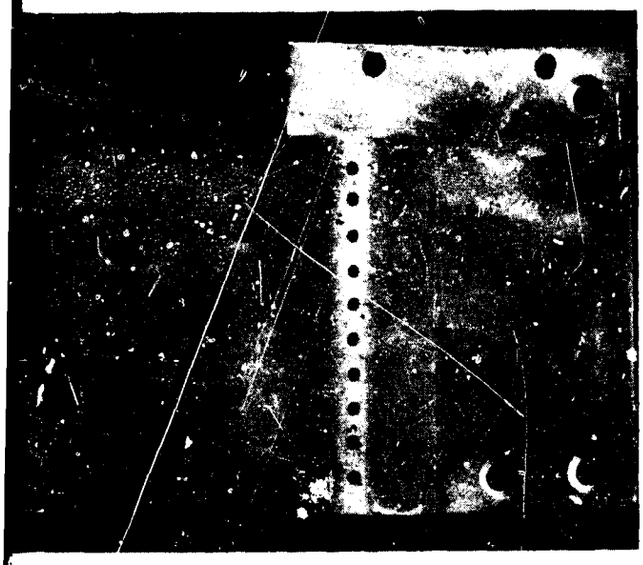

MAG: 250X

2200°F
6 HOURS

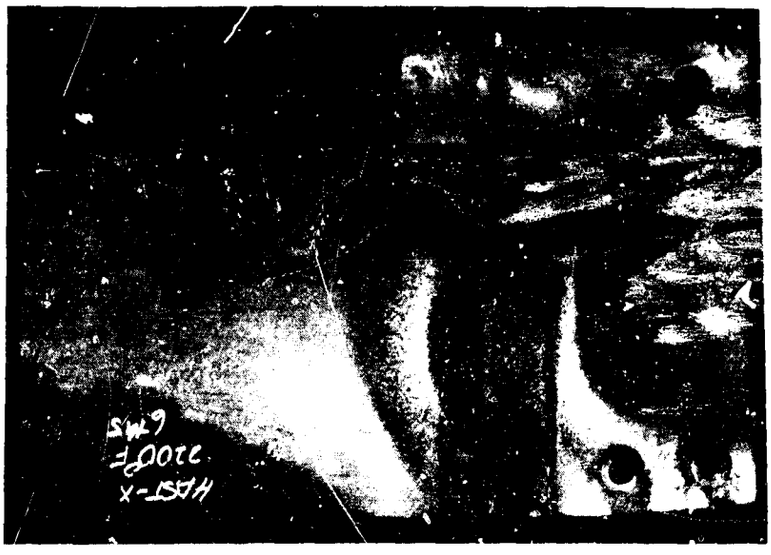

MAG: 250X

Endurance Test Results for Hastelloy X Specimen
XP-77872/XP-77420/XP-76019

2

1800°F
10 HOURS

2000°F
10 HOURS

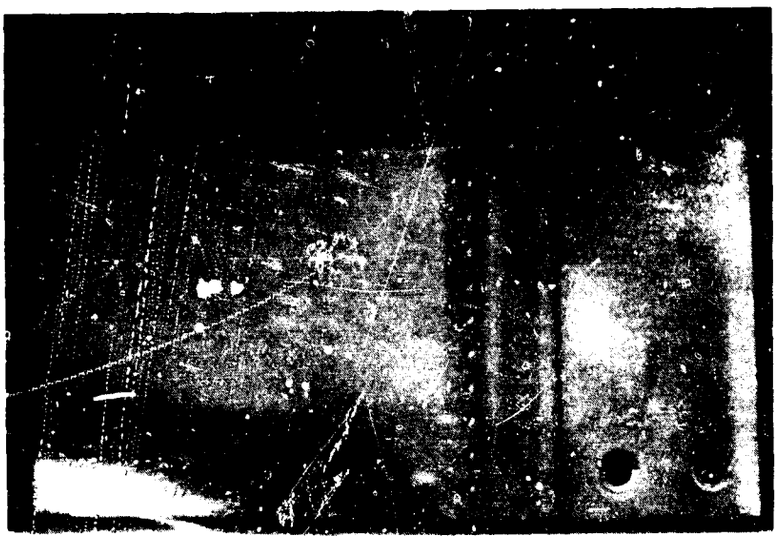

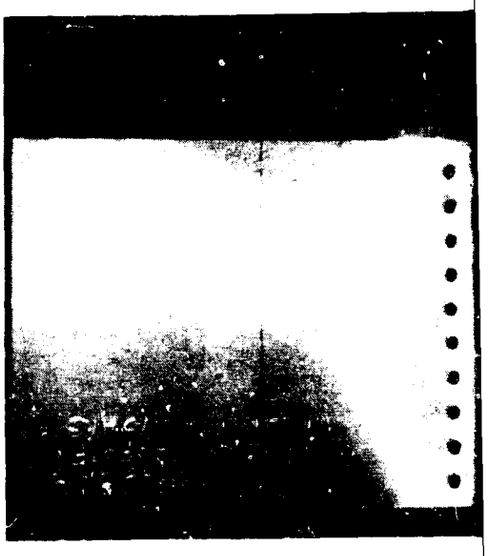

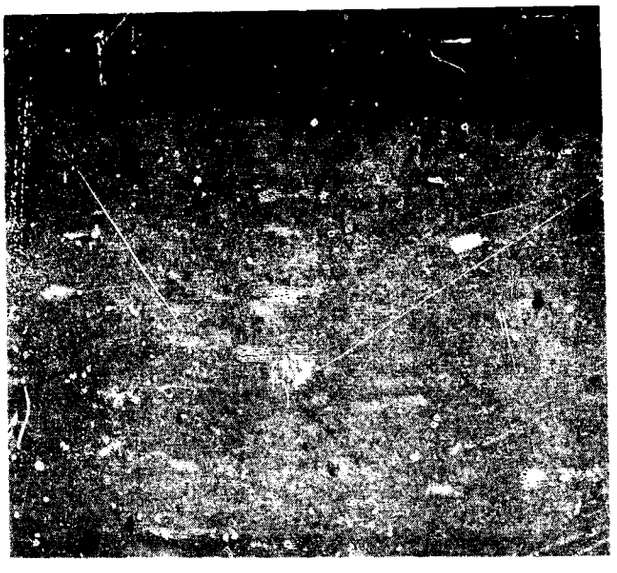

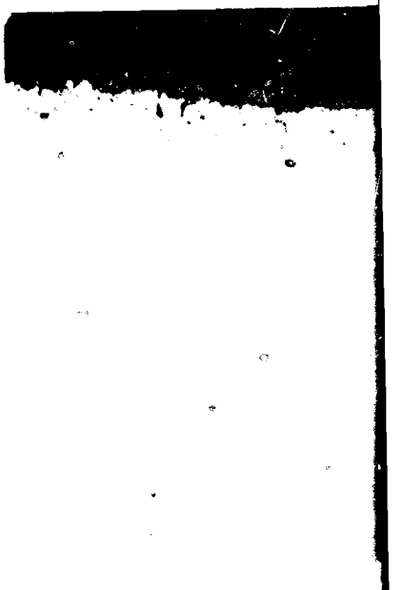

MAG: 500X

Figure 93 Phase I Endurance Test Results

NOFORN

UNCLASSIFIED

1

2000°F
10 HOURS

2200°F
10 HOURS

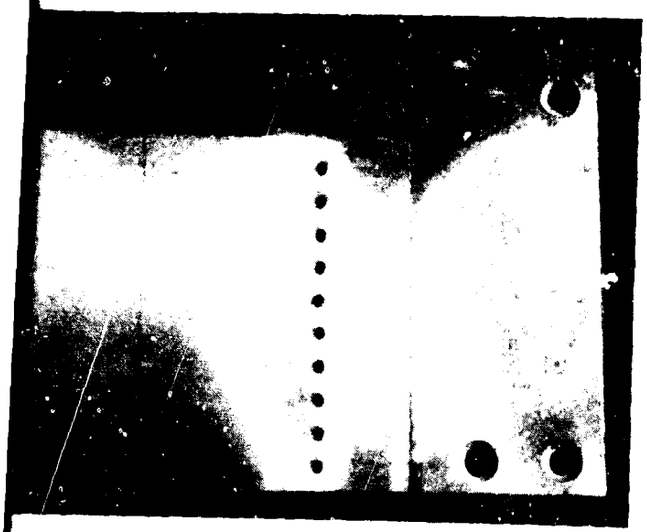

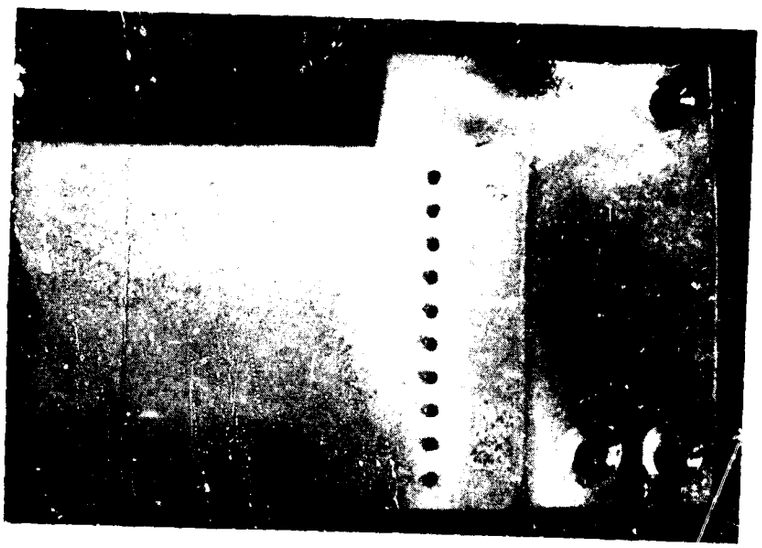

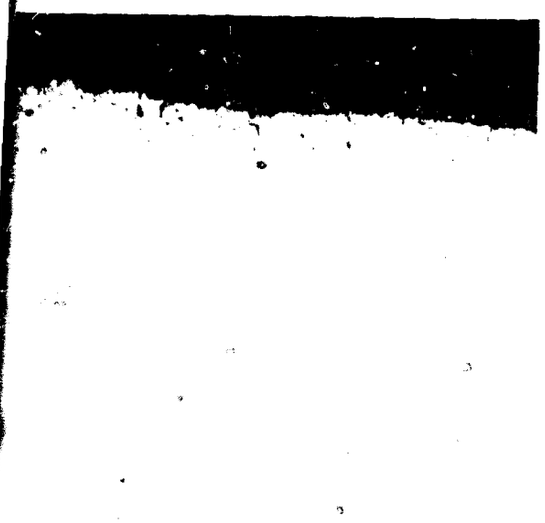

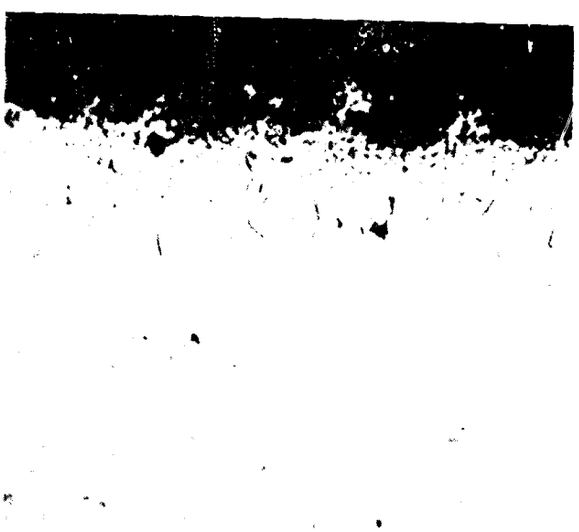

MAG: 250X

MAG: 250X

e I Endurance Test Results for Incoloy 804 Specimen
XP-77873/XP-77421/XP-76620

2

1800°F
10 HOURS

2000°F
10 HOURS

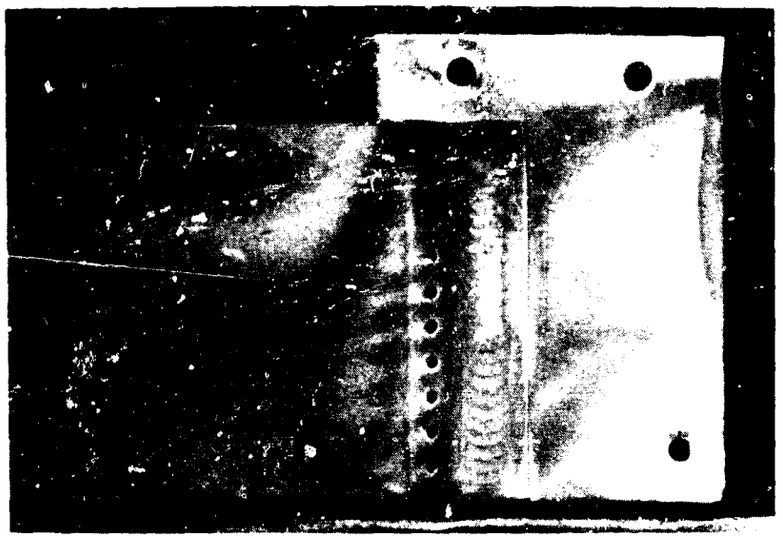

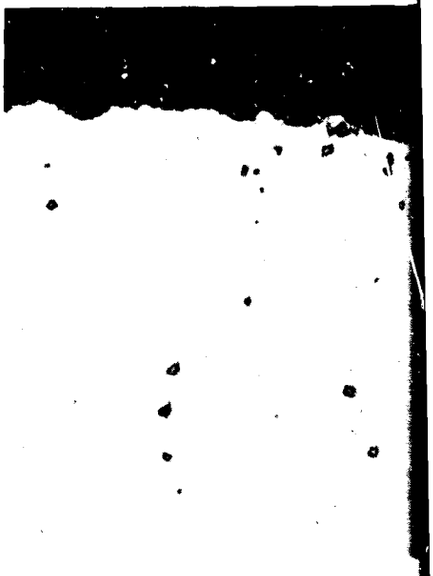

MAG: 500X

Figure 94 Phase I Endurance Test Results fo
X

NOFORN

UNCLASSIFIED

2000°F
10 HOURS

2200°F
10 HOURS

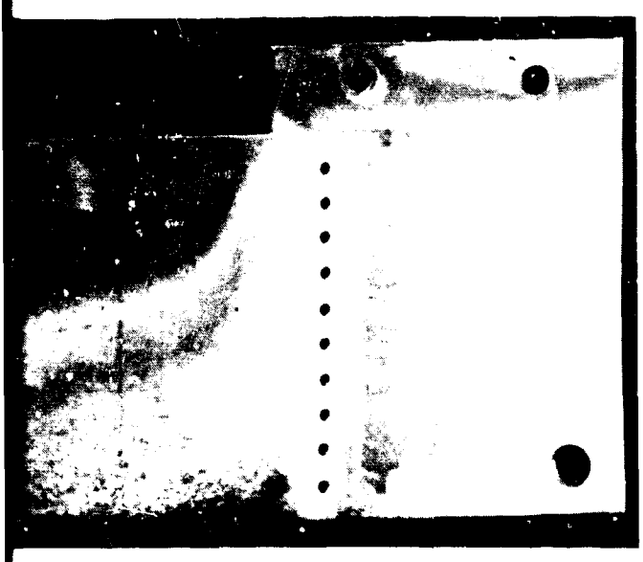

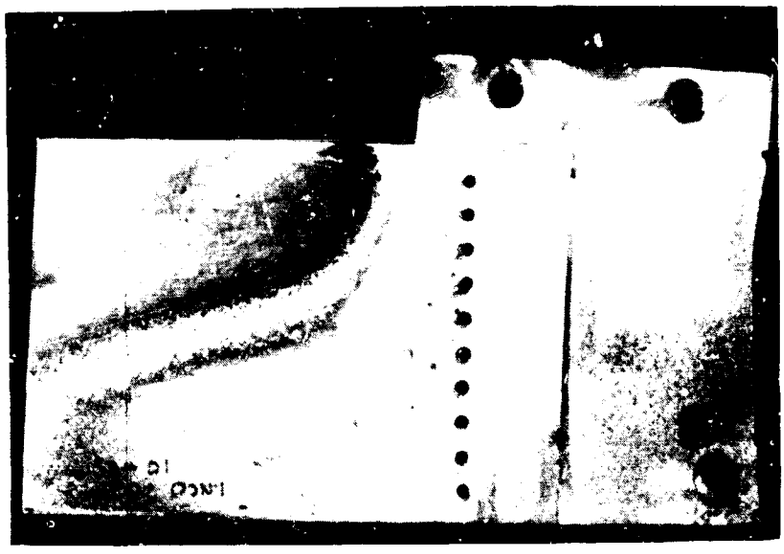

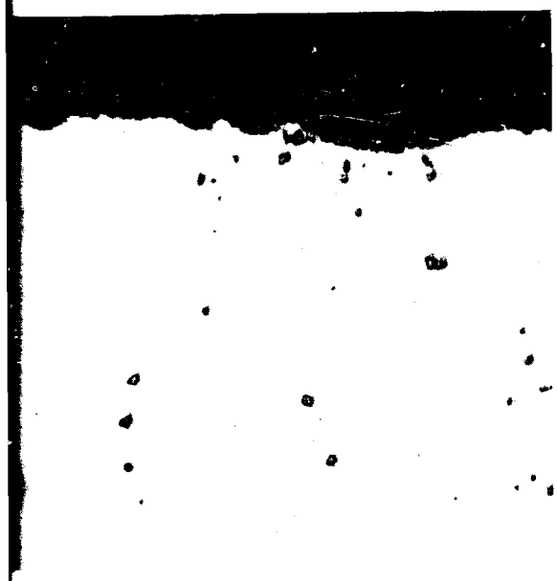

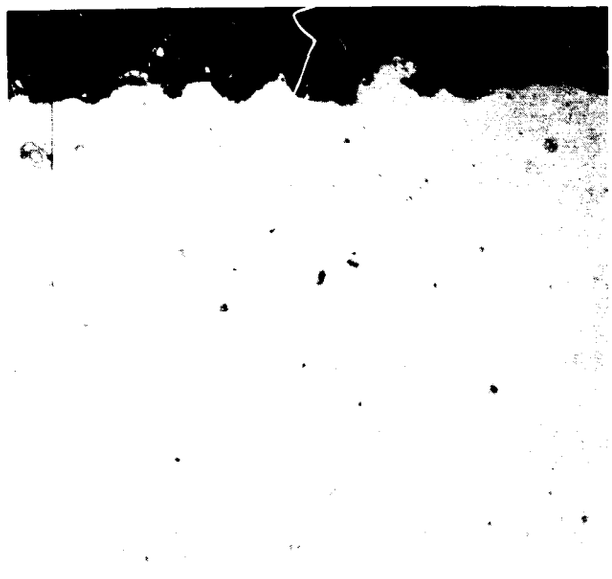

MAG: 250X

MAG: 250X

I Endurance Test Results for Inconel 702 Specimen
XP-77873/XP-77421/XP-77620

2

1800°F
10 HOURS

2000°F
8 HOURS

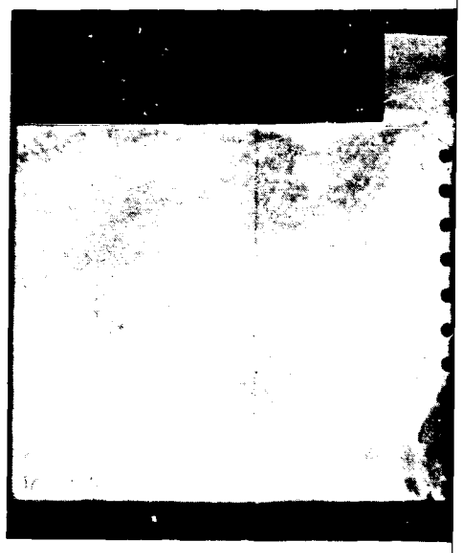

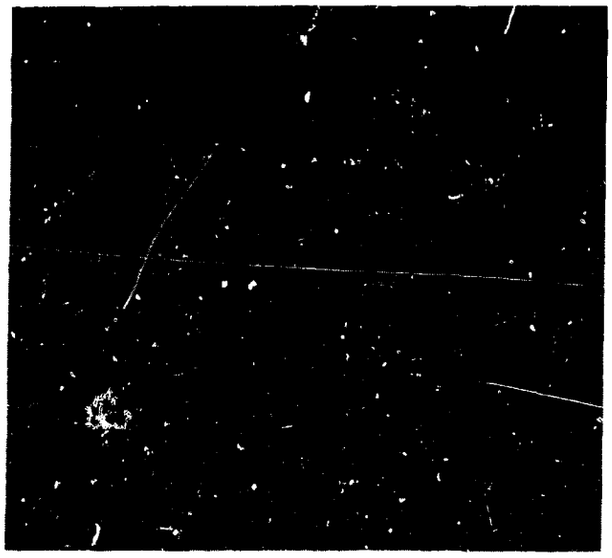

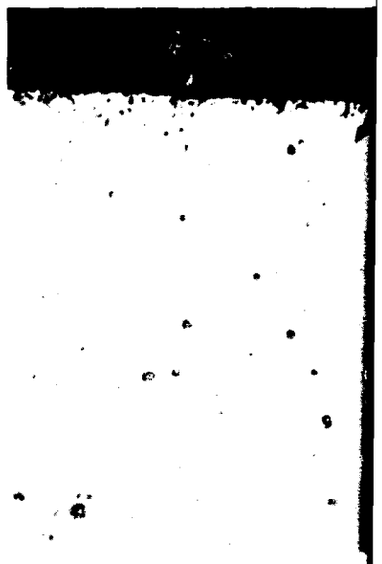

MAG: 500X

Figure 95 Phase I Endurance Test Result

NOFORN

UNCLASSIFIED

1

2000°F
5 HOURS

2200°F
10 MINUTES

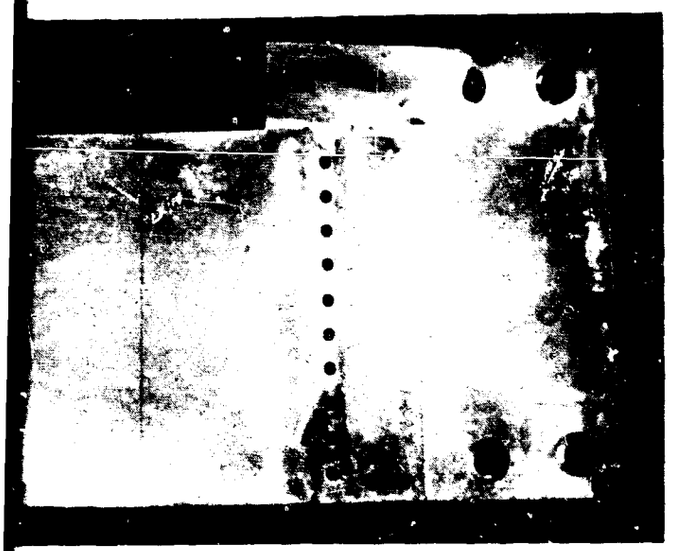

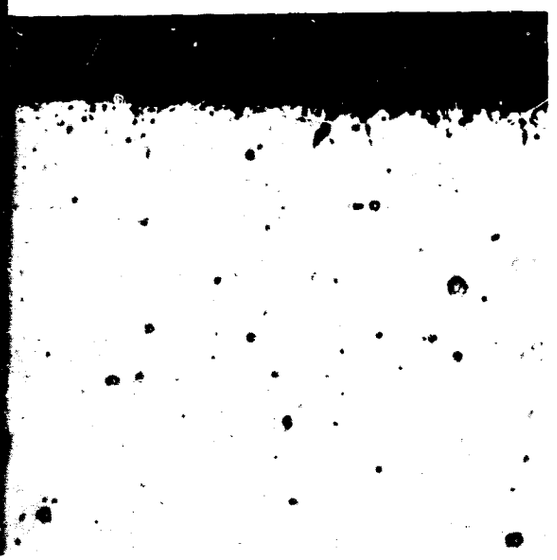

MAG: 250X

MAG: 250X

e I Endurance Test Results for Inconel 625 Specimen
XP-77872/XP-77420/XP-76019

2

1800°F
10 HOURS

2000°F
10 HOURS

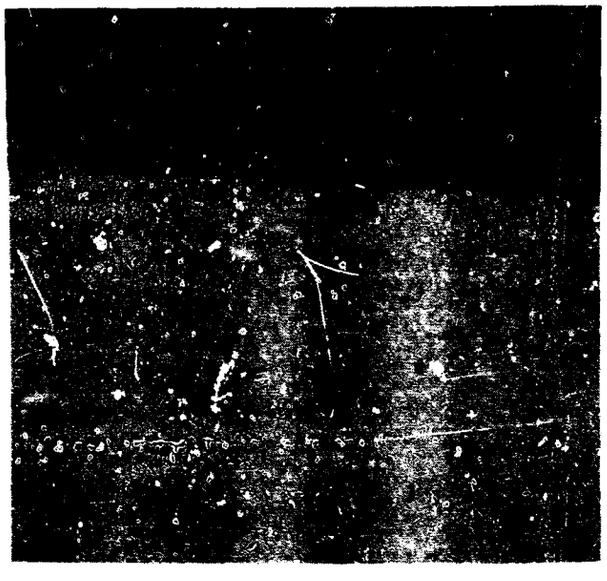

MAG: 500X

Figure 56 Phase I Endurance Test Results for XP-

NOFORN

2000°F
10 HOURS

2200°F
4 HOURS

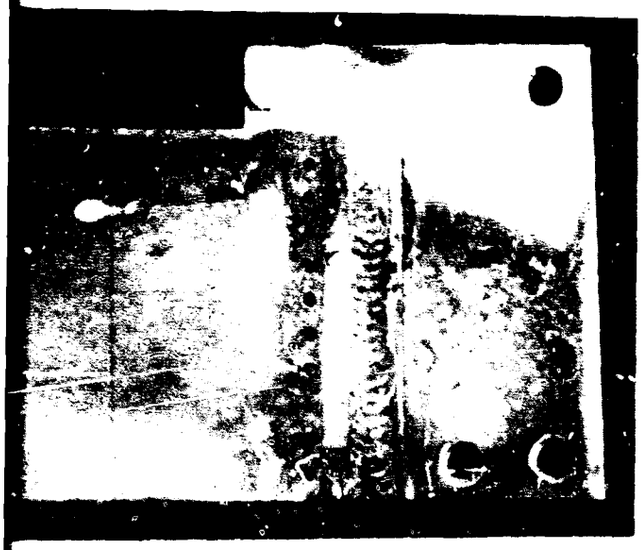

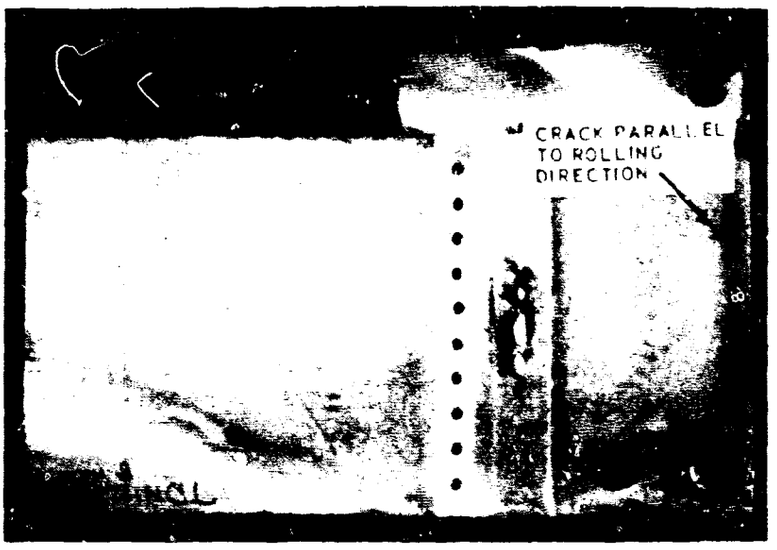

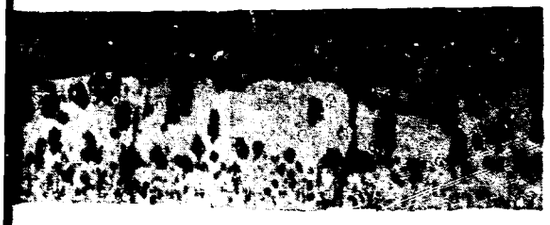

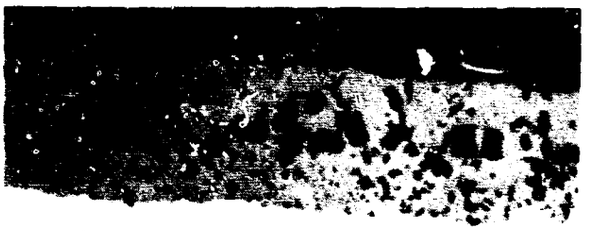

MAG: 20X

MAG: 20X

Endurance Test Results for TD Nickel Specimens
XP-17870 XP-77119 XP-76671

2

1800°F
10 HOURS

2000°F
10 HOURS

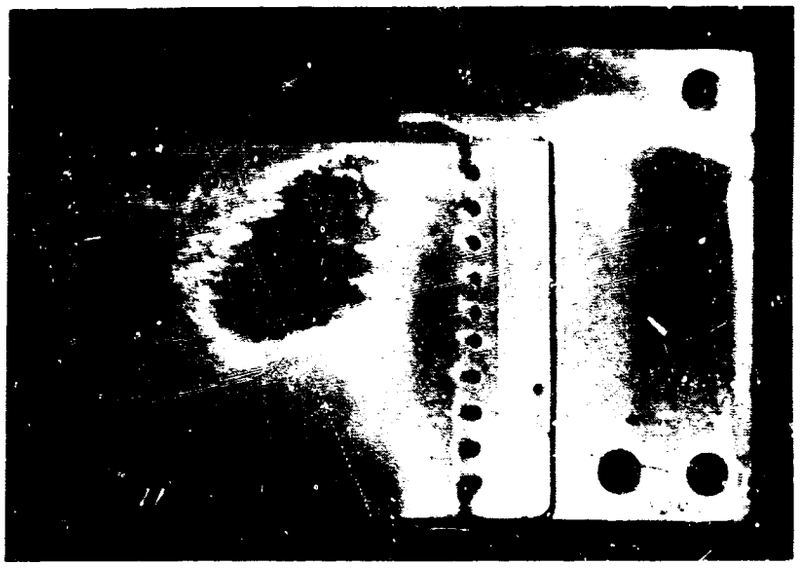

Figure 97 Phase I Endurance Test Results

NOFORN

UNCLASSIFIED

2000°F
10 HOURS

2200°F
10 HOURS

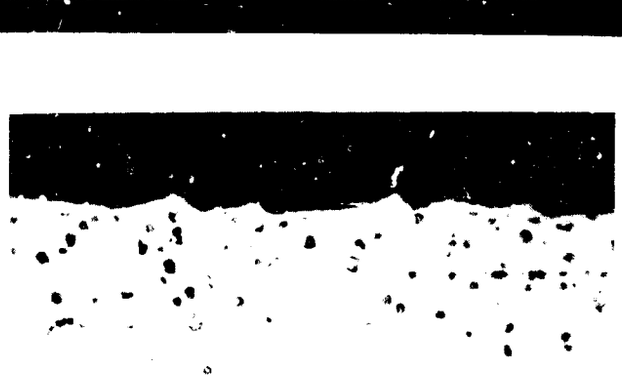

MAG: 250X

MAG: 250X

Endurance Test Results for TD Nickel-Chrome Specimen
XP-77870/XP-77419/XP-76621

1800°F
10 HOURS

2000°F
10 HOURS

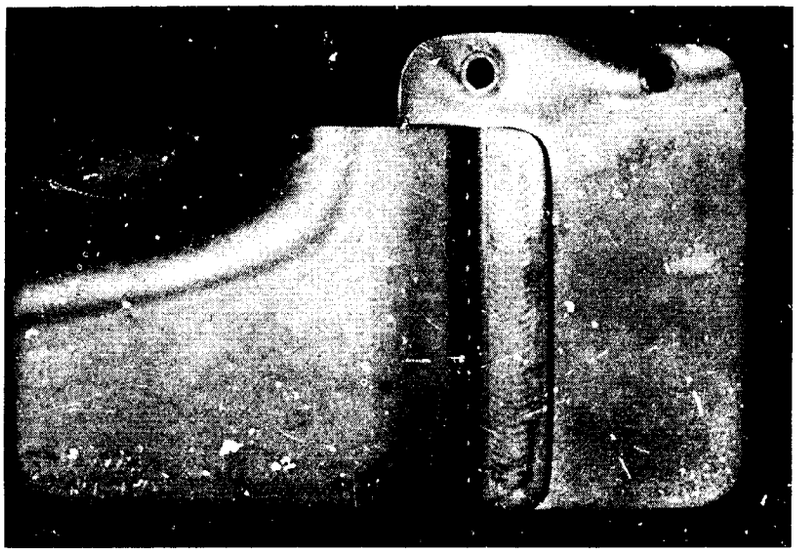

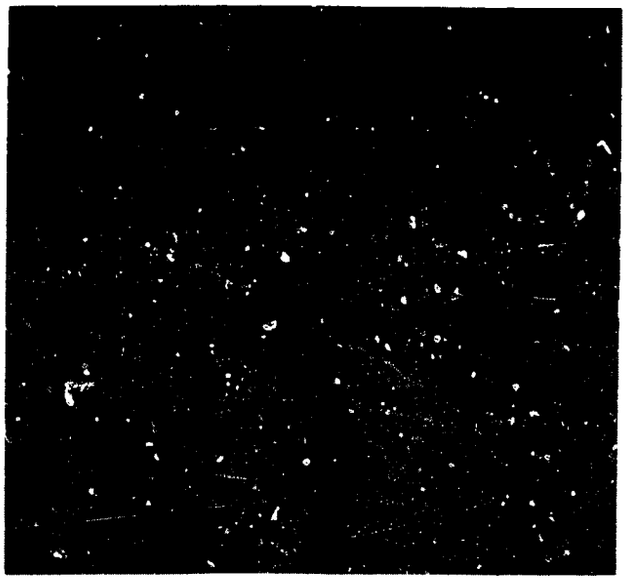

MAG: 500X

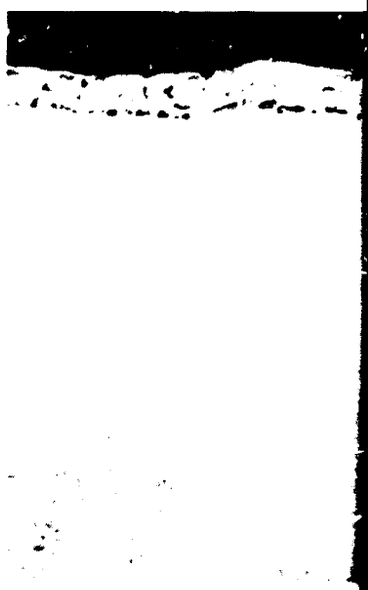

Figure 98 Phase I Endurance Test Re
TD Nickel Specimen

NOFORN

UNCLASSIFIED

2000°F
10 HOURS

2200°F
10 HOURS

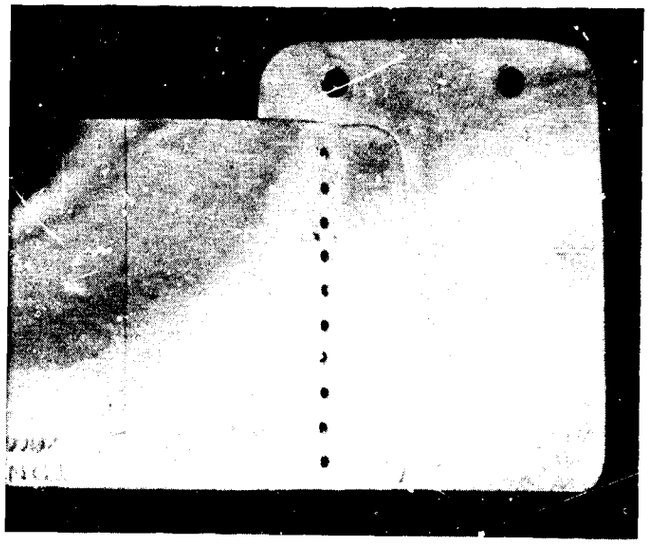

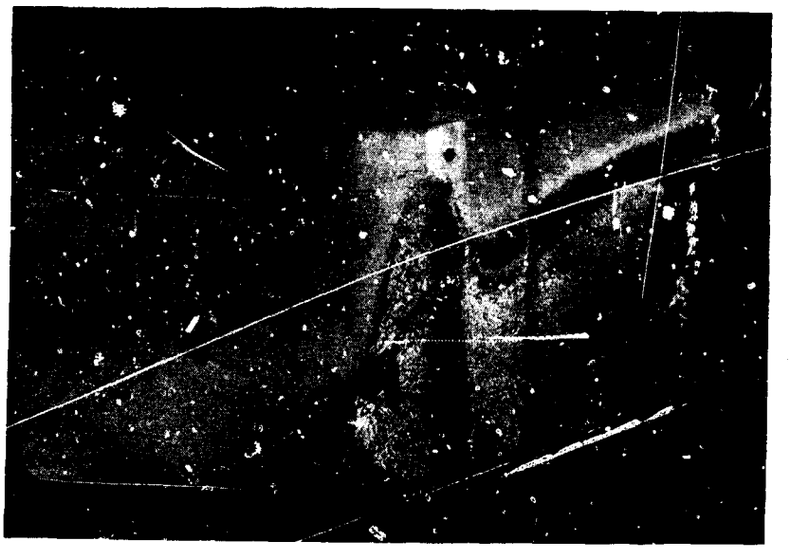

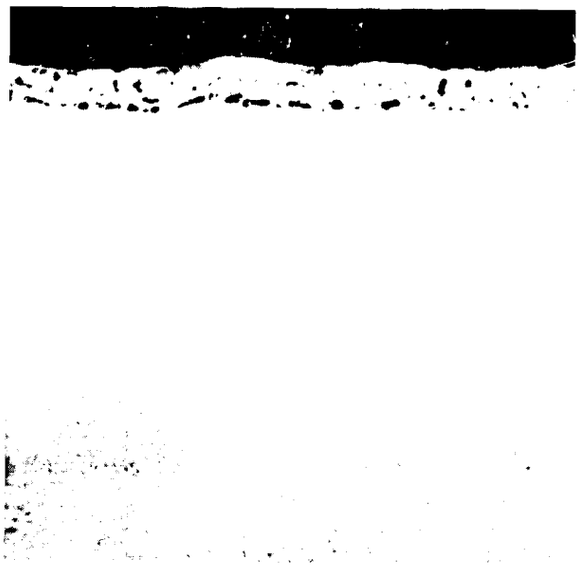

MAG: 250X

MAG: 250X

ase I Endurance Test Results for Chrome-Aluminide-Coated Nickel Specimen XP-77871/XP-77418/XP-76623

2

1800°F
10 HOURS

2000°F
10 HOUR.

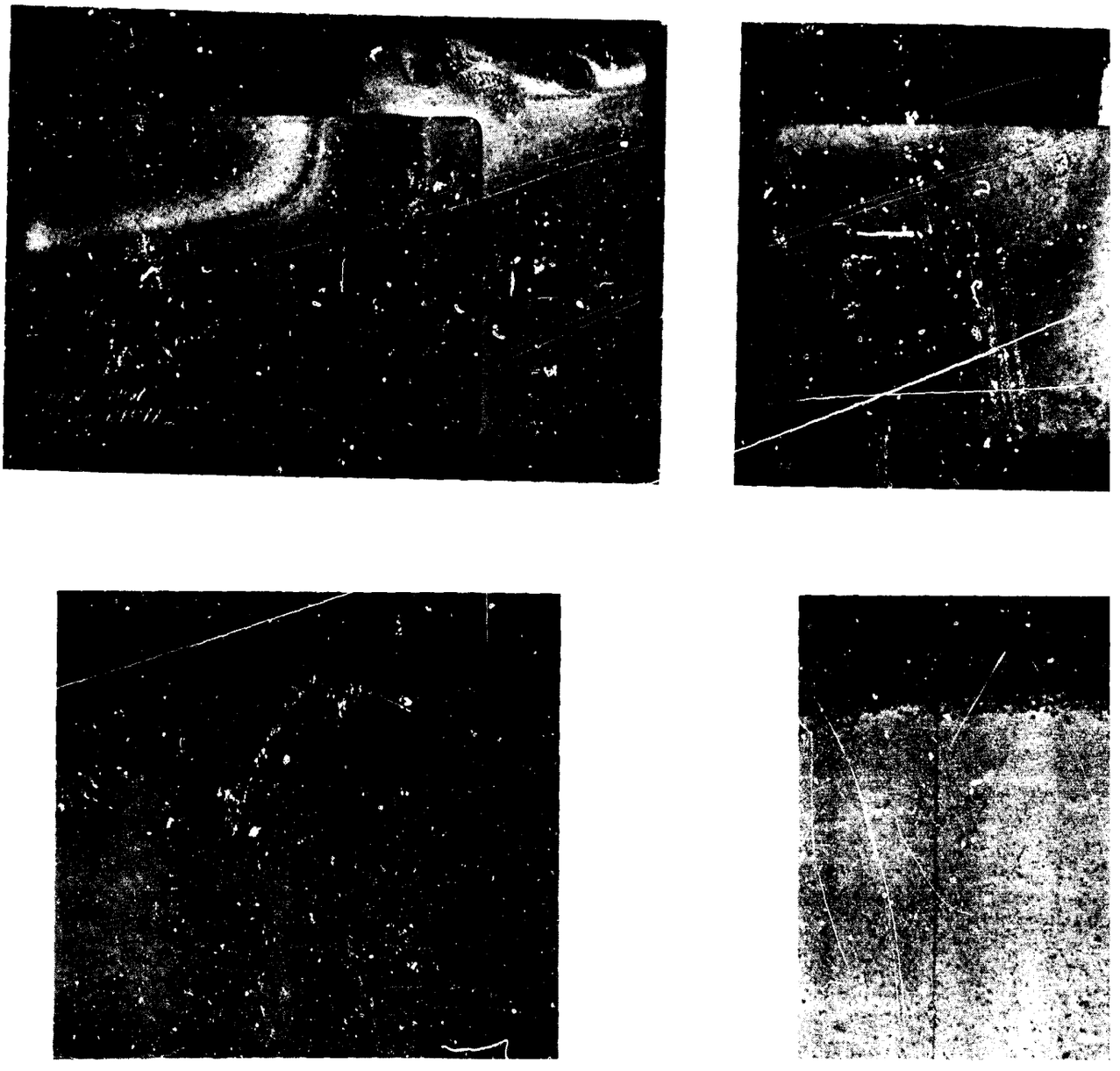

MAG: 500X

Figure 99 Phase I Endurance Test Result TD Nickel-Chrome Specimen

NOFORN

2200°F
6 HOURS

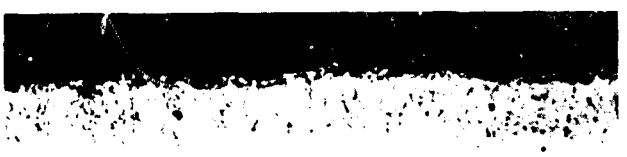

MAG: 250X

MAG: 250X

ılts for Chrome-Aluminide-Coated
XP-77871/XP-77418/XP-76623

2

1800°F
10 HOURS

2000°F
1 HOUR

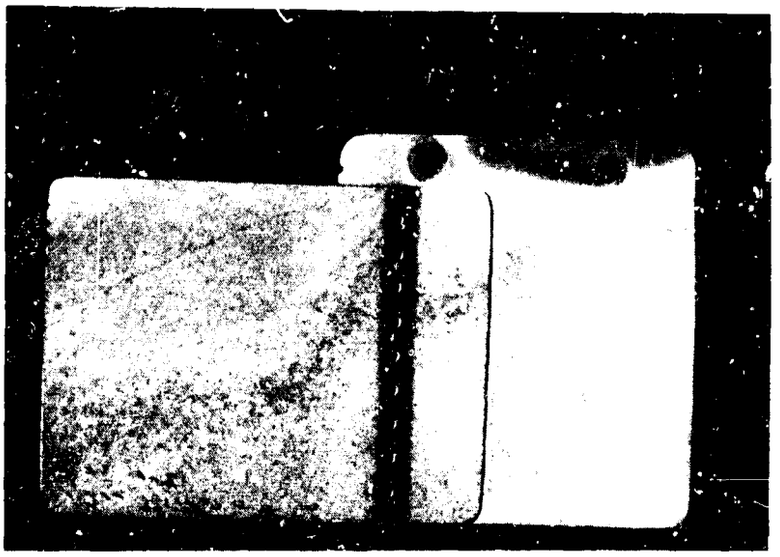

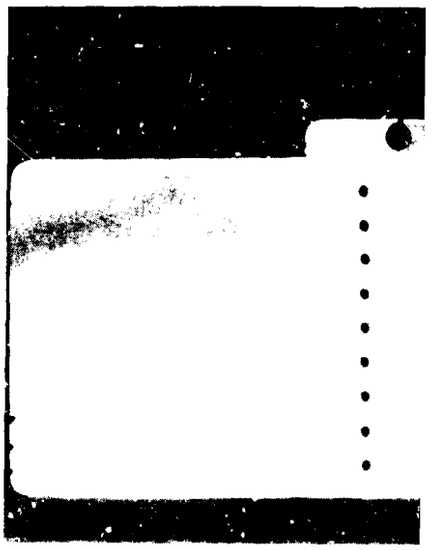

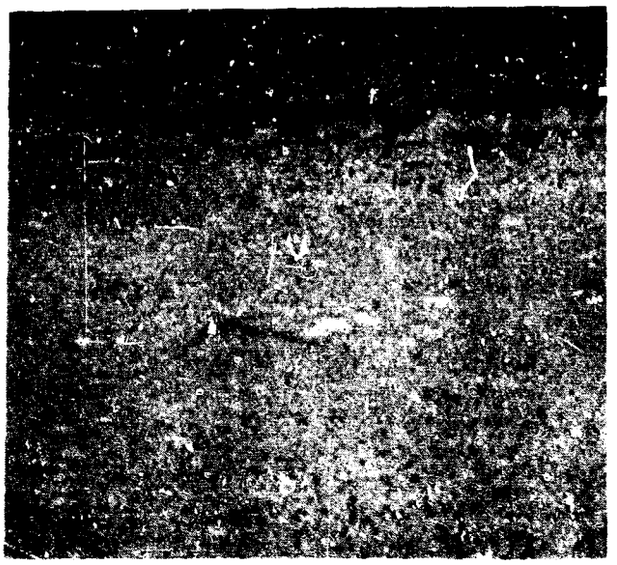

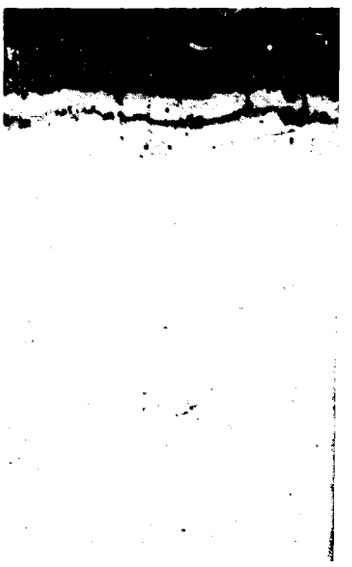

MAG: 500X

Figure 100 Phase I Endurance Test Result

NOFORN

UNCLASSIFIED

1

2000°F
1 HOUR

2200°F
2 HOURS

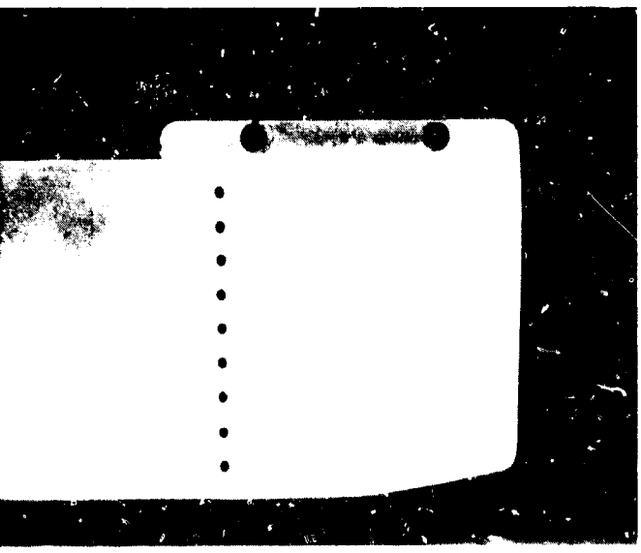

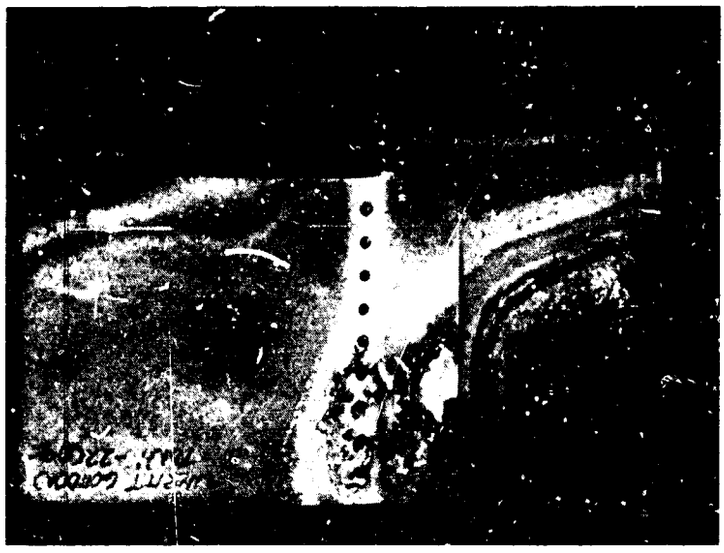

MAG: 250X

MAG: 250X

Endurance Test Results for DS Nickel-Chrome Specimen
XP-76622/XP-77869/XP-77417

1800°F
10 HOURS

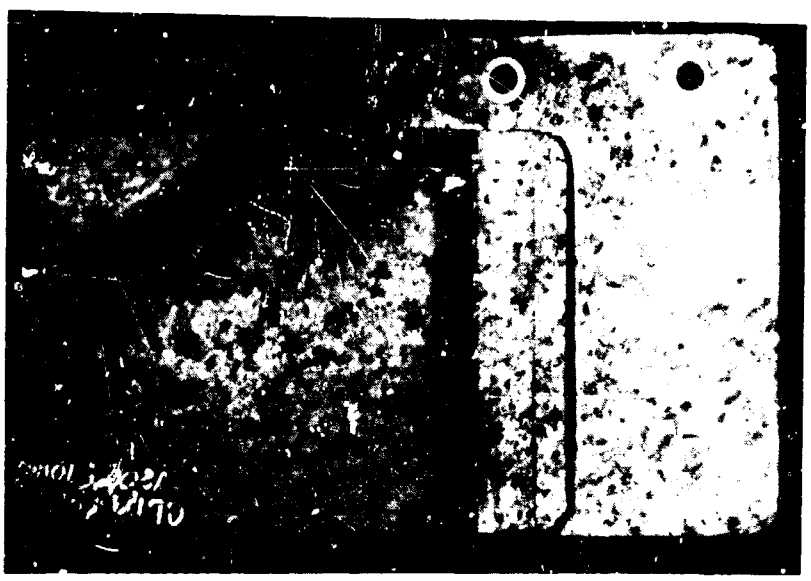

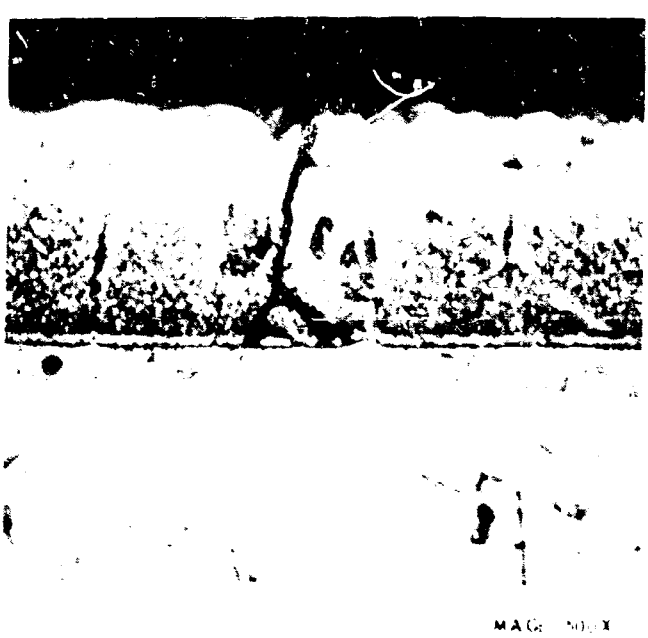

MAG 500X

Figure 101 Pr
Sp

NOFORN

UNCLASSIFIED

1

2200°F
10 HOURS

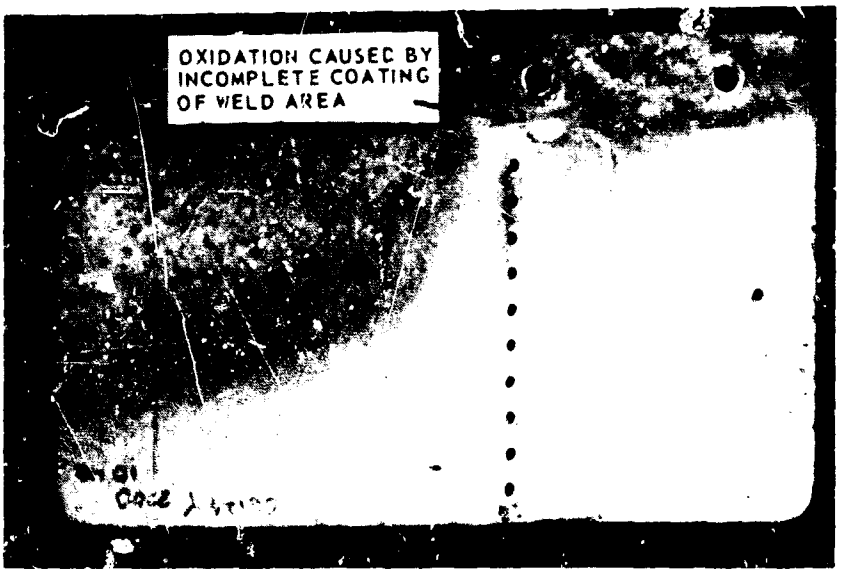

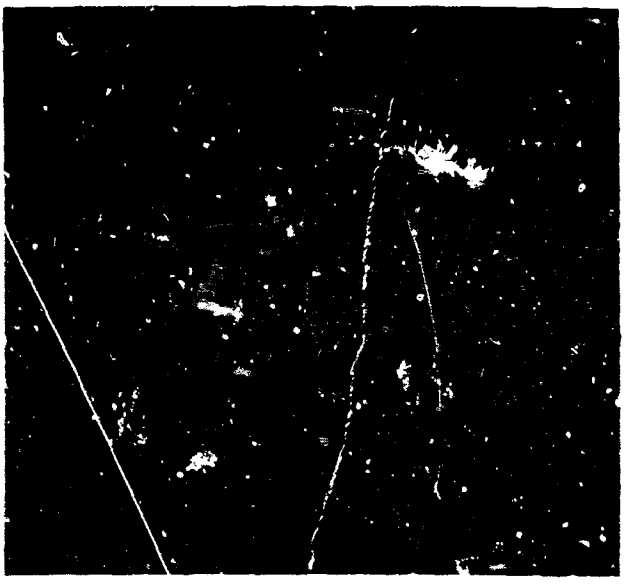

MAG: 250X

Coated Cb-129Y
-77869 XP-77417

2

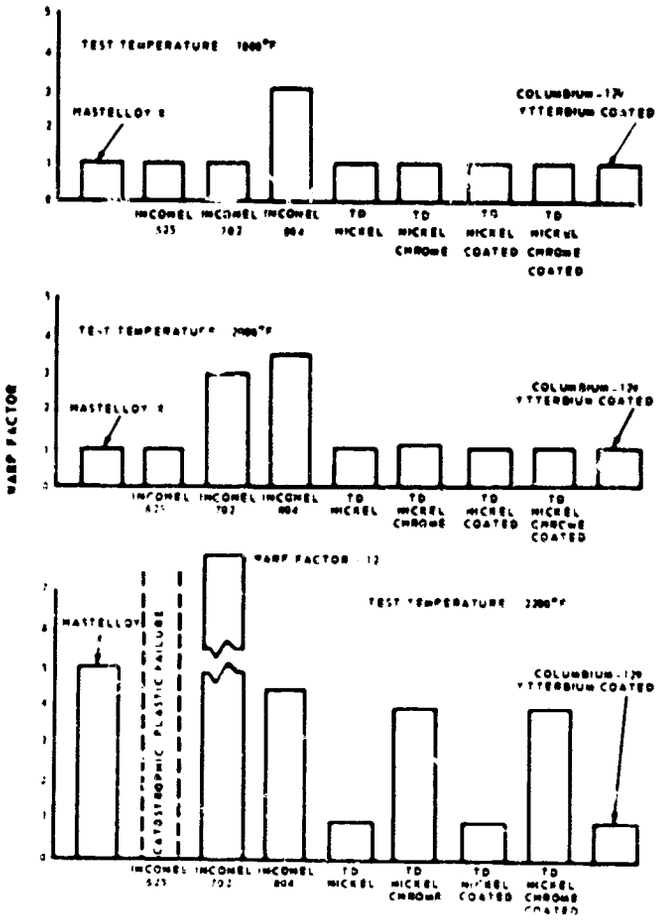

Figure 102 Relative Warpage Experienced by Phase I Endurance Test Specimens

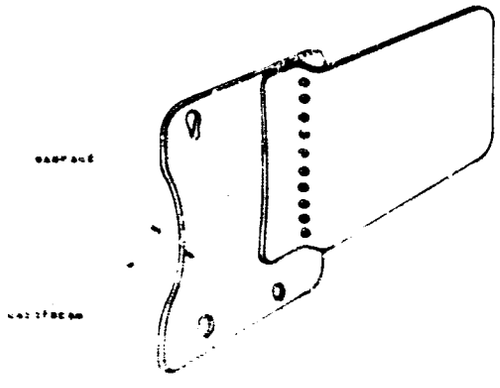

Figure 103 Location Where Warpage Was Measured on Phase I Endurance Test Specimens

NOFORN

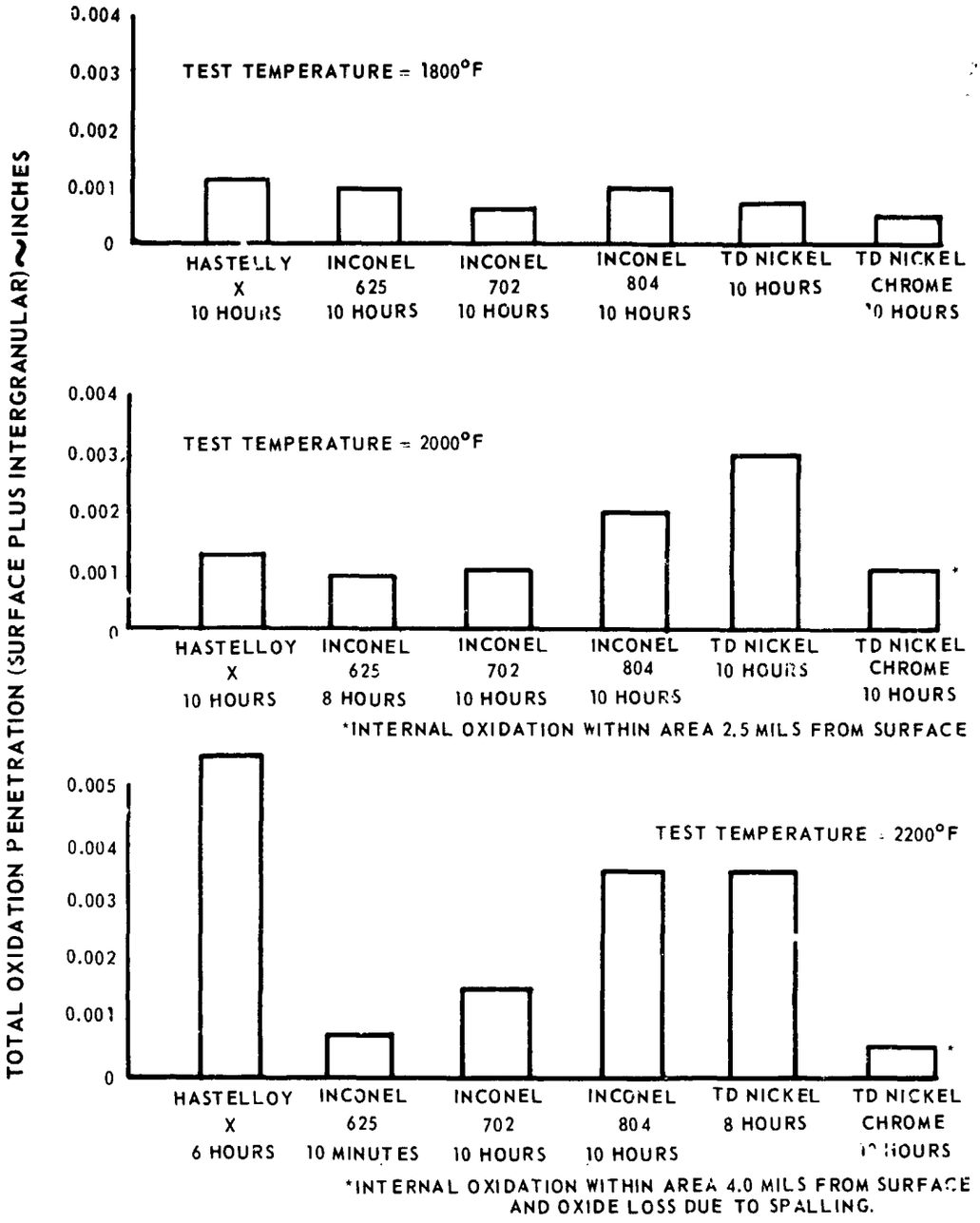

Figure 104 Oxide Penetration in Phase I Endurance Test Specimens

NOFORN

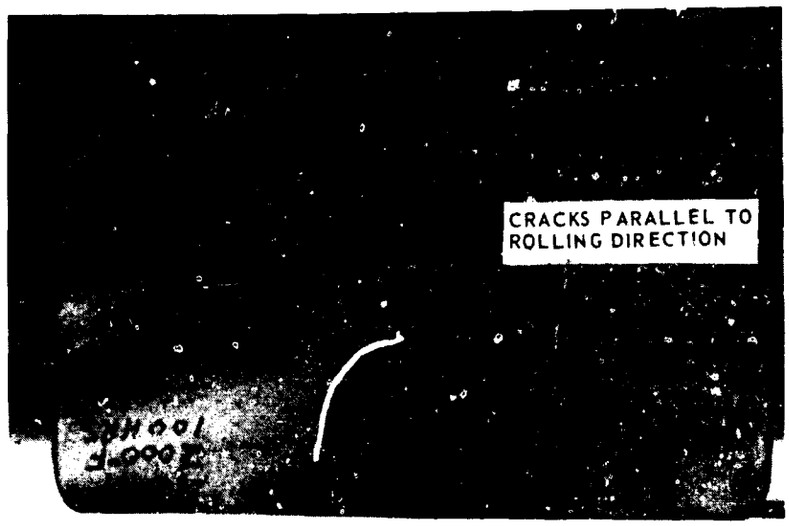

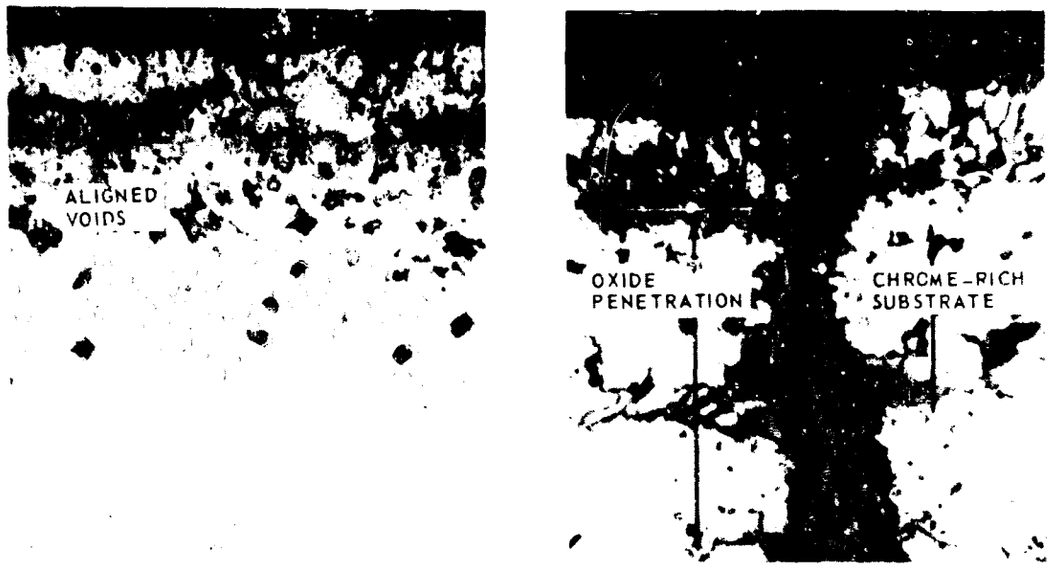

100 HOURS, 2000°F MAG: 500X

Figure 105 Phase II Endurance Test Results for Chrome-Aluminide-Coated TD Nickel Specimen XP-78420

NOFORN

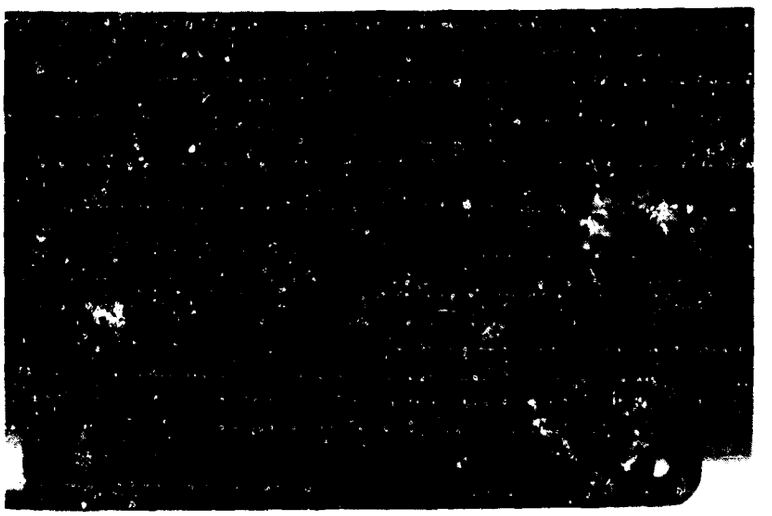

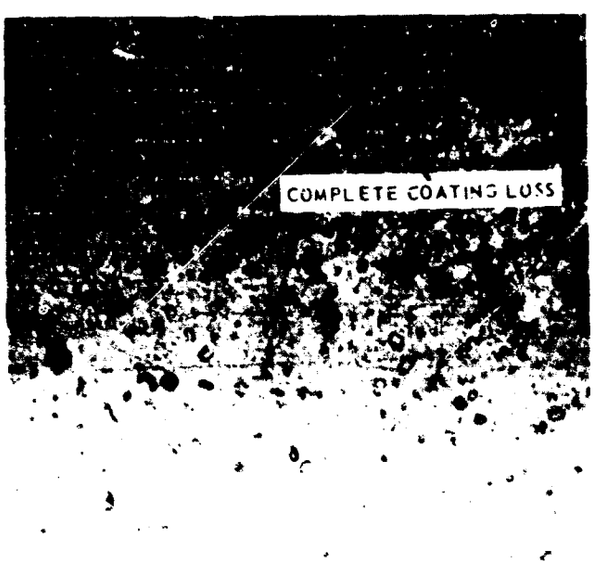

Figure 106 Phase II Endurance Test Results for Chrome-Aluminide Coated TD Nickel-Chrome Specimen XP-78420

NOFORN

gressed with considerable spalling occurring at the leading edge and in the areas around the cooling holes. Metallographic examination revealed an adherent oxide scale in the regions where the coating had spalled from the specimen, with internal oxidation and some porosity occurring in the chrome-rich region beneath the scale.

(U) It is evident from the results of the Phase II tests that coated TD nickel has greater resistance to cyclic thermal stress in a combustion stream than coated TD nickel-chrome alloy. However, consideration of the TD nickel-chrome alloy should not be closed since methods of applying coatings of thoriated nickel alloy have not yet been extensively developed.

F. CONCLUSIONS AND RECOMMENDATIONS

(U) None of the materials tested demonstrated an ability to withstand a combustion gas stream at 2000°F at Mach 0.3 to 0.4 for long periods. Best results were obtained with chrome-aluminide-coated TD nickel, but cracks were observed in this specimen after only 40 hours of testing and oxidation followed the cracks. The second best material was chrome-aluminide-coated TD nickel-chrome alloy, but this material deteriorated significantly during 100 hours of cyclic testing at 2000°F. However, the coating procedure used noticeably degraded the fatigue life and the formability of this material. With a better coating procedure, the thermal capabilities of the material might be improved together with the fatigue life and formability. All other materials tested suffered excessive oxidation and dimensional distortion after exposure to the hot gas stream for periods of ten hours or less.

(U) It is also recommended that the development of coated TD nickel-chrome and refractory Cb-129 Y be continued. TD nickel chrome is superior to TD nickel in the uncoated condition with respect to oxidation resistance and fatigue life, and, with proper coating procedure development, this material may also prove to be superior in the coated condition. Refractory Cb-129 material demonstrated excellent high-temperature capabilities during these tests, but was disqualified because of coating defects.

UNCLASSIFIED

Security Classification

DOCUMENT CONTROL DATA - R & D

(Security classification of title, body of abstract and indexing annotation must be entered when the overall report is classified)

1. ORIGINATING ACTIVITY (Corporate author)	2a. REPORT SECURITY CLASSIFICATION
Pratt & Whitney Aircraft Division United Aircraft Corporation East Hartford, Connecticut	Unclassified - NOFORN 2b. GROUP

3. REPORT TITLE

ADVANCED TURBINE ENGINE GAS GENERATOR CONCEPTUAL STUDIES AND FEASIBILITY EXPERIMENTAL TEST PROGRAM (U)
VOLUME III: MATERIALS SECTION (TABLE LXXV)

4. DESCRIPTIVE NOTES (Type of report and inclusive dates)

Final Report

5. AUTHOR(S) (First name, middle initial, last name)

Frederick G. Groh

6. REPORT DATE	7a. TOTAL NO. OF PAGES	7b. NO. OF REFS
April 1969	125	0

8a. CONTRACT OR GRANT NO.	9a. ORIGINATOR'S REPORT NUMBER(S)
AF33(657)-15504 b. PROJECT NO. 681B c. P. E. C. No. 63216F d.	PWA-3219 9b. OTHER REPORT NO(S) (Any other numbers that may be assigned this report) AFAPL-TR-69-35, Volume III

10. DISTRIBUTION STATEMENT

All distribution of this report is controlled. Qualified Defense Documentation Center users will request through AF Aero Propulsion Laboratory (RTD), [redacted], Wright-Patterson AFB, Ohio 45433

11. SUPPLEMENTARY NOTES	12. SPONSORING MILITARY ACTIVITY
Special Handling Required Not Releasable to Foreign Nationals	Air Force Aero Propulsion Laboratory Research and Technology Division Wright-Patterson Air Force Base, Ohio

13. ABSTRACT

Materials research and development was performed under Contract AF33 (657)-15504 on diffusion bonding of titanium, machining of small-diameter holes, determination of the abrasive properties of materials in a simulated jet-engine environment, and determination of the properties of selected materials in a high-temperature corrosive and erosive environment. Satisfactory diffusion bonds were formed in hollow titanium specimens at a temperature of 1800°F under isostatic pressure of 10,000 psi using machined steel mandrels to support the walls of the cavities within the specimens. Although satisfactory results were obtained using steel mandrels, the difficulty of accurately machining mandrels to fill cavities with complicated shapes makes this technique impractical for production processes. Five-mil diameter holes, which were subsequently coated to reduce the diameter to three mils, were successfully drilled into 80-mil thick alloys by the ECID (electrochemical impingement drilling) and the EDM (electrochemical discharge machining) processes. Low-cycle fatigue testing of specimens with arrays of three-mil diameter holes indicated the superiority of directionally solidified U-700 alloy over other forms of the same alloy and over Mar-M-509 alloy. None of the materials evaluated for abrasion properties demonstrated satisfactory abradability concurrently with a capability for withstanding the jet-engine environment, nor did any of the materials evaluated for use in a high-temperature corrosive and erosive environment meet the program requirements. Best results were obtained with chrome-aluminide-coated TD nickel, but cracks were observed in the specimen after only 40 hours of testing, and oxidation followed the cracks.

DD FORM 1473 REPLACES DD FORM 1473, 1 JAN 64, WHICH IS OBSOLETE FOR ARMY USE.

NOFORN

UNCLASSIFIED

Security Classification

14. KEY WORDS	LINK A		LINK B		LINK C	
	ROLE	WT	ROLE	WT	ROLE	WT
Diffusion Bonding of Hollow Blades Drilled Small-Diameter Holes Abradable Material Development High Temperature Materials						

NOFORN

SUPPLEMENTARY

INFORMATION

Pratt & Whitney Aircraft DIVISION OF UNITED AIRCRAFT CORPORATION

In reply please refer to
VWT:A:mhb - Eng. 2G5

June 26, 1969

To: Defense Documentation Center
Cameron Station
Alexandria, Virginia 22314

Subject: NOFORN Notice on ATEGG II Final Technical Report (U)
(AFAPL-TR-69-35)

The NOFORN notice (not releasable to foreign nationals) was printed on all pages of the ATEGG II Final Technical Report (U), AFAPL-TR-69-35, including Volume III, which was unclassified. However, Change 5 (dated 7 February 1969) amends paragraph 5.9a of the Air Force Regulation Manual AFR 205-1, "Safeguarding Classified Information," to read that "the NOFORN notice shall not be applied to any ... unclassified material."

In view of this amendment, all recipients of the ATEGG II Final Technical Report are being notified that the NOFORN notice is not applicable to unclassified material and may be disregarded where it appears on unclassified pages.

UNITED AIRCRAFT CORPORATION
Pratt & Whitney Aircraft Division

V. W. Thompson
Assistant Program Manager